Alma Mater Studiorum – Università di Bologna

DOTTORATO DI RICERCA IN

Scienze Biotecnologiche, Biocomputazionali, Farmaceutiche e Farmacologiche

Ciclo XXXIII

Settore Concorsuale: 05/G1

Settore Scientifico Disciplinare: BIO/14

TITOLO TESI

Evaluation of the theranostic use of miRNAs in correlation to the radiopharmaceutical $^{64}CuCl_2$ in glioblastoma

Presentata da: Serena Valentini

Coordinatore Dottorato

Prof.ssa Maria Laura Bolognesi

Supervisore

Prof.ssa Patrizia Hrelia

Supervisore

Dott.ssa Beatrice Giacobbi

Esame finale anno 2021

Table of Contents

Abstract

Background: Glioblastoma multiforme(GBM) is one of the most prevalent and aggressive malignant primary brain tumors in adult patients. $^{64}CuCl_2$ is an innovative radiopharmaceutical investigated as theranostic agent in GBM patients. The therapeutic scheme is still under evaluation, therefore the research focused on the possibility of radioresistance development. The actors responsible for modulating radioresistance could be miRNAs, thus their potential use was investigated both in radioresistant cell lines and in GBM patients plasma samples.
Methods: Radioresistant cell lines were generated by exposing U87MG, U373MG lines to increasing doses of radiation for 32 weeks. Cell membrane permeability alterations and DNA damage were assessed to characterize the lines. Moreover, ^{64}Cu cell incorporation and subcellular distribution were investigated measuring gamma-radiation emission. miRNA expression was evaluated: in parental and radioresistant cell lines, both in cell pellet and media exosomes; in plasma samples of GBM patients using TaqMan Array MicroRNA Cards.
Results: Radioresistant lines exhibited reduction in membrane permeability and in DNA DSBs indicating the capability to skip the drug killing effect. Cell uptake assays showed internalization of ^{64}Cu both in the sensitive and radioresistant lines. Radioresistant lines showed a different miRNA expression profile compared to the parental lines. 5 miRNAs were selected as possible biomarkers of response to treatment (miR-339-3p, miR-133b, miR-103a-3p, miR-32-5p, miR-335-5p) and 6 miRNAs as possible predictive biomarkers of response to treatment (let-7e-5p, miR-15a-5p, miR-29c-3p, miR-495, miR-146b-5p, miR-199a-5p). miR-32-5p was selected as possible molecule to be used to restore $^{64}CuCl_2$ responsiveness in the radioresistant cell lines.
Conclusion: This is the first study describing the development and characterization of $^{64}CuCl_2$ radioresistant cell lines useful to implement the approach for dosimetric analysis to avoid radioresistance uprising. miRNAs could bring to a better understanding of $^{64}CuCl_2$ treatment, becoming a useful tool both in detection of treatment response and both as molecule that could restore responsiveness to $^{64}CuCl_2$ treatment.

1. Background information

1.1 Glioblastoma Multiforme

Glioblastoma multiforme (GBM) is one of the most prevalent and aggressive malignant primary brain tumours in adult patients, usually with poor prognosis, low survival rates and limited therapeutic opportunities (Louis et al., 2007, Taylor et al., 2019). Glioblastomas represent the most frequent malignant tumour of the CNS in adults, with an annual incidence of around 1/33,330, prevalence is estimated at 1/100,000 people (orpha.net).

Epidemiological studies estimate that more than 250,000 new cases of central nervous system (CNS) tumours worldwide are expected every year with variable incidence rates (http://www.cancer.gov/types/brain/hp/adult-brain-treatment-pdq). Although glioblastoma is considered a rare tumour (Orphanet 360), malignant gliomas are the third leading cause of cancer among people between 15- 34 years old accounting for 2.5% of the global cancer death toll, making it as one of the deadliest human tumours. Among gliomas, glioblastoma multiforme represents the 50%, with a maximum incidence in patients aged more than 65 years (Taylor et al., 2019).

GBM manifests itself as headache of increasing intensity, nausea, vomiting, and seizures. These disorders are caused by the tumor mass which, expanding inside the skull, causes an increase in pressure and dilation of the cerebral blood vessels. The disorders can also be neurological and non-specific, such as personality disorders or state of consciousness, moreover memory, language alterations. Moreover, motor deficit or hemiparesis can develop in GBM patients (Gately et al.,2017; AIOM 2019). Despite current multimodality treatment efforts during the past two decades, including new neurosurgical techniques, radiation therapy and novel chemotherapeutics, patient survival time from initial diagnosis has not significantly increased and the vast majority of patients succumb to the disease within 2 years (Stupp et al., 2005; Carmeliet et al., 2000; Hanahan et al., 2000; Nasulewicza et al., 2004). Current standard of care for GBM patients consists of surgical resection followed by radiotherapy plus concomitant and maintenance chemotherapy with temozolomide according to the Stupp protocol (Stupp et al., 2005). Median PFS and OS are only 6.9 and 14.6 months, respectively. The literature defines the relapse as inevitable, with a mean time to progression of about 6,9 months. At the time of relapse, treatment options were very poor and

the result in term of disease control is unsatisfactory. Due to the absence of successful surgical and medical treatments currently available for GBM, it is a crucial health public issue for which an early diagnosis and an accurate tumor classification is of key importance to select a personalized treatment.

1.1.1 Classification

The international standard for gliomas nomenclature and diagnosis is WHO (World Health Organization) classification: gliomas are classified into grade I to IV on the basis of the level of malignancy that is determined by the histopathological criteria. In particular, grade I are gliomas with low proliferative potential lesions and for which surgical procedures can be effective, whereas grade II to IV gliomas are highly malignant and invasive. Glioblastoma multiforme arises from the neuroepithelial tissue group of the brain, astrocytoma, and is characterized by common uncontrolled proliferation, diffuse tissue penetration, neurodegeneration and for these reasons it is considered the most aggressive, invasive and undifferentiated brain tumor classified as Grade IV astrocytoma (Louis et al., 2007). Glioblastomas are classified into three subtypes, depending on the status of the isocitrate dehydrogenase (IDH) gene mutation: Primary glioblastomas (IDH-wild-type), secondary glioblastomas (IDH-mutant), and unclassified glioblastomas (NOS). It is important to note that unclassified glioblastomas (NOS) do not belong to a specific glioblastoma category, given their diagnostic and genetic heterogeneity; for that reason, they cannot be classified within any other group (Lukas et al., 2019).

The primary subtype arises de novo without clinical and histological evidence of precursor lesion, accounting 90%~95% of GBMs. They are more common among elders, especially after the age of 50 years. Secondary GBMs develop from progression of pre-existing lower-grade astrocytic tumours and anaplastic astrocytomas over the course of 4-5 years. They account for 5% to 10% of GBMs and are more common among young people (Hanif et al., 2017). Primary and secondary GBMs show similar histological characteristics but they differ in genetic and epigenetic profiles and are thought to develop from different cells of origin. They have a significantly different clinical outcome; in fact, primary GBM arise rapidly from non-neoplastic brain and progress quickly, whereas tumors with mutated IDH1 and IDH2 have improved prognosis (Ohgaki et al., 2012).

Moreover, from a molecular point of view four GBM subtypes can be identified: proneural, neural, classical, and mesenchymal, that were identified on the basis of the gene expression profiles and are essential to develop specific clinical strategies (Sasmita et al., 2017).

1.1.2 Pathogenesis of GBM

1.1.2.1 Cancer Stem Cell theory

The traditional view held that GBM took origin from the malignant transformation of differentiated glial components of the CNS as astrocytes and oligodendrocytes (Chesler et al., 2013). The discovery of multipotent stem cell and lineage-restricted progenitor cell populations in the CNS of the postnatal mammalian brain, and subsequent identification of stem-like cells in several primary brain tumors including glioblastoma has led to the challenge of this hypothesis and to the development of the Cancer Stem Cell (CSC) theory. This theory postulates that rather than the de-differentiation of mature cell populations being the mechanism behind glioma genesis, gliomas are instead derived from the malignant transformation of cells derived from this newly defined neural stem cell (NSCs) or lineage-restricted progenitor population NCS-derived astrocytes and oligodendrocyte precursor cells (OPCs)(Figure 1). Neural stem cells (NSC) give rise to neural and glial progenitors that then differentiate into the major cell types of the CNS neurons, oligodendrocytes and astrocytes. BTIC (or Glioma Initiating cells) have been theorized to come from terminally differentiated cells (Figure 1-[1]) which acquire genetic mutations which endow them with a proliferative advantage a slow accumulation of critical mutations results in its transformation. Normal NSCs give rise to progenitors with limited proliferative and self-replicative capacity. BTIC have been theorized to form as a result of NSC (Figure 1-[2]) or neural progenitor transformation GBM can also arise through differentiation of mature glial or neuronal lineages (Figure 1-[1]) (Agnihotri et al., 2013; Hung et al., 2019).

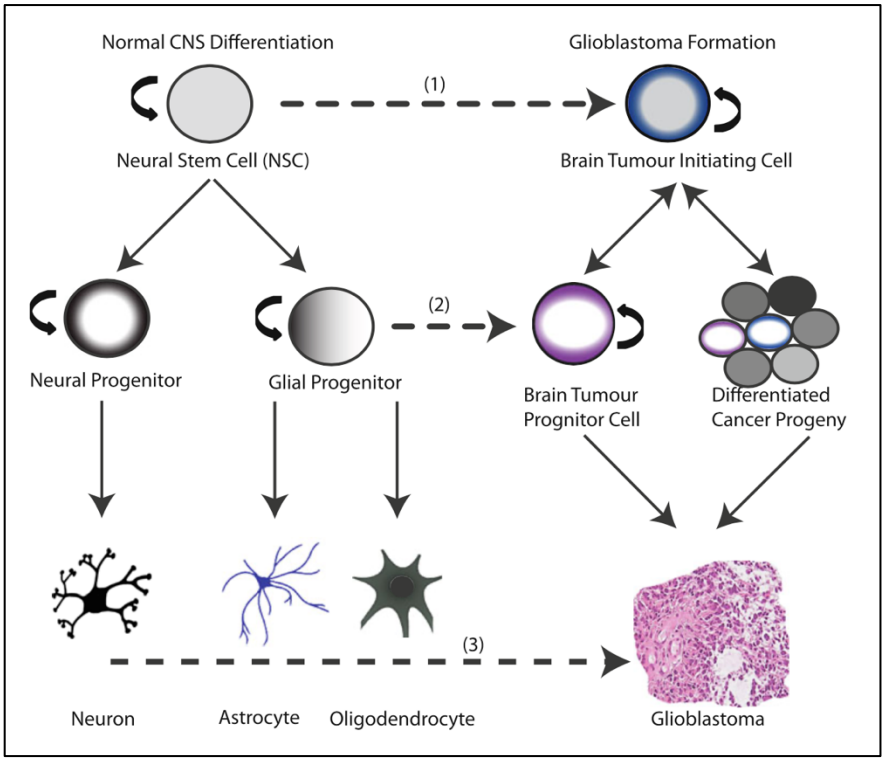

Figure 1.Putative cells of origin in GBM. Normal CNS differentiations and CNS tumor formation. Curved arrows represents ability to self-renew (Agnihotri et al., 2013).

Moreover, accumulating evidence suggests that these glioblastoma-derived stem-like cells are responsible for the invasiveness and resistance to treatment that characterizes glioblastoma (Chesler et al., 2013) or could have a role in influencing patients' survival (Pallini et al., 2010).

The cellular origin is a major determinant of the molecular subtype and may contribute to tumor development. Consistent with this concept, it was found that tumors derived from different cellular origins exhibited different behaviours in GBM mouse models. This observation suggests that the cellular origin could significantly contribute to GBM development and indicates the importance of deepening this aspect on the light of new drug discoveries (Yao et al., 2018).

1.1.2.2 Localization

The most frequent location for GBM is cerebral hemispheres; with 95% of these tumors arise in supratentorial region; while in only a small percentage occurs in cerebellum, brainstem and spinal cord (Hanif et al., 2017). In the study of Tyler et al. the authors studied the predilection occurrence of GBM with a density map

(Figure 2) showing that, in a total of 217 patients, GBM exhibit a strong predilection occurrence in proximity to the sub-ventricular zone (SVZ). This area which lies adjacent to the lateral wall of the lateral ventricle, is a site where neural stem cells (NSC) and astrocyte precursors are located in the adult brain (Steed et al., 2016).

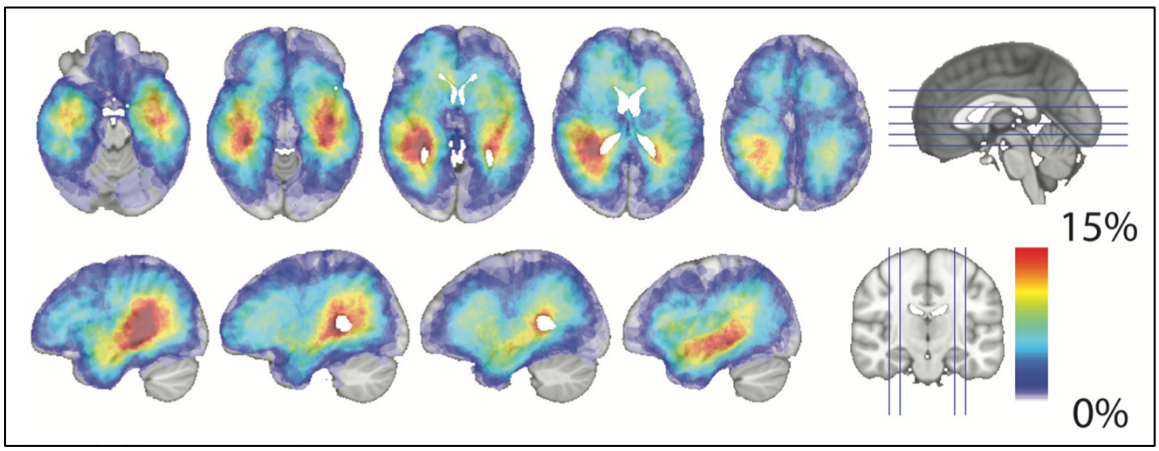

Figure 2. Glioblastoma density map. Red indicates the highest frequency of overlap and light blue indicating the lowest frequency of overlap (Steed et al., 2016)

During neural development, NSCs migrate radially and differentiate into various progenitor cells during this process. NSCs and progenitor cells are, thus, located at varying distance from the SVZ. The available data suggest that mutations occurring in these cell populations may give rise to glioblastomas. If the cell of origin contributes toward subtype-specific pathogenesis, then one would expect clustering of select subtypes with respect to distance from the SVZ. The quantitative tumor density map of glioblastoma subtypes demonstrates that these subtypes occupy distinct regions of the brain. Intriguingly, the subtypes exhibit regional associations with regard to the SVZ, an area of critical importance in neurogenesis and glioblastoma pathogenesis. The perineural and neural glioblastomas exhibit anatomic tropism reminiscent of NSCs (in proximity to the SVZ) and show gene expression patterns resembling these cells. In contrast, the classical and mesenchymal glioblastomas exhibit a more diffuse distribution and are found farther from the SVZ - a distribution that is similar to those of neural progenitor cells. These findings provide clinical evidence that subtype biology may be related to differing cells of origin. Glioblastoma subtypes occupy different regions of the brain and vary in proximity to the SVZ. These findings harbor

implications pertaining to the pathogenesis of glioblastoma subtypes., providing clinical evidence that subtype biology may be related to different cell of origin (Teed at al., 2016). Glioblastoma development occurs in the trans-barrier space of the blood-brain barrier (BBB), which prevents the translocation of polarized and/or high-molecular-weight substances from the bloodstream towards the brain. The development of the tumor influence BBB functionality, that is often observed in gliomas affecting peripheral blood detectable levels of tumor biomarkers. The rapid growth of glioblastoma cells creates areas of local hypoxia, which triggers the process of angiogenesis moreover, changes in the expression of aquaporin proteins in the components of the BBB have been linked with the tumor progression of the glioblastoma. However, glioblastoma, show intact BBB areas, especially at the periphery of the tumor, representing one of the main obstacles against their response to drug treatments (Slanted et al., 2019). This could be one of the reasons of the very low incidence of extracranial GB metastasis that is equal to 0.5%, despite the local aggressiveness of this tumor (Lah et al., 2020).

1.1.2.3 Macroscopic and Histological Features

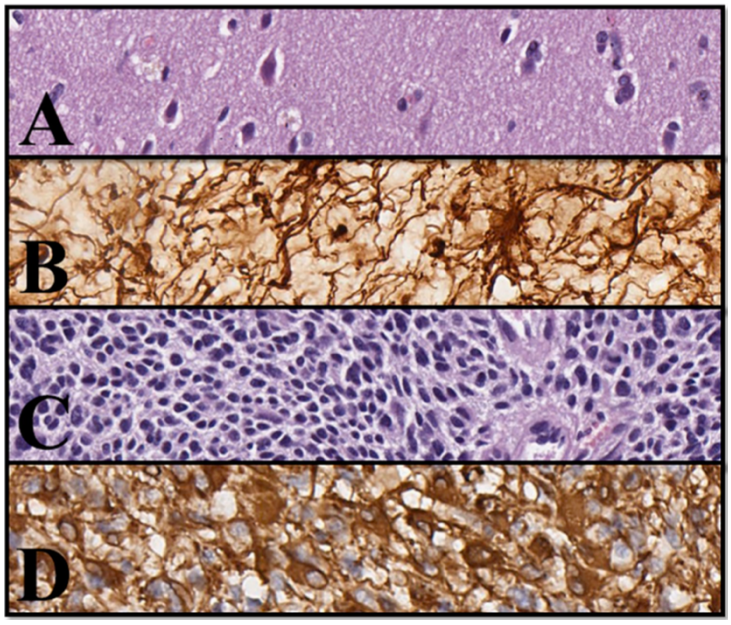

Figure 3. Cellular contrast between healthy brain tissue and GBM. A) Healthy brain tissue, H&E; B) Healthy astrocytes, ICH stain with GFAP; C)Hypercellularity and cellular atypism of GBM, H&E D) Neoplastic astrocytes of GBM, ICH stain with GFAP (Stoyanov et al., 2018)

Glioblastoma is histologically defined by neoplastic cells with astrocytic characteristics and the presence of either endothelial proliferation, often in a glomeruli morphology, microvascular proliferation, and/or necrosis, which may resemble a pseudo palisading pattern (a false fence of neoplastic cells, surrounding an area of necrotic tissue) (Lukas et al., 2019). A characteristic of GBM is the variation in gross appearance of the tumor from one region

to the other. Some of the regions appear as soft and yellow in colour due to necrotic tissue, but other tumor regions result firm and white, and some regions show marked cystic degeneration and hemorrhage. The tumor usually is represented by a a single, irregular shaped lesion which usually arises in the white matter (Hanif et al., 2017). Some of the change in cellular biology in GBM can be observed via light microscope as they form the cellular and tissue hallmarks of the condition. Changes in genetic information, resulting in alteration, suppression and expression of genes compared to their physiological levels in healthy astrocytes lead to not only cellular, but also extracellular matrix reorganization (Figure 4). These features are used as the diagnostic medium, by which GBM is verified pathologically (Stoyanov et al., 2018). The tumor mass is characterized by highly proliferating tumor cells, necrosis, and neoangiogenesis. Large areas of necrosis are surrounded by tumor cells arranged in a pseudopalisading pattern. Tumor microenvironment includes ECs and pericytes, reactive astrocytes, GBM-associated stromal cells, extracellular matrix, immune infiltrate of T lymphocytes and Treg cells, myeloid-derived suppressor cells (MDSCs), NK cells, activated resident microglia, cells (MDSCs), peripheral monocyte-derived macrophages, and GBM cancer stem cells (GCSCs).The peritumoral tissue may present tumoral cells and it harbors ECs and pericytes, GBM-associated stromal cells, extracellular matrix, reactive astrocytes, oligodendrocytes, inflammatory cells, and peritumoral tissue cancer stem cells (PCSCs). In addition, persistent neurons are found in the white matter (D'Alessio et al., 2019).

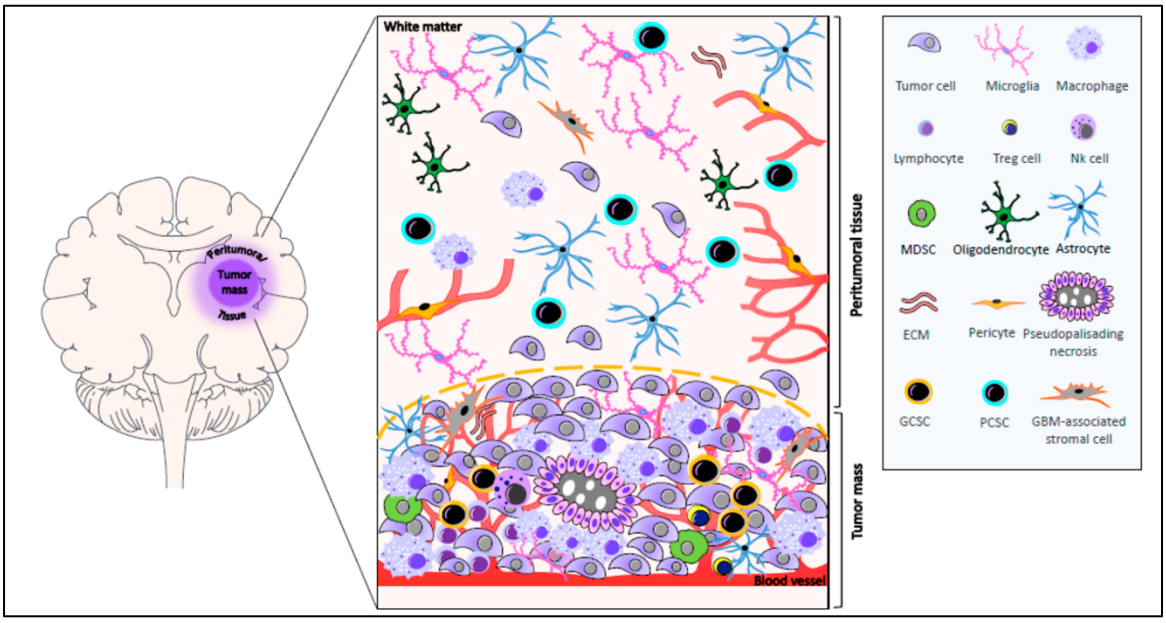

Figure 4. Tumoral and peritumoral GBM tissue pattern

The area surrounding the tumor represents the invasion front of GBM into the neighboring tissue and, for this reason, it is assuming a growing interest in translational research. While, in the past years, few data were present in the literature regarding the biomolecular characterization of peritumoral tissue, recently, several studies focused on this topic with the aim of optimizing surgical resection, better defining its role in GBM progression, and finding new therapeutic targets.

1.1.2.4 Genetic and molecular alterations

Classification only based on histopathology could not describe all the malignant features of GBMs, especially their responses to treatment. Due to these pitfalls of traditional classifications, molecular parameters have been added for GBMs classification. Molecular markers that carry both diagnostic and prognostic information add useful tools to traditional classification by redefining tumour subtypes within each WHO category. Nowadays, molecular markers have become an integral part of tumour assessment in modern neurooncology, helping for clinical decisions in GBMs (Soomro et al., 2017). At the molecular level in primary GBMs, loss of heterozygosity (LOH) at 10q is the most frequent genetic alteration observed in 69% patients, followed by EGFR amplification (34%), tumour protein 53 (TP53) mutations (31%), p16INK4a deletion (31%), and phosphatase and

tensin homolog (PTEN) mutation (24%). In secondary GBMs, LOH 10q and TP53 mutations are the most frequent as they are present in 63% and 65% patients, respectively, while other genetic alterations are infrequent (4%-19%). LOH 10q alteration has been observed in both primary and secondary GBMs while TP53 mutation mostly in secondary GBMs (Table 1). EGFR amplification, IDH ½ mutation, TP53 mutation and PTEN mutation rates are distinctive signatures between primary and secondary GBMs (Soomro et al., 2017; Pirtoli et al., 2016).

Table 1. Common mutations in GBM

Genetic alteration	Primary GBM	Secondary GBM
LOH 10q Mutation[1]	70%	63%
EGFR Amplification[2]	35%	8%
TP53 Mutation[3]	30%	65%
PTEN Mutation[4]	25%	4%
IDH Mutation[5]	5%	80%
MGMT promoter methylation[6]	42%	79%
[1]LOH: Loss of heterozygosity, [2]EGFR: epidermal growth factor, [3]TP53:tumor protein p53, [4]PHT: Phosphatase and tensin homolog, [5]IDH: Isocitrate dehydrogenase, [6]MGMT: O6-methyl guanine-DNA (deoxyribonucleic acid) methyltransferase		

Recent data from The Cancer Genome Atlas (TCGA) let to classify GBM on gene expression-based molecular classification (Figure 5) into classical, mesenchymal, proneural and neural subtype (Hanif et al., 2017; Sasmita et al., 2017). Proneural GBMs have lower incidence rate and characteristics of oligodendroglial cells, express genes which correlate with neuron development. They arise mainly in younger patients with secondary glioblastoma and have a good prognosis. Neural GBMs arise from astrocyte and oligodendrocyte lineage cells and manifest the expression of neuron-related genes. Their main characteristics are high level of epidermal growth factor receptors (EGFRs) and expression mode most similar to normal brain tissues. Classical GBMs express the markers of neuron precursor cells and stem cells. They show the characteristics of astrocytes while mesenchymal GBMs share the characteristics of cultured astrocytic gliomas (Soomro et al., 2017, Silantyev et al., 2019).

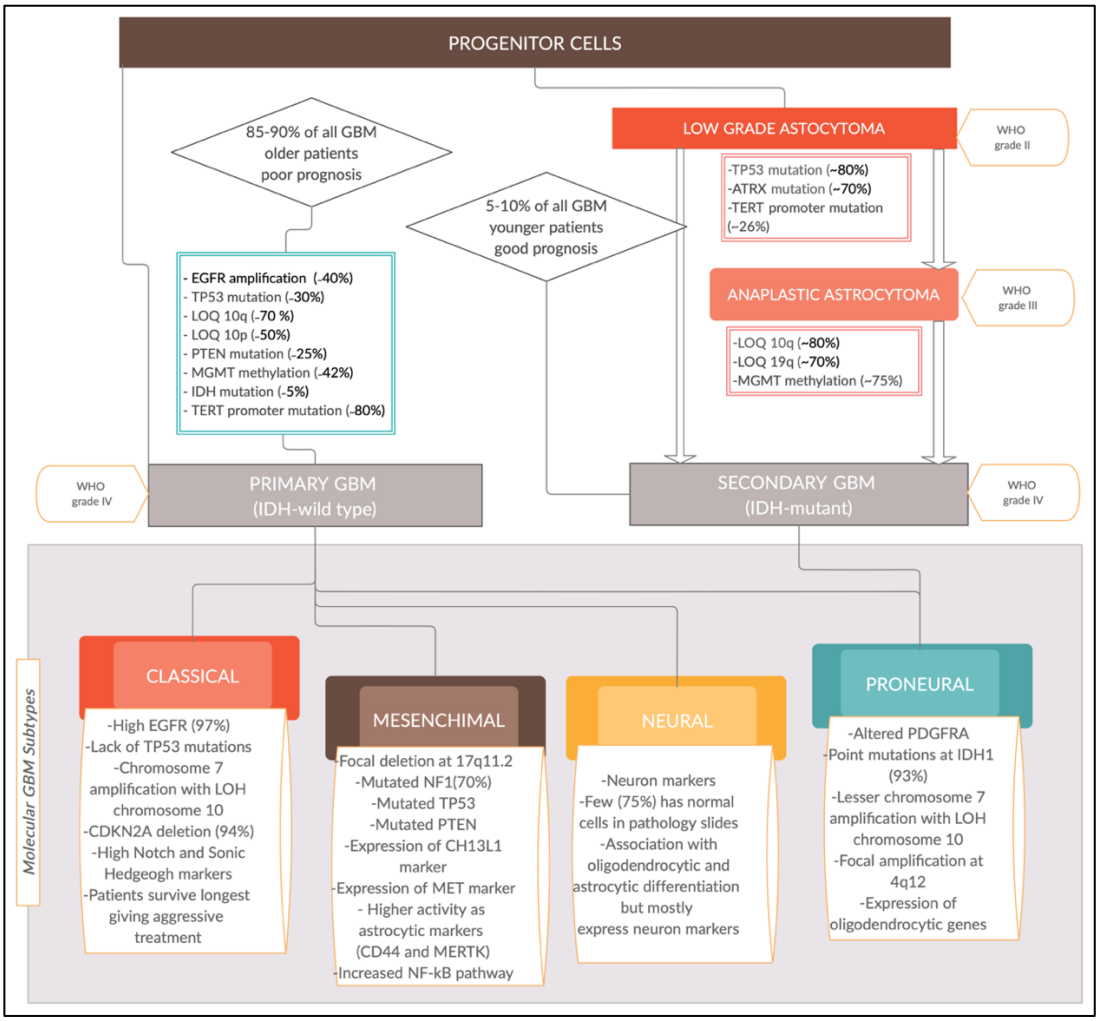

Figure 5.Molecular GBM Subtype

1.1.3 Diagnosis

In order to diagnose GBM, patients are usually subjected to a preliminary neurological exam to identify which area of the brain may be affected by the tumor. This is commonly followed by imaging tests, such as computed tomography (CT) and magnetic resonance imaging (MRI), to determine the location and the size of the tumor. Finally, the histopathological analysis performed on a tissue sample will ascertain the type of tumor and its aggressiveness. The extreme heterogeneity of these tumors makes cancer therapies increasingly challenging. Together with inter-tumor heterogeneity, intra-tumor heterogeneity represents a crucial field of investigation of GBM since it requires the study and the comprehension of an assortment of biomolecular features such as genetic and

epigenetic abnormalities, the identification of precise molecular markers, and the rate of cell growth and death of tumor cells (D'Alessio et al., 2019).

1.1.3.1 Molecular Biomarkers of GBM

A number of clinically significant glioma genetic biomarkers are currently analyzed as routine practice. Among these biomarkers, the most representative are: IDH1/2 mutation status, MGMT promoter methylation, EGFR, PDGFR and IDH, tumor protein p53 (Table 2). In addition to these also Circulating tumor cells (CTCs) and miRNAs could harbor prognostic values which could be useful for patients monitoring. The methods for the analysis of these genetic biomarkers and the identification of nucleic acid mutations include: Direct sequencing, high-resolution melting (HRM), immunohistochemistry, droplet digital PCR (ddPCR), and several others (Silantyev et al., 2019, Sasmita et al., 2017). The use of these advanced techniques permits to classify histologically indistinguishable GBM by the presence/absence of genetic mutations, which has an important therapeutic, prognostic, and experimental value.

Table 2. GBM biomarkers (Sasmita et al., 2017)

Biomarker	Source and Analysis	Significance	Regulation	Functional relevance
MGMT	Source: Biopsy Analysis: PCR with pyrosequencing and SYBR Green Technology	Prognostic and predictive biomarker	Upregulated (+)	Methylated MGMT promoter confers better prognosis upon chemoradiotherapy with TMZ adjuvant
EGFR	Source: GBM cancer tissue Analysis: PCR or transfected cell line study	Prognostic biomarker	Upregulated (+)	EGFR mutation and amplification remodel landscape of GBM tumor cells via RTK/RAS/PI3K, FOXG1 or SOX9 pathways
PDGFR	Source: GBM cancer tissue biopsy Analysis: PCR or mRNA in situ hybridization techniques	Prognostic biomarker	Upregulated (+)	PDGFRA mutation and amplification serve as potential drug target and localize within tumor cells only
IDH	Source: GBM cancer tissue biopsy Analysis: PCR, immunohistochemistry or spectroscopy	Prognostic biomarker	Upregulated (+)	Mutation catalyzes the production of 2-HG, leading to DNA hypermethylation and eventually gliomagenesis
LOH 10q	Source: GBM cancer tissue biopsy Analysis: Utilize microsatellites and PCR amplification	Prognostic biomarker	Upregulated (+)	Deletion of PTEN, TP53 and NF1 which are tumor suppressors genes
TP53	Source: GBM cancer tissue biopsy Analysis: qRT-PCR	Prognostic biomarker	Upregulated (+)	Regulates MVA pathway to promote tumorigenesis,

				negatively regulated by MDM2
CTC	Source: Body fluids Analysis: Telomerase assay and immunostaining	Prognostic biomarker	Upregulated (+)	Distinguishes molecular subtypes and also radionecrosis from tumor progression

1.1.3.2 Imaging techniques

MRI is the gold standard in the initial evaluation and diagnosis of patients with suspected GBM. The typical appearance of GBM on MRI is an irregularly shaped heterogeneous mass with a hypotense core representing necrosis and a ring of enhancement, as well as surrounding vasogenic edema causing mass effect. However, in pathological specimens, glioma cells go far beyond the abnormality shown in these imaging techniques (Zygogianni et al., 2018).

A minimum of T2 weighted FLAIR and pre- and post-gadolinium contrast enhanced T1 weighted imaging is recommended (Figure 6). CT provides baseline information regarding location and may provide additional information such as the presence of calcification or hemorrhage. Recent studies have shown that the addition of diffusion and perfusion weighted MRI can help to distinguish GBM from other tumor types. (Lundy et al., 2020). Not only diagnosis, but also treatment planning and treatment response of glioblastomas are mostly based on conventional magnetic resonance imaging (MRI) characteristics, including T1- weighted gadolinium-enhanced (T1-Gad), T2-wheighted and fluid-attenuated inversion recovery (FLAIR) sequences (John et al., 2019). Glioblastomas are highly infiltrative with tumor cells extending well beyond the contrast-enhancing tumor mass. Glioma-infiltrated no enhancing regions commonly show high signal intensity on Y2/FLAIR sequences but cannot be differentiated accurately from pure vasogenic edema that shows similar signal changes on MRI. Therefore, no enhancing

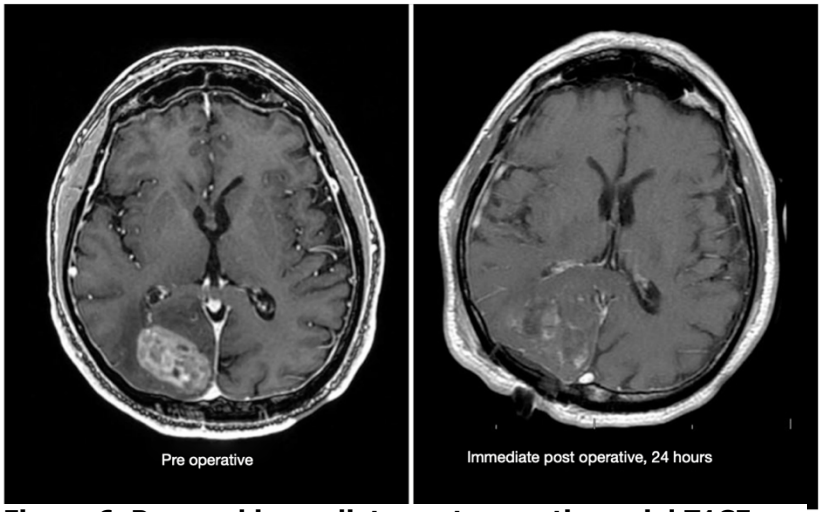

Figure 6. Pre- and immediate post-operative axial T1CE weighted MRI images of GBM (Skukla et al., 2017)

glioblastoma-infiltrated regions are difficult to detect, and they may be undertreated. On post-treatment MRI, progressive contrast enhancement can indicate glioblastoma progression or radiation injury, but these 2 pathologies (which can coexists) are difficult to differentiate by conventional MRI (John et al., 2019). Advanced imaging techniques as PET, can improve detection of high-grade gliomas and their differentiation from nontumorous lesions, edema, or therapy-related changes.

Nuclear Imaging

Molecular imaging by the use of positron emission tomography (PET) is increasingly being implemented into clinical practice for treatment planning and response monitoring of GBM. The most common is fluorodeoxyglucose 18F-FDG PET imaging that allows the functional imaging of glucose metabolism, but imaging of brain tumors present unique challenges because of the high background glucose metabolism of normal gray matter masking detection of malignant lesions. Thus, the use of 18F-FDG-PET in brain tumors albeit is limited (Alexiou et al., 2012). For GBM it is recommended the use of radio-labeled amino acid tracers such as [18F]fluoro-ethyl-L-tyrosine (18F-FET) and [11C]methionine(11C-MET), that are currently applied in clinical practice (Gotz et al., 2013). Other amino acid tracers currently under investigation include 18F- FDOPA (phenyl alanine) PET, a dopaminergic tracer, and alpha 11C-L-methyl-tryptophan PET, a tryptophan analog (Drake et al., 2020).

11C-MET it was considered a valuable tracer because methionine, an essential amino acid, could be used in protein synthesis, but due to its short half-life (20 minutes) and low sensitivity other PET tracers have been developed. 18F-FET shows rapid uptake, has a much longer half-life time (120 minutes) and is only taken up by cells through specific L- transporters—LAT2—that are highly and predominantly expressed on glioma tumor cells. This guarantees a high and selective uptake of the tracer in tumor tissue, with a low background signal in normal brain tissue or in surrounding inflammatory areas. Thus, 18F-FET-PET shows higher sensitivity and specificity for the detection of malignant gliomas (Verduin et al., 2018). 18F-FET PET currently has multiple potential clinical applications including the monitoring of treatment response and can distinguish tumor recurrence from radiation necrosis or pseudo progression. Literature data

have shown that 18F-FET-PET has a higher diagnostic accuracy than conventional MRI in differentiating glioma recurrence from posttreatment tissue changes. Correlation between different types of AA-PET standard uptake values (SUV) and molecular markers, in the context of radiogenomics, is currently under investigation (Dissaux et al., 2020). A recent study demonstrated the relationship between 11C-MET-PET and IDH1 mutation and found that SUVmax and SUVratio were inversely correlated with IDH1 mutation (Kudulaiti et al, 2019). To assess the potential of radiogenomics as a diagnostic and predictive tool, well-defined preclinical models with specific driver mutations are needed that can be used to validate the sensitivity and specificity of radiogenomics. The ability to identify prognostic or molecular response markers based on imaging features derived from routine diagnostic procedures (MRI, PET, and computed tomography (CT)) providing an attractive way of predicting treatment response in GBM.

1.1.4 Therapeutic Management

The treatment of brain tumors represents a unique challenge considering the presence of the BBB (blood brain barrier), a highly selective semipermeable barrier that separates blood from the brain. The BBB, composed by endothelial cells of capillaries, astrocytes surrounding the capillary, and pericytes embedded in the capillary basal lamina. There are different variables that can affect molecules crossing capabilities as lipophilicity, molecular weight and charge. The BBB is able to prevent the CNS access to large molecules ($>$ 400 Da) and 98% of small molecules drugs (Taylor et al., 2019). Therapeutic management of newly diagnosed glioblastoma typically involves first, surgical resection reducing the tumor load and establishing a histopathological and molecular diagnosis. Following surgery, adjuvant radiotherapy is given with concomitant and maintenance chemotherapy (Lukas et al., 2019).

Surgery

Resection confirms the diagnosis and improves overall survival and progression-free survival while providing seizure control. It is important to individualize the neurosurgical approach to biopsy or excise a brain tumor according to a patient's KPS index, co-morbidities, cooperation and neurocognitive status as well as the tumor' s location proximity to the surface and eloquent cortex (Zygogianni et al.,

2018). A classification of the amount of removal is usually adopted for prognostic evaluation into three categories, as follow: gross total resection (GTR: in respect of preoperative imaging and intraoperative findings), subtotal resection (STR: a gross complete removal of the tumor is not achieved), and biopsy-only (BO: any attempt to ablative or even cytoreductive surgery is judged impossible or not advisable) In newly diagnosed GBM patients surgery consists of maximal safe resection, respecting tumor shape, size, proximity to blood vessels or functionally determinant brain regions. The anatomical localization of the tumor in the brain may affect patient's survival, with the possibility to conditionate the surgical excision (Pirtoli et al., 2016). Surgery plays an important role in the management of glioblastoma, however, due to the invariably infiltrative nature of the disease, even macroscopically complete resection is not curative, due to the frequency of disease recurrence.

Radiation therapy

In 1978, the trial published its results providing solid evidence on the efficacy of radiation therapy (RT) over best supportive care or chemotherapy (carmustine), while the combination therapy had a non-significant benefit. Since then, RT has become part of the adjuvant treatment of GBM following surgery. The prescribed dose of 60 Gy was established by a retrospective study by Walker, which showed that the treatment efficacy strongly depends on an increase in dose (Verduin et al., 2019). Currently, the standard of care for patients up to age 70 is the Stupp regimen, which consists of adjuvant RT concomitant with temozolomide (TMZ) since it significantly improved median, 2- and 5-year survival. It is widely accepted that partial brain irradiation is superior to WBRT (whole-brain RT) as there is no difference in overall survival, while irradiation of healthy brain tissue and later radiation-induced toxicity is limited. External-beam radiation should begin within 8 weeks following surgical resection or biopsy. Conventional RT consists of a total dose of 60 Gy in 1.8–2.0 Gy per fraction is given to the visible tumor with a 2–3 cm margin with the purpose of including the microscopic invasive disease. Total treatments last approximately 6 weeks (Lukas et al., 2020). However, 90% of the tumors recur at the original site after RT, thus strategies to increase local radiation dose are the subject of clinical radiobiology research for improving patient's outcome (Pirtoli et al., 2016).

Systemic therapy

Actually, GBM treatment schedule consists of neurosurgery, concurrent chemoradiation therapy, and adjuvant temozolomide. This provides a median progression-free survival of almost 7 months. There is no standard treatment for the recurrent setting. Systemic treatment options include a temozolomide rechallenge, lomustine, and antiangiogenic therapy such as bevacizumab. However, effectiveness of these treatment options is limited (Verduin et al., 2019). Temozolomide is a DNA-alkylating chemotherapy agent that is designed to cross the blood-brain barrier reaching therapeutic concentrations. This drug adds a methyl group to the DNA residues at the O6, N3, N7 positions that, if not repaired, leads to DNA strand breaks and cytotoxicity. Oral administration of Temozolomide, used concomitantly to radiotherapy followed by 6 cycles of maintenance (150-200 mg/m2 x 5/28 days), is considered a world-wide standard of care (Lukas et al., 2020). However, despite this increase in survival with radiotherapy and temozolomide, tumor progression and recurrence typically occur due to the development of resistance to temozolomide and moreover, temozolomide has been associated with many side effects.

Other chemotherapeutic approaches for GBM treatment include anti-angiogenic agents as anti-VEGF monoclonal antibody (Bevacizumab), anti-FGF antibodies, monoclonal antibodies targeting EGFR (e.g., Erlotinib and Gefitinib) and tyrosine kinase inhibitors (Taylor et al., 2019). These target therapies, either alone or in combination with traditional RT and CHT are under evaluation, but unfortunately, clinical trials have not yet given significant results in term of patient survival improvement. The approval of "CAR-T (Chimeric Antigens Receptor Cells-T) therapy" via T cell engineering is an innovative approach against GBM. The development of CAR-T cells provided results which are consistent with its usefulness compared to antibody-based immunotherapy as the engineered T cells can penetrate solid GBM tumors and recruit supporting molecules into the cancer microenvironment for a better immune response. In spite of benefit one of the main concerns with the use of CAR-T cells are the cytokine storm. Recently, another innovative approach to fight GBM is Optune, FDA-approved device, which deliver electric fields to the tumor location to disrupt cancer cell division (https://www.accessdata.fda.gov). Therefore, the scarse treatment opportunities

for GBM patients, keep opened the challenge to find effective agents for the worldwide community.

Radioresistance

Even in consideration of technological progresses, as the upgrade in radiotherapy technology from 2-dimensional whole-brain radiotherapy to 3-dimensional conformal radiotherapy, and more recently to intensity-modulated radiation therapy (IMRT) and volumetric arc radiation therapy (VMAT), unfortunately GBM are notoriously resistant to radiotherapy and molecular details of radioresistance remain largely unknown. Anyways different mechanisms have been identified including tumor microenvironment, hypoxia, metabolic alteration, glioma stem cells, tumor heterogeneity, microRNAs, cell cycle, and DNA damage and repair, that contribute to the development of GBM radioresistance (Figure 7).

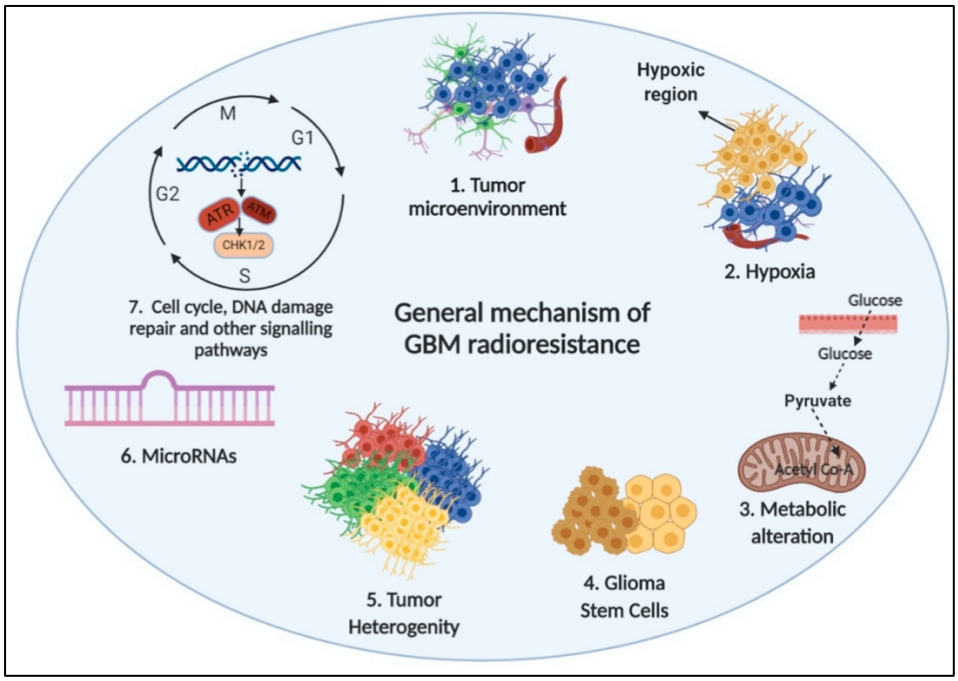

Figure 7. Identified mechanism of GBM radioresistance (Ali et al., 2020)

The most relevant process to cellular radiosensitivity are DNA damage pathways. Ionizing radiation can induce base damage, single-strand breaks, double-strand breaks (DSBs), sugar damage, and DNA-DNA and DNA-protein cross linking. DSBs are the most important damage as they are harder to repair than other DNA lesions. Mammalian cells have developed specialized pathways to sense, respond to and repair these different types of damage. The DNA damage response (DDR)

is a complex and coordinated system that allows cells to detect DNA lesions, signal their presence and promote their repair. DDR is not a single pathway but a group of highly interrelated signaling pathways, each of which controls different effects on the cell. One of the earliest events of the DDR is the phosphorylation of a protein called histone H2AX. This phosphorylated form known as γH2AX, is necessary for the recruitment of many other proteins involved in the DDR. One of the pathways reported to be intricately involved in this resistance is the Notch signaling pathway. Inhibition of Notch 1 and 2 restores radiosensitivity in glioma stem cells, and Notch has been reported to induce radioresistance in GBM through regulation of the PI3-kinase/Akt pathway (Ali et al., 2020). In GBM, the increase in expression and activity of AKT contributes to tumor progression, recurrence, and radioresistance. Radiation activates Akt in GBM and thereby contributes to the development of radioresistance, enhancing DNA damage repair (DDR) by promoting γ-H2AX foci resolution in irradiated glioma cells, whereas downregulation of AKT facilitates unrepairable DNA double strand breaks (DSB) in irradiated U251 glioma cells (Chautard et al., 2010). A critical role of promoting radioresistance could be the presence of Glioma Initiating Cells The fraction of glioma cells expressing CD133, a marker for both neural and GICs, increases after irradiation. CSCs have altered DNA damage response and repair pathways, and this causes resistance to exogenously induced DNA damage that leads to the failure of tumor therapy. It was also shown that GICs become radioresistant through the overexpression of proliferating cell nuclear antigen (PCNA)-associated factor (PAF). PAF is a DNA damage-regulated factor that controls the accessibility of DNA translation synthesis (TLS) enzymes to PCNA, thereby facilitating DNA damage bypass. After irradiation of GICs, PAF associates with PCNA to release TLS Pol η, resulting in restoration of error-free DNA synthesis and, in turn, glioma stem cell proliferation and radioresistance (Schulz et al., 2019). In the process of radioresistance also p53 have been found involved, different forms of p53 status in GBM lines have been correlated to radiation response (Kastan et al., 1991), and radiosensitivity (Williams et al., 2009), suggesting multiple mechanisms underlay intrinsic cellular radiosensitivity. Hypoxia is associated with tumor angiogenesis and invasiveness, therapeutic resistance, and poor prognosis. A few studies have shown close-knit association between hypoxia and radioresistance in glioma. Kessler et al. discovered that DNA-PKcs, acting on the NHEJ pathway of DDR,

regulates HIF- 1α expression and confers radioresistance to gliomas (Kessler et al., 2010). Hypoxia seems to increase cell proliferation, self-renewal, and promote stemness maintenance in GSCs with intrinsic radioresistance. In the hypoxic microenvironment, the expression of hypoxia inducible factors (HIF-1α and HIF-2α) is elevated, with HIF-1α expression detected both in GSCs and non-GSCs, and HIF-2α expression observed in GSCs exclusively. Although the detailed molecular interactions remain unclear, it is not hard to find the pivotal role of hypoxia inducible factors, HIF-1α and HIF-2α in glioma radioresistance (Han et al., 2017). In conclusion, the curative potential of radiotherapy depends on the scale and quality of DNA damage in the exposed tumor tissues. Ionizing radiation induces different types of DNA damage with DNA double-strand breaks (DSBs) as major lethal DNA lesions. If the levels of radiation-induced DSBs exceed the DNA repair capacity of tumor cells, this might result in cell cycle arrest, tumor cell senescence, and death. The cell fate decision following radiation exposure depends on the amount of critical DNA damage. If the level of DNA lesions is low, DNA repair mechanisms and DNA damage checkpoints are activated, the cell cycle progression arrest in the presence of DNA damage and allow cells to repair DNA before returning to the proliferative pool. But, if the amount of DNA damage is unrepairable, the cells activate death programs. The first of the "5R" of radiation biology is "Repair" and refers to DNA repair as one of the key determinants of tumor cell survival after radiation therapy (Schultz et al., 2019).

1.2 Copper Chloride

Copper(64Cu)Chloride ($^{64}CuCl_2$) is a revolutionary molecule in the field of Nuclear Medicine, that is a medicinal product involving the application of radioactive substances in the diagnosis or therapy. Actually, this active substance is marketed under the name of "Cuprymina", with the European Marketing Authorization number EU/1/12/784/001 of which ACOM- Advanced Center Oncology Macerata-SRL is the Marketing Authorization Holder. This radioisotope Copper-64 is produced by a cyclotron and it has a half-life of 12.7 hours that permits to distribute the molecule all over Europe. Cuprymina is a radiopharmaceutical precursor, so it can be used only linked to a carrier molecule, that is specific for each tumor type. However, the company is developing the product as "$^{64}CuCl_2$

solution for injection", a ready to use solution that can be injected to patients alone without the link to other carrier molecules. Actually, this solution is an Investigational Medicinal Product (IMP) under clinical development both as diagnostic and theranostic agent in glioblastoma (GBM).

1.2.1 Theranostic era in Nuclear Medicine

During the last few years, in the field of nuclear medicine unprecedented advances have been shown: one of the main driving forces is the so-called "theranostic" concept that combines the use of a diagnostic biomarker with a therapeutic option. Although the use of term "theranostic" is quite recent, the general concept of using a radioactive compound for diagnostic target-expression confirmation and subsequent radionuclide therapy has been established in nuclear medicine for more than 70 years, with the use of radioiodine for diagnosis and therapy of benign and malignant thyroid disease being arguably the most successful molecular radiotherapy in history. Recent developments have significantly broadened the scope of radionuclide imaging and therapies that now extends to neuroendocrine tumors, prostate cancer, or hematologic malignancies (Lapa et al., 2019). A definition of theranostic involves the administration of a diagnostic agent:

- to determine localization in the site or disease state under study as a surrogate for a potential therapeutic agent with similar chemical properties.
- to examine its biodistribution as predictive of off-target (adverse) effects of the potential therapeutic agent.
- as an aid in determining the optimal therapeutic dosage or activity to be administered, based on the anticipated tumoricidal doses measured in the tumour site (*i.e.,* dosimetry); and/or
- to monitor the response to this treatment.

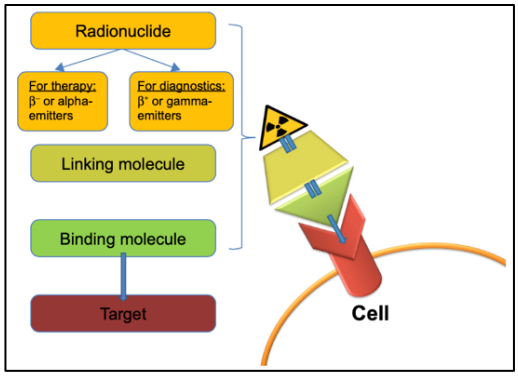

Figure 8. Theranostic mechanism in Nuclear Medicine

The crucial point for the application of a theranostic agent is the dose that, systemically administered, should reach the target in sufficient quantities. The dose should be optimized for an individual patient, molecular radiotherapy is often administered in an activity chosen to result in the highest acceptable whole-body dose or critical tissue radiation dose (Yordanova et al., 2017). Ideally, theranostics compounds implicate chemically and biologically identical compounds. Radioiodine and MIBG (iobenguane) meet this ideal but few others do. Actually, the market offers the so called "theranostic pairs" that is a combined use of a diagnostic agent and a therapeutic one (Table 3). Most of that are not chemically or biologically but they are similar enough in biodistribution that the diagnostic agent adequately predicts the biodistribution of the therapeutic analogue. The diagnostic radiometals ^{111}In and 68Ga and their therapeutic counterparts ^{90}Y and ^{177}Lu, are all trivalent metals which can be attached to a targeting moiety with the same chelator but there are differences in their chemical structure which can affect their biological properties. The market not always is able to completely follow scientific principles, in fact patent status of a molecule may limit its availability for clinical use or simply, product availability could be limited as in the case of ^{86}Y that has been used for diagnostic PET imaging prior to therapy with ^{90}Y labelled compound, but nowadays there is a very limited availability of ^{86}Y making its use not very widely applicable (Ballinger et al., 2018)

Table 3. Theranostics agents in current clinical use (Ballinger et al., 2018)

Clinical indication	Diagnostic agent	Therapeutic agent
Hyperthyroidism or thyroid cancer	^{123}I-iodide	^{131}I-iodide
Adrenergic tumours	^{123}I-iobenguane	^{131}I-iobenguane
Bone metastasis from prostate cancer	^{99m}Tc-MDP	^{223}Ra chloride
Non-Hodgkins lymphoma	^{111}In-ibritumomab	^{90}Y- ibritumomab
Neuroendocrine tumours	^{68}Ga-DOTATATE	^{68}Lu-DOTATATE
Prostate cancer	^{68}Ga-PSMA-11	^{177}Lu-PSMA-617

The combination of targeted cancer imaging and therapy is a considerable achievement for personalized medicine. Theranostic medicine could improve patient selection, reduce side effects, and enhance therapeutic efficacy. The detection of potential targets can help predict whether a patient will benefit from a particular treatment. Theranostics can be useful for estimating the potential

response and eventual toxicity and during the treatment, theranostics can be applied in monitoring the therapy course.

1.2.2 Copper in tumors

Copper is one of the most important trace metals in humans, being surpassed in abundance only by iron and zinc (Sun and Anderson, 2004). The body of a healthy human adult weighing 70 kg contains approximately 110 mg copper (Linder, 1991), and it is estimated that 0.6–1.6 mg copper are ingested every day with about 50% being absorbed (Linder et al., 1998). Studies with copper-64 and copper-67 have identified albumin (Mr = 66 kDa) and transcuprein (Mr = 270 kDa) (Weiss and Linder, 1985) as immediate chelators of copper after entry from intestinal cells into the interstitial fluid and blood plasma. There is a high-affinity site for Cu^{2+} at the amino terminus of most albumins, but the binding affinity of transcuprein is even higher. Copper is exchangeable between these two plasma proteins, and most of the copper bound by albumin and transcuprein is rapidly deposited in the liver, and to a lower extent, the kidney. In the liver, copper can be incorporated into the protein ceruloplasmin (CP) during its synthesis, and the holoprotein is subsequently secreted. CP cannot exchange its copper with other plasma components, and it is the main carrier that delivers copper to organs other than liver and kidney. Excess copper usually is not stored in mammals. The rate of excretion is the main process maintaining copper homeostasis (Linder and Hazegh-Azam, 1996).

Copper is the 29th element in the periodic table and belongs to the group 11 transition metals along with silver and gold. Two stable and nine radioactive isotopes are known, respectively. Although Cu(III) and Cu(IV) oxidation states have been reported, copper chemistry is largely dominated by Cu(I) and Cu(II) compounds. Copper(I) forms numerous complexes with both organic and inorganic ligands. Because of the "soft" character (Pearson definition) of this ion, Cu(I) strongly prefers ligands having soft donor atoms such as sulfur comprised, for example, in cysteine and methionine, aromatic nitrogen (e.g., sp2 hybridized nitrogen in pyridine and histidine systems) and phosphatase (e.g., in tertiary phosphine).

Switching from the unstable reduced Cu(I) state to stable oxidized Cu(II) one or vice versa both in conventional bench chemical reactions and in physiological

conditions, copper is involved in redox reactions and is crucial for the function of several enzymes and proteins. As a consequence, it takes part to several important mechanisms such as energy metabolism regulation, mitochondrial respiration, antioxidation and collagen cross-linking. Copper, essential trace element with many physiological functions, plays an important role in tumor angiogenesis and is able to stimulate endothelial cell proliferation (Hu, 1998). Copper metabolism, that is tightly regulated through sophisticated homeostatic mechanism in physiological conditions, is profoundly altered in neoplastic disease together with its cellular deposition—from cytoplasm in normal tissue to intranuclear and perinuclear zones in tumors (Fuchs and Lustig, 1989). Cellular ionic copper in excess damages different types of biomolecules through cytotoxicity and by mediating the generation of the highly reactive hydroxyl radical (Valko et al., 2005, Gaetke and Chow, 2003). In addition to the metabolic alteration of copper, high levels of this metal have been found both in serum and in tumor tissue in a large variety of neoplasms. In particular, several preclinical studies have shown an effect of copper on tumor development. A comparison between malignant and normal tissue show that copper has an almost 50% higher concentration in neoplastic tissue (Jørgensen et al.,2013; Ishida et al., 2013). Similarly, studies a highly significant increase in both serum copper level and ceruloplasmin level was observed in patients with various types of tumors (Fisher and Shifrine, 1978, Pizzolo et al., 1978, Scanni et al., 1979).

In particular, several authors (Canelas et al., 1968, Kaiser and Gullotta, 1980) reported an increased copper content in brain tumors and this increase in copper content was in correlation with malignity of tumors (Wollemann, 1974).

According to these premises, the presence of an elevated copper concentration in cancer cells may be potentially used to differentiate healthy from transformed cells, becoming the target for novel diagnostic and therapeutic agents (Daniel et al., 2004). In particular, the use of different ponderal and radioactive doses of ^{64}Cu in patients with glioblastoma multiforme should be promising in the diagnostic setting and especially for therapeutic purpose.

1.2.3 Copper-64 decay

Copper has the atomic number Z = 29, and isotopes with 23 to 51 neutrons (copper-52 to copper-80) occur naturally or have been generated and studied. All isotopes from copper-60 to copper-69 have a half-life of one minute or more, or are not radioactive (copper-63 and copper-65). Copper-60, copper-61, copper-62, copper-64, and copper-67 all possess half-lives, decay modes, and energy spectra that make them potentially suitable for molecular imaging and/or targeted radiotherapy (Sun and Anderson, 2004). The half-lives range from just under 10 minutes to 62 hours. Beta minus, positron and gamma emission occur and enable various copper isotopes to be used for targeted radiotherapy, and imaging by positron emission tomography as well as gamma scintigraphy. Copper-64 is the only copper isotope that possesses three decay modalities, and it has a half-life (12.7 h) allows for efficient clinical imaging at delayed scan times, exploiting better target-to-background signal; furthermore, it allows for the convenient distribution of the radiopharmaceuticals after its synthesis at centralized production sites, and for easier management of scheduled activities at the clinical nuclear medicine facilities. The detailed decay scheme of copper-64 is shown in Figure 9. It can undergo electron capture (EC) and β+ emission to nickel-64, and β– emission to zinc-64. Both daughter nuclides are stable.

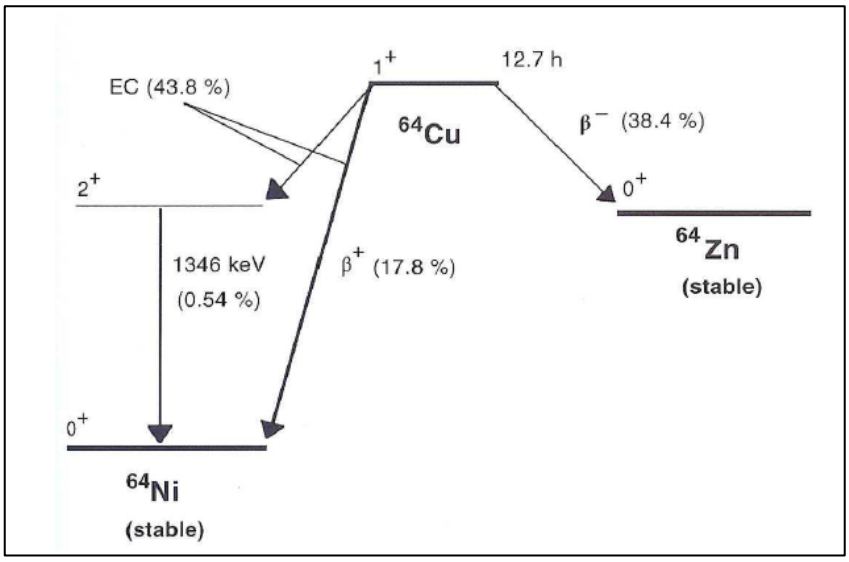

Figure 9. Decay scheme of copper-64

Then Figure 9 shows the maximum energies and intensities of all particles and electromagnetic rays emitted that have energies over 1 keV. Electron capture

(Intensity I = 43.8%) involves a p→n conversion, monoenergetic neutrino emissions, and branching to either the 1345.77 keV-level (I = 0.54%) or the ground state (I = 43.3%) of nickel-64. The excited level of nickel-64 decays via a 1346 keV γ-ray to the ground state. Electron capture is also accompanied by characteristic Auger and X-ray emissions, which result from filling the electron vacancy in the inner electron shell with higher-level electrons. Decay by positron emission (I = 17.8%) also produces the nickel-64 daughter and is accompanied by neutrino emission and γ annihilation radiation (I = 35.6%). Decay via β– emission (I = 38.4%) to the ground state of zinc-64 is accompanied by antineutrino emission. In addition to beta minus, ^{64}Cu decays also by Auger electron emission leading to tumor cell DNA damage that may enhance cancer therapy. Auger electrons from ^{64}Cu decay have an average of 2 keV of energy, 126 nm range in tissue (Howell, 1992) and are considered high-LET radiation.

1.2.4 Targeted radiotherapy with Auger effect

In 1925, the irradiation of a cloud chamber with low-energy, Xray photons, resulted in the production of multiple electron tracts and this lead to the discovery of the Auger effect: the ejection of inner-shell electrons from the irradiated atoms, the creation of primary electron vacancies within these atoms, a complex series of vacancy cascades composed by both radiative and nonradiative transitions, and the ejection of very low-energy electrons from these atoms (Auger, P., 1925, Sur les rayons b secondaires produits dans un gaz par des rayons X. Comptes Rendues Hebdomadaires des Seances de l'Academie des Sciences, 180, 65–68).

Low-energy electrons are also ejected by many radionuclides that decay by electron capture (EC) and/or internal conversion (IC). Both of these processes introduce primary vacancies in the inner electronic shells of the daughter atoms which are rapidly filled up by a cascade of electron transitions that move the vacancy towards the outermost shell (Howell et al., 1992).

Typically, an atom undergoing EC and/or IC emits several electrons with energies ranging from a few eV to approximately 100 keV. Consequently, the range of Auger electrons in water is from a fraction of nanometer to several hundreds of micrometers. The majority of these electrons travel short distances up to ~ 500 nm from the decay site and deposit all their energy in a small spherical volume of

few cubic nanometers. From a radiobiological point of view, it is important to notice that the organization of genomic double-stranded DNA and proteomic sequences are all within the range of these high-LET (≤8–26 keV/mm), low-energy (≤1.6 keV), short range (≤130 nm) electrons (Kassis et al, 2004) (Table 4).

Table 4. Electron energies needed to traverse various conformational states of DNA in mammalian cells and their respective LET (Kassis, 2004)

Conformational DNA states	Diameter (nm)	e^- energy (eV)	LET*
Double-stranded DNA	2	45	18
Two loops of double-stranded DNA on nucleosome	6	140	25
Nucleosome	11	245	21
Chromatin fiber	30	550	15
Chromonema fiber	60-130	92-1550	11-8

In fact, the crucial link of the Auger effect to biology come with the ability to incorporate radioactive elements into the nuclear DNA: when an atom is taken into a cell and decays within the range of tumor cell DNA, the emitted Auger electrons can impart very high cytotoxicity to mammalian cells creating DNA damage. Considering the fraction of atoms decaying within the mammalian cell nucleus and/or the proximity of the decaying atoms to nuclear DNA, the sharp increase in the LET of low-energy electrons occurs only when the radionuclide is within or in close proximity (< 1μm). There are several indications that high-LET radiation can efficiently kill radio resistant cells, including cancer stem cells, so this has focused the interest in exploring cancer therapeutic potential of Auger electrons (Cui et al., 2011).

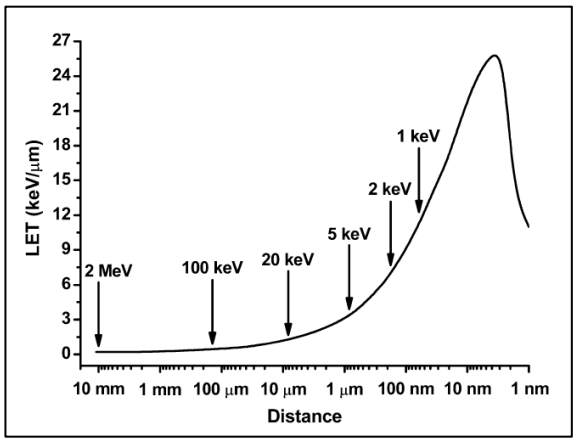

Figure 10. LET of electrons as function of distance. Electron energy values along the track are shown. Electron energies needed to traverse various conformational states of DNA in mammalian cells and their respective LET (Kassis, 2004)

Among all the radionuclides, the Auger electron emitter investigated most extensively is iodine-125 since Carlson et al (1963) that demonstrated this kind of radioactive decay for iodine-125. There is a very steep distance-dependence between the distance of the decaying Auger nuclide from DNA and the efficiency of double-strand break induction. Several in vitro/in vivo studies with compounds labelled with the Auger-electron emitting radionuclide Iodine-125, e.g., intercalators (Kassis et al. 1989) and groove binders (Kassis et al. 1999) have demonstrated that a decaying iodine atom does not need to be covalently incorporated into the DNA of the target cell to produce Auger-electron induced-double-strand break or effective cell kill, if it is placed in sufficient proximity to the DNA. Kiess et al (2015) have considered Iodine-125, with the short range of emission (<10 μm), suitable for treating micro metastases while sparing normal tissues. They used highly specific small molecule targeting the prostate-specific membrane antigen (PSMA) to deliver 125I to prostate cancer cells. PSMA-targeted radiopharmaceutical therapy with the Auger emitter 125I-DCIBzL yielded highly specific antitumor efficacy in nude mice, suggesting promise for treatment of prostate cancer micro metastases.

Another radionuclide that has an important potential application in radionuclide therapy is Copper-64 and it is more and more evaluated as a possibility to treat cancer. ^{64}Cu is an attractive radionuclide for positron-emission tomography because it emits moderate energy positrons (Emax 0.653 MeV) that provide good spatial resolution (0.7 mm). The half-life of ^{64}Cu (12.7 h) is also compatible with the pharmacokinetics of peptides or antibody fragments that recognize tumour-associated receptors overexpressed on cancer cells tumour-associated receptors overexpressed on cancer cells. In addition to its positron emission, ^{64}Cu emits β-particles (0.573 meV), Auger and internal conversion (IC) electrons, and γ particles. Auger electrons that are emitted during the electron capture (40%) decay of ^{64}Cu have low energy (2 keV) and a subcellular range <1 μm (Howell, 1992) and are considered high-LET radiation. The Auger electrons of ^{64}Cu have been studied in several works for radiation treatment of tumours. The cytotoxicity of ^{64}Cu in tumour cells from DNA damage was explained by Obata et al. (2005), inhibition of cell proliferation and induction of apoptosis was observed at 24h and 36h after treatment; but only McMillan et al (2015), studying DNA double strand breaks and chromosomal aberration after ^{64}Cu-ATSM treatment, demonstrated

the direct evidence that high-LET Auger electrons are the primary cause of cells death, and not positrons or other low-LET radiations.
In conclusion, Auger electron emitters radiopharmaceuticals will play a major role as radiotherapeutic agents for cancer treatment in the future.

1.2.5 Copper Chloride theranostic mechanism

The isotope Copper-64 is an authentic tracer for the in vivo characterization of copper metabolism in the tumor tissue. The potential promising diagnostic use of $^{64}CuCl_2$ PET/CT has been demonstrated in preclinical studies in different tumor types such as breast, prostate or melanoma (Peng et al., 2006; Cai et al., 2014, Qin et al.,2014) but also in the clinical setting. In patients affected by prostate cancer $^{64}CuCl_2$ PET/CT seems to show superior characteristic comparing to the clinical standard 18F-FCH (Capasso et al., 2015; Piccardo et al.,2017). Instead, the potential promising therapeutic use is quite new and is focused on GBM.

The double mechanism of $^{64}CuCl_2$ is first of all of a "real theranostic" agent as described by Gutfilen et al. (2018) in fact the same tracer, from a chemical and biological point of view, could be administered both for diagnosis and for therapeutic purpose. Once injected, the radiopharmaceutical follows the physiopathological path inside the human body. Although the exact mechanism of Cu^{2+} absorption by human calls has not yet been fully elucidated, it is known that, in the blood stream, Cu^{2+} ions are bound to plasma proteins, such as ceruloplasmin, albumin, and transcurrent, which transfer them to the outer cell membrane, where they are reduced to Cu+ ions by reductase enzymes. In this reduced oxidation state, Cu+ ions are then transported across the cell membrane by the human copper transporter 1 (hCTR1) where they subsequently bind to the tripeptide glutathione (GSH) that, hypothetically is thought to behave as primary Cu+ acceptor. Intracellular copper trafficking is mediated by chaperones which typically receive Cu+ immediately after it enters the cell. Storage and the subsequent redistribution of copper ions to the other tissues mainly occurs through the liver. The chaperon ATOX1 seems to be the responsible for delivering the Cu+ ions to the cell nucleus and to the copper transporter ATP7A of the secretory pathway for incorporation into copper requiring proteins that pass through the trans-Golgi network, moreover ATP7A also translocate to the plasma

membrane pumping excess cytosolic copper out of the cell, and to the vesicles/phagosome (Boschi et al., 2018). Different studies connect the alter metabolism of copper in tumor cells with the overexpression of CTR1 (Pamar et al. 2018, Peng et al., 2006; Cai et al.,2014), that result overexpressed in different types of tumors, bringing higher uptake in tumor cells comparing to normal cells. This could be the reason of selectivity of this radiopharmaceutical towards tumor cells and the scarse side effects.

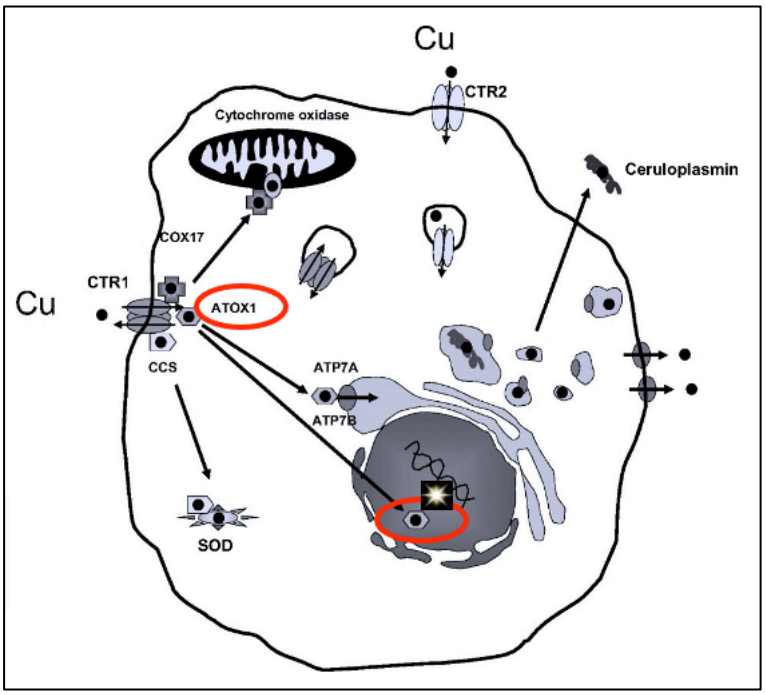

Figure 11. Schematic rapresentation of Copper flux in the cell

In case of copper-64 the dose makes the effect: lower doses make the diagnostic agent, characterized by a beta+ emission useful for PET/CT imaging visualization; higher doses, that still are under evaluation could make the therapeutic agent thanks to the specific target, the nucleus of tumor cells, and thanks to the Auger electrons, that are able to cause cell death of tumor cells. This mechanism permits to apply this radiopharmaceutical as a theranostic agent for GBM.

1.2.6 Copper Chloride in Glioblastoma

In glioblastoma, different authors showed the increment of copper content in tumoral brain tissue (Daniel et al., 2004, Jørgensen 2013). Anyways, only in the study of Ferrari et al. (Ferrari et al., 2015), on xenograft mouse model of glioblastoma have emerged the possible application of $^{64}CuCl_2$ both as diagnostic and therapeutic agent. U87MG cell lines were injected subcutaneously on the back of the neck, near the shoulder, in 6 weeks old Athymic nu/nu male Balb/c mice. Experiments were performed in animals bearing 3 weeks old tumors. In this study three groups of mice were compared: 20 no-treated animals, 20 animals treated with a single administration of 9 mCi of copper64, and 20 animals treated with a multiple-dose regimen of 1,5 mCi x 6 days of copper 64, one injection each day. Mice were then submitted to a microPET scan after 1 hour and after 18 hours post injection. MicroPET images showed a well visualization of all the tumors grafts at both acquisitions. There was a prominent activity in the tumors in comparison to the shoulder. Notably, the authors found a significant increase in survival in mice treated with $^{64}CuCl_2$ compared to controls. On the basis of pre-clinical findings, now the company is developing -$^{64}CuCl_2$ - as a possible theranostic agent in adult GBM patients, sponsoring a phase I clinical trial titled "Phase I study of $^{64}CuCl_2$ as theranostic agent in patients with relapse or progression of glioblastoma multiforme (GBM)" that is on-going. This trial has the aim to evaluate the potential theranostic use of $^{64}CuCl_2$ in the management of patients with recurrent or progressive glioblastoma multiforme. In particular, patients included are Recurrent/progressive GBM patients after surgery and standard radiotherapy-chemotherapy, second/third line of treatment and/or candidates to support therapy only. In the trial the IMP tested is the radiopharmaceutical - $^{64}CuCl_2$ solution for injection - as a theranostic agent. The first dose is injected at a diagnostic regimen to test if there is evidence of tumor uptake, in case of no uptake (visualized in the PET/CT) the treatment doesn't start. The treatment is composed by a dose escalation scheme, patients receive 7 doses of the radiopharmaceuticals once a week. $^{64}CuCl_2$ PET/CT is also performed at a follow up to evaluate this imaging technique also for monitoring response to treatment. The use of different ponderal and radioactive doses of $^{64}CuCl_2$ in patients with glioblastoma multiforme should be promising in the diagnostic setting and

especially for therapeutic purpose. $^{64}CuCl_2$ PET/CT could become a useful tool for monitoring the effects of copper-modulating therapy, permitting to verify the increased copper uptake by GBM cells that may reflex increased demand for more copper ions due to uncontrolled growth of cancer tissue.

1.3 miRNA

MicroRNAs (miRNAs) are a class of small (~19–24 nucleotides in length), endogenous, evolutionarily conserved RNAs that function as post-transcriptional regulators of gene expression. miRNAs were discovered in 1993 by Lee and colleagues in the nematode Caenorhabditis elegans, in particular have been noticed a downregulation of the protein LIN-14 (Lee et al.,1993). Since then, miRNAs have been detected in all animal model systems and some were shown to be highly conserved across species. New miRNAs are still being discovered and their roles in gene regulation are well recognized. Actually, miRBase, the primary online repository for all potential miRNA sequences, annotation, nomenclature, and target prediction miRNA genes, counts 38589 miRNAs (miRbase.org). The primarily function of miRNAs, by binding to complementary target sequences in messenger RNA (mRNA) and interfering with the translational machinery, thereby preventing or altering the production of the protein product. In most cases, miRNAs interact with the 3'UTR of target mRNAs to suppress expression (Figure 12) by means of a perfect, or unperfect pairing. However, interaction of miRNAs with other regions, including the 5'UTR, coding sequence, and gene promoters, have also been reported (Broughton et al., 2016).

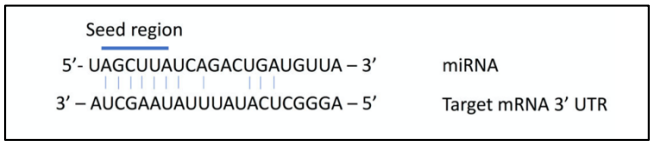

Figure 12. miRNA pairing with 3'UTR target region of mRNA

Most target sites on mRNAs have only partial base complementarity with their corresponding microRNAs. Each microRNA is able, however, to bind to at least 100 different mRNAs. Furthermore, each mRNA molecule can contain multiple binding sites for different microRNAs, creating a complex regulatory network. At least 30% of human genes are regulated by miRNAs (Ross et al., 2007). Before the discovery

of miRNAs, it was known that much of the human genome was not translated into proteins, so-called introns, but the function wasn't known. Nowadays, it is known that this "junk DNA" is involved in gene expression regulation. About half of all currently identified miRNAs are intragenic and processed mostly from introns and relatively few exons of protein coding genes, while the remaining are intergenic, transcribed independently of a host gene and regulated by their own promoters (Bhaskaran et al., 2014).

Biogenesis

The biogenesis of miRNA is classified into canonical and non-canonical pathways. The canonical biogenesis pathway is the dominant pathway by which miRNAs are processed (Lin et al., 2015). In this pathway (Figure 13), the first step consists of the transcription of a short genomic sequence by an RNA polymerase II in the nucleus, and primary miRNA (pri-miRNAs) are capped, sliced and polyadenylated. An individual pri-miRNA can either produce a single miRNA or contain clusters of two or more miRNAs that are processed from a common primary transcript. These long pri-miRNAs are cleaved by Microprocessor, which comprises the RNase III enzyme DROSHA and its essential cofactor, the double-stranded RNA (dsRNA)-binding protein DiGeorge syndrome critical region 8 (DGCR8). RNase III domains, each of which cleaves one strand of the dsRNA towards the base of stem–loop secondary structures contained within pri-miRNAs to liberate ~60–70-nucleotide hairpin-shaped precursor miRNAs (pre-miRNAs). Microprocessor recognizes the single-stranded RNA (ssRNA)–stem junction as well as the distance from the terminal loop region. It specifically cleaves the dsRNA ~11 bp from the junction with the flanking ssRNA to produce

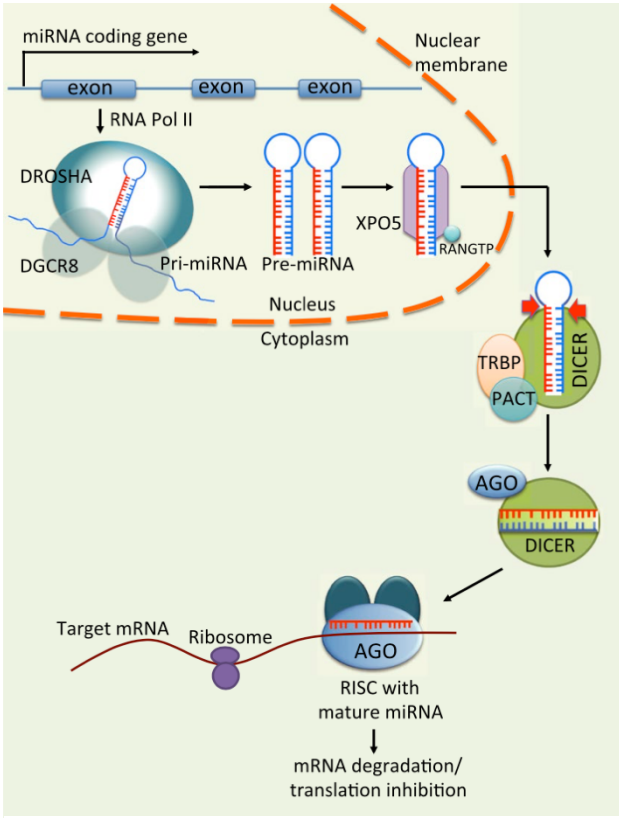

Figure 13.Biogenesis of miRNAs (Shea et al., 2016)

hairpin-shaped pre-miRNAs with an overhang at the 3’ end. The pre-miRNAs are then exported from the nucleus to the cytoplasm by exportin 5 (XPO5). The pre-miRNA is further processed in the cytoplasm by DICER, an RNase III enzyme that measures from the 5’ and 3’ ends of the pre-miRNA. DICER1 binding to the end of the pre-miRNA positions its two catalytic RNase III domains so that asymmetrical cleavage of the dsRNA stem, close to the terminal loop sequence, produces the mature ~22-nucleotide miRNA duplex with 2-nucleotide 3’ overhangs (Matsuyama-et-al-2019). The two strands of miRNAs are then separated by the RISC complex (composed by DICER1 with the Argonaute proteins (AGO1, AGO2, AGO3 or AGO4), based on various factors such as the thermodynamic asymmetry of the duplex and the stability of the base pairing at the 5 'end. The directionality of the miRNA strand determines the name of the mature miRNA form. The 5p strand arises from the 5’ end of the pre-miRNA hairpin while the 3p strand originates from the 3’ end. Both strands derived from the mature miRNA duplex can be loaded into the Argonaute (AGO) family of proteins (AGO1-4 in humans) in an ATP-dependent manner. For any given miRNA, the proportion of AGO-loaded 5p or 3p strand varies greatly depending on the cell type or cellular environment, ranging from near equal proportions to predominantly one or the other. The selection of the 5p or 3p strand is based in part on the thermodynamic stability at the 5’ ends of the miRNA duplex or a 5’ U at nucleotide position 1 (O’Brein et al., 2018). Generally, the strand with lower 5’ stability or 5’ uracil is preferentially loaded into AGO, and is deemed the guide strand. The unloaded strand is called the passenger strand, which will be unwound from the guide strand through various mechanisms based on the degree of complementarity. The passenger strands of miRNA that contain no mismatches are cleaved by AGO2 and degraded by cellular machinery which can produce a strong strand bias. Otherwise, miRNA duplexes with central mismatches or non-AGO2 loaded miRNA are passively unwound and degraded. To date, multiple non-canonical miRNA biogenesis pathways have been elucidated: using different combinations of the proteins involved in the canonical pathway, mainly Drosha, Dicer, exportin 5, and AGO2. In general, the non-canonical miRNA biogenesis can be grouped into Drosha/DGCR8-independent and Dicer-independent pathways. Pre-miRNAs produced by the Drosha/DGCR8- independent pathway resemble Dicer substrates. An example of such pre-miRNAs is mirtrons, which are produced

from the introns of mRNA during splicing. Another example is the 7-methylguanosine (m7G)-capped pre-miRNA. These nascent RNAs are directly exported to the cytoplasm through exportin 1 without the need for Drosha cleavage. There is a strong 3p strand bias most likely due to the m7G cap preventing 5p strand loading into Argonaute. On the other hand, Dicer-independent miRNAs are processed by Drosha from endogenous short hairpin RNA (shRNA) transcripts. These pre-miRNAs require AGO2 to complete their maturation within the cytoplasm because they are of insufficient length to be Dicer-substrates. This in turn promotes loading of the entire pre-miRNA into AGO2 and AGO2-dependent slicing of the 3p strand. The 3' -5' trimming of the 5p strand completes their maturation.

1.3.1 miRNA and cancer

MiRNAs not only play a key role as regulators of gene expression but represent a critical cellular factor in biological and pathological processes. These RNA fragments are involved in processes such as cell cycle control, apoptosis, cell differentiation, modulate inflammation and innate immunity by promoting macrophage differentiation and activation, are involved in hypoxia, skeletal muscle development and cardiac, insulin secretion and cholesterol metabolism (Bhaskaran et al., 2014). In addition to playing an important role in various cellular processes and functions, miRNAs play a crucial role in the initiation and development of a large variety of neoplasms; in fact, approximately 50% of miRNAs are located in the genomic regions associated with cancer (Tutar et al., 2015). In each cell type 200-600 miRNAs are usually expressed, and each cell type has its own miRNA expression profile. In the tumor there is therefore an alteration of the expression profile, which is characteristic for each neoplasm, thus allowing for a classification (Cheng et al., 2012).

In addition to being deregulated in cancer, a single miRNA can potentially perform a dualistic function by acting as an oncogene or tumor suppressor. In the first case, they are defined as oncomiRs: they are oncogenic miRNAs that have a causal role in the onset or maintenance of cancer. OncomiRs perform their function either by inhibiting tumor suppressor genes, or by inhibiting cellular differentiation or apoptosis-promoting genes that are normally upregulated in cancer (Wen et al.,

2015). Oncomirs are characterized by high levels of expression in tumors compared to control tissue, in contrast to tumor suppressor miRNAs which are under-expressed. The latter act by inhibiting oncogenes or genes that inhibit apoptosis or cell differentiation. In the literature there are various studies that report the aberrant expression of miRNAs in tumors, in which they undergo deregulation. In 2002, the first case of connection between miRNAs and cancer pathogenesis was reported; in particular Calin and colleagues observed that miR-15a and miR-16-1 were downregulated in B cells of patients with chronic lymphocytic leukemia (Calin et al., 2002). Subsequently, several cases of deregulated miRNA have been reported such as, for example, miR-34: the up-regulation of p-53 causes an increase in the expression of miR-34, which leads to inhibition of the proliferation of pancreatic cancer cells (Qing et al., 2009). In a 2005 study on lymphoma, the importance of miR-155 was highlighted, which plays a key role in the development of these tumors, accelerating it (Eis et al., 2005). MiR-17-92 is also deregulated in lymphoma, where it is under-expressed; in fact, this miRNA is downregulated in various neoplasms such as myeloma, medulloblastoma, lung cancer, breast, colon and prostate cancers (Farazi et al., 2011). Another miRNA that undergoes upregulation in cancer is miR-21, waived in glioblastoma, lymphoma, breast cancer, colon, rectum, pancreas, lungs, liver, stomach, thyroid, cervix (Sayed et al., 2011). MiR-26 acts both as an oncogene in glioma and glioblastoma; but also, as a tumor suppressor in breast, thyroid and hepatocellular carcinoma (Gao et al., 2011). Finally, miR-127 is also an example of downregulation in prostate and bladder cancer (Saito et al., 2006). The miRNA expression pattern is therefore specific for each type of tissue and cancer, and consequently they are examined as biomarkers of prognosis and diagnosis in cancer (Tutar et al., 2015).

1.3.2 miRNA in GBM

miRNAs are involved, as integral part in the development, and progression of gliomas (Adalz et al., 2013; D'Urso et al., 2012), due to their essential role as signaling pathways regulators of cancer pathogenesis (Delic et al., 2014; Gonzàlez-Gòmez et al., 2011). In GBM over 240 miRNAs have been identified in various GBM samples, most of them are upregulated while a few are downregulated compared to normal tissue, of these the mechanisms of action of

is reported in the literature, for others, the functional activities are yet to be fully characterized. As for other type of tumors, some microRNAs in GBM can function as oncogenes or oncomiRs, while others show antioncogenic features. The contribution of miRNAs to the development and progression of gliomas refers to their regulation of crucial mechanisms targeting developmental genes. miRNAs have shown crucial roles in apoptosis, proliferation and the cell cycle, the remodeling of the extracellular matrix, tumor infiltration and angiogenesis, invasiveness, stem-cell renewal, and DNA repair (D'Alessio et al., 2019). Individual miRNAs have been correlated with different glioma stages as in the study of Malkorn et al. (2019) in which 12 miRNAs have been identified as up-regulated (miR-9, miR-15a, miR-16, miR-17, miR-19a, miR-20a, miR-21, miR-25, miR-28, miR130b, miR-140, miR-210) and two (miR-184, miR-328) that were downregulated during progression. It is to note that miRNAs seem to like targeting developmental genes.

The first microRNA reported to be overexpressed in GBM compared to the normal brain tissue is miR-21, whose main function is to prevent the activation of the caspase-dependent apoptotic pathway, contributing to the onset of the malignant phenotype. miR-21 carries out its pro-genic effect by downregulating numerous targets including ANP32A, SMARCA4, SPRY2, IGFBP3, LRRFIP1, and RECK. Through these targets, miR-21 can influence numerous biological processes as cell cycle progression, promotion of invasion and metastasis and resistance to chemotherapies. Dysregulation of miRNA expression is one mechanism of cancer cells to bypass signals for programmed cell death. Antiapoptotic miRNAs target proapoptotic genes and are frequently upregulated with GBM. Again miR-21 is antiapoptotic enhancing tumor formation by targeting p53 signaling pathway and TGF-beta, as well as the mitochondrial apoptotic pathway. Considering all the pathways in which this miRNA is involved, it has a critical role in GBM pathogenesis and a promising target for therapeutic interventions. This primary GBM are characterized by amplification of EGFR, miR-7 which acts as tumor suppressor, directly targets EGFR and can independently repress the Akt pathway through targeting of its upstream regulators. In GBM is frequently downregulated, allowing for enhanced activation of the Akt pathway, increasing viability and invasiveness of tumor cells. Other miRNAs that are overexpressed in GBM and present different target involved in glioma genesis is miR-221 and miR-222. Both of them can

regulate cell death through targeting of p53-upregulated modulator of apoptosis (PUMA). Under normal conditions PUMA binds Bcl-2 and Bcl-x, rapidly inducing apoptosis. Thus, forced expression of miR-221/miR-222 and the subsequent downregulation of PUMA, promotes cell survival. The knockdown of miR-221/222 is able to induce cell death and decrease tumor growth.

Other microRNAs found upregulated in GBM, include miRNA-10b, linked to the regulation of the cell cycle and invasion of GBM cells. For example, the study by Gabriely et al. (2011) drew attention to miR-10b highlighting that the survival of patients with GBM expressing high levels of miR-10b was significantly reduced compared to those with low levels, indicating that miR-10b could contribute to growth of glioma in vivo. Furthermore, the inhibition of this miRNA, which is strongly up-regulated in GBM, in mouse models of human glioblastoma, has led to a significant reduction in tumor growth.

Concurrently, some microRNAs were found downregulated in GBM, such as miR-34a and miR-128, both have antiproliferative effect. miR-34a is able to repress CDK6, CCND1 and it is involved in the proliferative signaling pathway. Restoration of this miRNA could reduce CDK6 protein expression, inhibiting cell survival, proliferation, and invasion as well as inducing apoptosis (D'Alessio et al., 2019). Because of the failure of common therapies, many efforts focused on the identification of molecular targets in support of the diagnosis and the treatment of GBM. miRNAs have increased interest among scientific community, as versatile regulators of gene expression, can act as biomarkers and as therapeutic agents.

1.3.3 miRNA as biomarkers

It has been shown that miRNAs are integrally involved in brain gliomas' development and progression They are essential regulators of many key pathways implicated in tumor pathogenesis. Because miRNAs have been shown to play crucial roles in glioblastoma progression, invasion, tumor growth, and therapy responses, it is very likely that some miRNAs could be useful biomarkers in brain tumor patients (Barciszewska et al 2016).

There are many data showing that miRNA signatures can refine glioblastoma classification, differentiate GBM subclasses, as well as provide regulatory links to disrupted signaling pathways such as those facilitating cell growth. Some studies show lower miRNA expression in tumour samples, what can be a function of

cellular differentiation status. Microarray studies of glioma tissue have implicated a number of miRNAs involved in glioma formation and propagation. The application of miRNA as tissue biomarker could be useful to define diagnosis and prognosis but is invasive and in case of inoperable tumors it would be of difficult application. Moreover, for GBM it is necessary to identify biomarkers able to Monitor glioma development during or after completed treatment requires a reliable and quick test for biomarker detection from an easily accessible source, allowing a less extensive and more accurate disease monitoring in shorter time periods (as compared to neuroimaging). Furthermore, there could be a huge benefit from developing bio- markers for glioblastoma confirmation in order to avoid biopsy for patients with a high risk of surgery-associated mortality or small tumours in eloquent brain areas. This role could be entrusting to peripheral blood miRNA.

1.3.3.1 Liquid Biopsy

Liquid biopsies that enable the detection of circulating biomarkers confer the benefit of being non-invasive, thereby facilitating serial sampling and the ability to monitor potential dynamic changes in the tumour over the course of therapy. Tumors in general, including GBM shed tumoral content into the blood and cerebrospinal fluid (CSF). The detection of these biomarkers, such as proteins, miRNAs, cell-free nucleic acids (cfNAs), extracellular vesicles (EVs) and circulating tumour cells (CTCs), in a liquid biopsy can be used to complement standard risk-stratification methods, monitoring of treatment response and disease progression in GBM patients (Figure 14). The first treatment for GBM patients is surgery but resection or biopsy from a brain tumour can present risk to the patients, such as possible brain swelling within and around the tumour mass, or might even affect neurological functions, moreover some tumour might be inaccessible owing to their location.

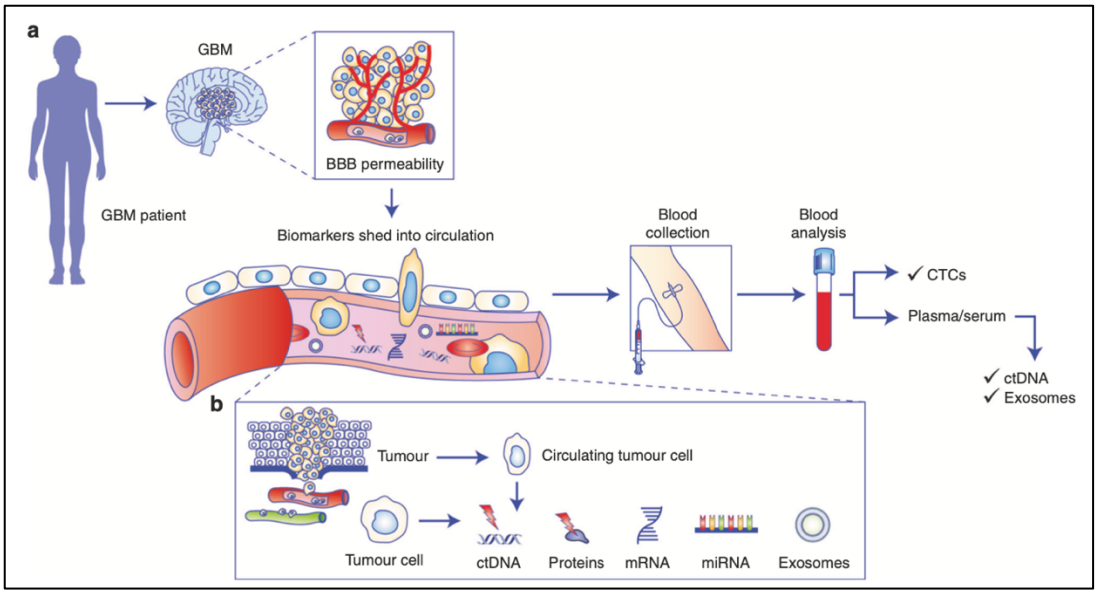

Figure 14. a) Schematic representation of biomolecular transportation from the brain tumor through the BBB into the circulation b) molecules that can be measured in liquid biopsies (Bark et al., 2020)

The sampling and analysis of these molecules in non-solid biological fluids is defined as a "liquid biopsy". Although liquid biopsy is often carried out by using a blood draw, other biofluids, such as saliva or urine, can be also used. Also, Cerebrospinal fluid (CSF) has also been used to investigate tumour-specific biomarkers in brain tumors, as it circulates along with the brain and spinal cord, and therefore has close contact with the CNS, but CSF collection requires an invasive lumbar puncture procedure (Bark et al., 2020). Liquid biopsy presents a minimally invasive way to capture tumour activities in real time to diagnose and predict disease progression. The first FDA-approved broad companion pan-cancer diagnostic test utilizes the presence of ctDNA within a liquid biopsy sample to test for the presence of a number of solid tumours, including non-small-cell lung cancer, colorectal cancer, breast cancer, ovarian cancer and melanoma. For liquid biopsies to be successfully used in GBM, it is assumed that tumour-specific material would cross the BBB. It has been noticed that in GBM the permeability of the membrane is augmented, with a tight junction decrease, supporting the access of pro-inflammatory immune cells. The EVs derived from glioma cells were shown to cross the intact BBB and were detected in the blood of GBM patients. This highlight the importance of EVs in liquid biopsies since EVs can be detected in cases in which the BBB is not compromised.

Liquid biopsy could therefore be a helpful tool to complement current strategies for predicting GBM prognosis, by allowing a more dynamic view of tumour characteristics, and response to chemotherapy, by providing a platform to monitor treatment responses. For brain tumors, where noninvasive procedures are complex, precarious, and may be nonrepresentative for outcome, circulating biomarkers pose a realistic option. For the inoperable patients, which mostly occurs in the recurrent setting, circulating biomarkers could be the source of a molecular profile of the relapsed tumor, allowing clinicians to identify potentially druggable molecular alterations driving recurrence (Verduin et al., 2019).

1.3.3.2 Circulating miRNAs

Tumor tissues miRNA profiles may help determine tumor grades, disease prognosis, and therapeutic targets, but fluid is more feasible for non-invasively diagnosing GBM. Circulating miRNAs have been detected in various biological fluids, in particular in plasma, serum, milk, tears, saliva, urine, amniotic, cerebrospinal, and semen fluids, and in ascites (Makarova et al., 2015). Circulating miRNAs could be useful biomarkers considering that is much less invasive than repeatedly taking tumor tissues biopsies. The relationship between miRNA existing in the peripheral fluids and miRNA expression in the GBM tissues is still unclear. Circulating miRNAs are appealing biomolecules to be considered as cancer biomarkers also because of their stability, which sustain a high temperature or extreme pH conditions that would damage other cell components. It has been noted that miRNAs in serum are not digested by the RNase and other conditions. miRNAs levels can be determined by various methods without any difficulty (Chakraborty et al.,2016). In table below (Table 5) are shown some miRNA evaluated as potential biomarkers.

Table 5. Potential circulating miRNA as biomarkers in GBM (Banelli et al., 2017)

Biomarker	Source and Analysis	Significance	Regulation and prevalence in GBM	Functional relevance
miR-21	Source: Body Fluids* Analysis: PCR	Prognostic and predictive biomarker; also allows patient stratification	Upregulated (+)	Modulates PTEN, RECK, FasL and PDCD4 for GBM cells to proliferate - Hypotize to play a role in CSC differentiation with Fas ligand as its main target

miR-10b	Source: Body Fluids* Analysis: PCR	Prognostic and predictive biomarker	Upregulated (+)	Alternative splicing of RSRC1 and MBNL or by activation of caspases accompanied by inhibition of Bcl-2 pathway to induce excessive proliferation
miR-15b	Source: Body Fluids* Analysis: PCR	Prognostic and predictive biomarker	Downregulated (-)	miR-15b downregulation correlates with cell cycle progression
miR-137	Source: Body Fluids* Analysis: PCR	Prognostic and predictive biomarker	Downregulated (-)	miR-137 downregulation is hypothesized to be negative regulation of gene target, GLIPR-1

In comparison to normal controls the plasma levels of miR-21 and miR-342-3p were shown to be significantly altered in GBM patients and miR-342-3p positively correlated with glioma' histopathological grade. Also, miR-29 shows high diagnostic potential, allowing to differentiate between patients of stage I-II with stage III-IV. Furthermore, the miR-454-3p expression in the post-operative plasmas is markedly downregulated in comparison to the pre-operative plasmas, and a correlation of worsening prognosis of glioma was observed with increasing miR-454-3p expression. Moreover, a huge increase in miR-210 expression was found in GBM patients' serum samples compared to controls, and it was associated with the tumour grade and patient's poor outcome. It was also noted that miR-15b is inversely correlated with worsening histopathological status of GBM and various other gliomas (Sasmita et al., 2018).

microRNA-10b seems to be deeply involved in glioblastoma progression because its expression levels clearly correlate with tumour grade and it is under development in the clinical stage, recently a clinical trial titled "Evaluating the Expression Levels of MicroRNA-10b in Patients with Gliomas" [ClinicalTrials.gov Identifier: NCT01849952] have been closed. The trial testing the hypothesis that in primary glioma samples mir-10b expression patterns will serve as a prognostic and diagnostic marker. Several studies have shown that miR-128 levels were increased in patient peripheral blood, although it was decreased in GBM tissues. In blood of glioblastoma patients, compared with controls, miR-128 overexpression has been identified. Thus, the level of miR-128 in blood may serve as a biomarker for detecting GBM (Huang et al., 2018). However, it was noticed

that miR-128 false levels could be falsely elevated due to the miRNA that are released from red blood cells. miR-21 level was also increased in patient serum, brain tissue and exosome, but this miRNA is upregulated in several cancers, therefore it would be difficult to detect GBM only with this miRNA (Huang et al., 2018). But in general, it is difficult to predict GBM from only one miRNA, this is the reason because "miRNA panels" are currently used as biomarkers in different tumor types. Numerous companies developed new miRNA-based diagnostic tools, the first company focusing on miRNA-based diagnosis assays was Rosetta Genomics, they launched in 2012 miRviewTM Mets a miRNA panel allowing the identification of cancers of unknown or uncertain primary origin (CUP). Nowadays exists panels available for thyroid cancer, pancreatic cancer, cardiovascular disease, but still not approved panel for GBM that are still under development (Bonneau et al). Actually, there are on-going clinical trials validating miRNAs as possible biomarkers in GBM as "Establishment of a Signature of Circulating microRNA as a Tool to Aid Diagnosis of Primary Brain Tumors in Adults (miRNA)" [ClinicalTrials.gov Identifier: NCT03630861].

However, literature data propose different miRNA panels. The first panel is composed by three serum miRNAs: miR-106a-5p, miR-182, and miR-145-5p in which miR-106a-5p resulted up-regulated, miR-182 and miR-145-5p resulted downregulated, this panel have been associated with short-term (two years) survival of GBM patients. Another panel is composed by 5 serum miRNAs 222-3p, miR-182, miR-20a-5p, miR-106a-5p, and miR-145-5p. In this panel, up-regulated miR-222-3p, miR-20a-5p, and miR- 106a-5p, and down-regulated miR-182 and miR-145-5p were correlated with a lower probability of two-year disease-free survival (Zhao et al., 2017-a).

The specific miRNA signature in plasma samples derived from GBM patients before tumour resection would be very useful for planning the necessary degree of resection and adjuvant therapies. A significant difference in serum miRNA profile was found between untreated high-grade astrocytoma (grade III-IV) and controls in a genome-wide miRNA analysis. Seven miRNAs (miR-15b, miR-23a, miR-133a, miR-150, miR-197, miR-497, miR-548b-5p) were markedly decreased in grade II-IV patients and showed high specificity (97.87%) and sensitivity (88.00%) for prediction of malignant astrocytomas. Furthermore, these miRNAs were also elevated in serum after operation, and some of them could be proposed as non-

invasive biomarkers of malignant and benign cases, astrogliosis and other primary brain tumours (Barciszewska et al., 2016). Moreover, it is important to note that circulating miRNA could help monitoring therapeutic response or predict therapeutic effects. For example, high levels of miR-10b and miR-21 were observed in most GBM patient serum during the bevacizumab (BVZ) treatment period compared to the pre- treatment levels. miR-10b and miR-21 levels expressed were negatively correlated with increased tumor diameters in the BVZ-treated group but not in the TMZ-treated group. Therefore, the potential role of miRNA as biomarkers of prognosis, diagnosis, treatment response or resistance is emerging even in GBM.

1.3.3.3 Exosome and Exosomal miRNAs

Exosomes, a kind of EV have also been put forth as a possible source of macromolecules for analysis in liquid biopsy for brain tumors. Exosomes, membrane-bound vesicles of 40–100 nm in diameter, are present in almost all biological fluids. They are released from most cell types into the extracellular space after fusion with the plasma membrane. Exosomes can be found in multiple types of extracellular fluids, such as blood, urine, amniotic fluid, saliva, cerebrospinal fluid, and even breast milk EV is a global term used for all types of vesicles secreted by cells. EVs are classified according to their size, biogenesis process, and physical nature. Among the EVs, the best characterized are the exosome, which are released by exocytosis when multivesicular bodies (MVBs) fuse with the plasma membrane, releasing them in the extracellular space (Figure 15). MVs are referred to as ectosomes or microparticles and formed by direct blebbing of the outward plasma membrane and released into the extracellular matrix. Another type of EV is the apoptotic body formed during cellular blebbing and fragmentation upon apoptosis (Jurj et al., 2020).

Lipids and proteins are the main components of exosome membranes, which are enriched with lipid rafts. In addition to the proteins, various nucleic acids have recently been identified in the exosomal lumen, including mRNAs, microRNAs (miRNAs), and other non-coding RNAs (ncRNAs).

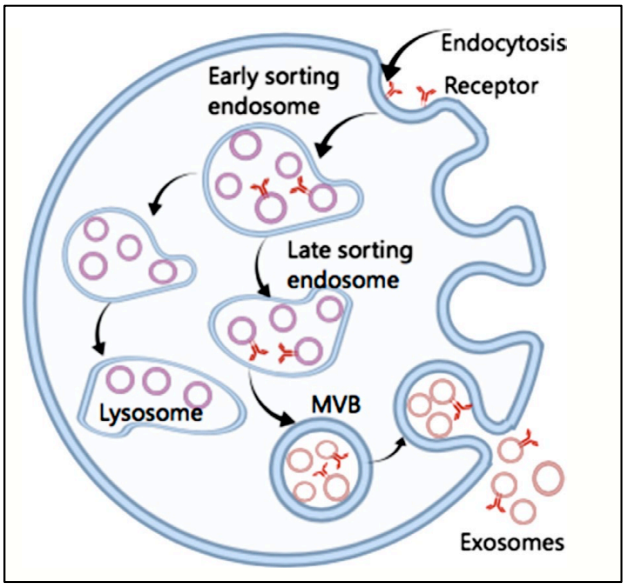

Figure 15. Exosome released in the extracellular environment

These exosomal RNAs can be taken up by neighboring cells or distant cells when exosomes circulate, and they subsequently modulate recipient cells. The discovery of their function in genetic exchange between cells has brought increasing attention to exosomes. They have now been shown to play a crucial role in intercellular communication functioning as a bridge for information exchange between cells, they can transport miRNAs and prevent RNA enzyme degradation, and can also affect cell-cell communication (He et al., 2018). EVs could be isolated from the serum brain tumor patients and the specific genetic alterations in the EGFR gene could be detected in the serum-derived EVs of these patients. Additional investigations in the serum of patients with brain tumors versus controls showed that distinct RNA expression patterns could be detected in the EVs of GBM patients as compared to controls (Ganesh et al., 2017). miRNAs are not randomly incorporated into exosomes and subset of miRNAs preferentially enter exosomes. Moreover, some reports have shown that exosomal miRNA expression levels are altered under different physiological conditions. In GBM exosomal levels of miRNA-21 from cerebrospinal fluids resulted associated with poor prognosis and tumor recurrence of glioma patients 198 glioma tissue samples, we verified that miR-21 levels associated with tumor grade of diagnosis and negatively correlated with the median values of patient overall survival time (Shi et al., 2015). The pilot study of Ebrahimkhani et al.(2018) selected seven miRNAs differentially expressed in serum exosomes from glioblastoma patients

relative to healthy controls. Serum exosomal miRNA signatures can accurately diagnose glioblastoma preoperatively. miRNA signatures identified are distinct from previously reported "free-circulating" miRNA studies in GBM patients and appear to be superior. In the study of Cai et al. (2018) circulating exosomal miR-148a levels were significantly higher in serum from GBM patients compared with serum from healthy volunteers. In T98G cells, inhibition of miR-148a suppressed cell proliferation and metastasis. In addition, the authors identified Cell adhesion molecule 1 (CADM1) as a target gene of miR-148a, moreover there was a strong negative correlation between exosomal miR-148a and CADM1 mRNA levels in samples of patients. Moreover, miR-148a antagonist increased p- STAT3 protein level to activate STAT3 pathway. miR-148a delivered by exosomes may promote cancer cell proliferation and metastasis via targeting CADM1 to activate STAT3 pathway, suggesting a predictor and therapeutic target role of exosomal miR-148a in GBM patients (Cai et al., 2018). Another miRNA examined as diagnostic and prognostic value in association with hypoxic conditions in patients with glioma is miR-210. A significant increase in serum exo-miR-210 levels was observed in patients with glioma compared with healthy controls. Furthermore, serum exo-miR-210 levels from patients with glioblastoma were markedly decreased following surgery and upregulated once more at the recurrences of primary tumors, indicating that exo-miR-210 could reflect alterations in malignant glioma loads. Finally, increased serum exo-miR-210 expression was positively associated with high levels of hypoxia-inducible factor 1a and reflected hypoxia in patients with glioma highlighting the usefulness of exosomal miRNAs as a diagnostic, prognostic and hypoxic biomarker to reflect glioma status and hypoxic signatures (Lan et al., 2019). Moreover, Yue et al. showed that exosomal miR-301a contributed to glioblastoma resistance to radiotherapy. Hypoxic GBM cells secreted the exosomal miR-301a, which could be transferred to responsive cells that were originally in normoxic conditions, but then became resistant to radiation. Exosomal miR-301a directly targeted TCEAL7 genes, which function as tumor suppressors in GBM progression, and actively suppressed their expression in normoxic glioma cells. TCEAL7 down-regulated the Wnt/β-catenin signaling pathway via inhibiting β-catenin translocation from the cytoplasm to the nucleus (Ghaemmaghami et al., 2020). The study also found that exosomal miR-301a was over- expressed in the sera of glioma patients in comparison with healthy

individuals. The elevated levels of miR-301a containing exosomes were related to increased tumor grade and lower Karnofsky performance status scores. The levels of miR-301a containing exosomes in the serum were significantly decreased after surgery of the primary tumor and were elevated again after GBM relapse. Kaplan-Meier statistical analysis of tumor grade (III or IV) in patients with elevated amounts of the miR- 301a containing exosomes in the serum showed a shorter overall survival (OS) time in comparison with patients with a lower level. Exosomes are innovative and potential biomarkers considering their crucial role in communication can open new perspectives in miRNA role and functions.

1.3.4 miRNA in GBM radioresistance

The GBM radioresistance have shown involvement of microRNAs that effectively regulate radiation-related signal transduction pathways in GBM, and many studies have reported that the radiosensitivity of GBM can be altered by targeting these microRNAs. Different miRNA results involved in differential response of glioblastoma cells to ionizing radiation as miR-15a, miR-16, miR-143, miR-155 upregulated in glioblastoma cells after radiation treatment (Chaudry et al., 2010). Moreover, different miRNAs have been associated to radioresistance. One of the miRNAs involved in radioresistance is miR-181a, that showed downregulation in U87MG cell lines after IR exposure. This miRNA is involved in the PI3K/AKT and over-expression of miR-181a sensitized these cells to IR and led to downregulation of mRNA and protein level of BCL-2, associated with radioresistance (Chen et al., 2010).

miR-21 enhances resistance of glioma cells to radiation therapy, in fact the miR-21 expression levels positively correlated with resistance to radiation in glioma cells (Han et al., 2017). Anti-miR-21 treatment of U373MG and U87MG malignant GB lines resulted in an increased sensitivity to radiation. Moreover, it has been reported that miR-21 can mediate the radiation resistance of GBM cells by regulating important cell cycle genes as PDCD4 and hMSH2 (Chao et al., 2013).

Another study reported that miR-1, miR-125a, miR-150, and miR-425 induce radioresistance in GBM through upregulation of the cell cycle checkpoint response. Thus, these studies show that different microRNAs can regulate GBM radioresistance by modulating Akt signaling, cell cycle checkpoint responses, and DDR activity (Ali et al., 2020). The p53 tumor suppressor is involved in the

regulation of cell cycle checkpoints and apoptosis, and thus is part of the DNA damage response and can influence radiosensitivity. One of the direct targets of p53 is miR-34. The miR-34 family has shown upregulation after irradiation in different tumor types including GBM (Metheetrairut et al., 2013). In the study of Sasaki et al. the authors showed the high miR-34a expression level in the cells after irradiation at 60 Gy reduced the p53 expression level. This study suggests that apoptosis might be promoted by regulating the action of miRNAs, even in cells that have acquired radioresistance.

In the study of Moskwa et al. a functional screen identified miR-1, miR-425, miR-125, miR-150 as associated to radioresistance, in particular the overexpression promotes radioresistance through upregulation of cell-cycle checkpoint response. Conversely antagonizing with antagomiRs sensitizes GBM cells to irradiation, has suggested their potential as targets for inhibiting therapeutic resistance (Moskwa et al., 2014). In addition, overexpression of miR-221/222 confer radioresistance in GBM cells by regulating AKT, independently of PTEN status. Upon activation by miR-221/222 after irradiation, AKT modulates DNA-PKcs expression to enhance DNA damage repair (DDR) activity and thereby promote radioresistance (Li et al., 2014). These findings suggest that the regulation of miRNAs could become a novel therapeutic strategy to enhance the radiosensitivity of GScs and suppress the progression of glioblastoma. The response to treatment in GB patients is variable and probably depends on tumor heterogeneity that originates from genetic and epigenetic alterations which can influence the behavior of the disease. In this respect, the relation between miRNA and chemo- and radiotherapy has been extensively exploited to search for new possible therapeutic targets or to predict and improve the response to treatment.

1.3.5 miRNA-based therapeutics

The wide involvement of miRNAs in tumors suggests their usefulness as new ideal therapeutic targets. Considering that they can act as either oncogens or tumor suppressors, this corresponds to two different approaches to developing miRNA-based cancer therapies (Figure 16): a) reduce over-expressed miRNAs antagonizing onco-miRs or, b) molecules that mimic the action of miRNAs, with the aim of restoring the expression levels of tumor suppressor miRNAs (Tutar et al., 2015). Oligonucleotides or small molecules could be used in both approaches

to inhibit miRNAs directly or indirectly, targeting specific genes or transcription factors that modulate the expression of certain miRNAs. Overexpressed intracellular miRNAs can be inhibited via administration of synthetic antisense, single-stranded RNA-based oligonucleotides, called "antagomirs" or "antimiRs". These synthetic small RNA molecules have a complementary sequence to the miRNA to be inhibited and block the function of the corresponding miRNA by binding to it strongly (Takahashi et al., 2018). Efficient inhibition by antagomirs requires optimization of the oligonucleotides for high binding affinity, high resistance to nuclease degradation, low toxicity, and efficient in vivo delivery. These factors can be modified through alterations of the sugar, the nucleobase, the inter-nucleotide linkages, or with the addition of non-nucleotide modifiers (Shea et al., 2016). Phosphorothioate oligodeoxynucleotides were the most common type of first-generation antisense oligonucleotides, having high resistance to nucleases but low binding stability and high toxicity.

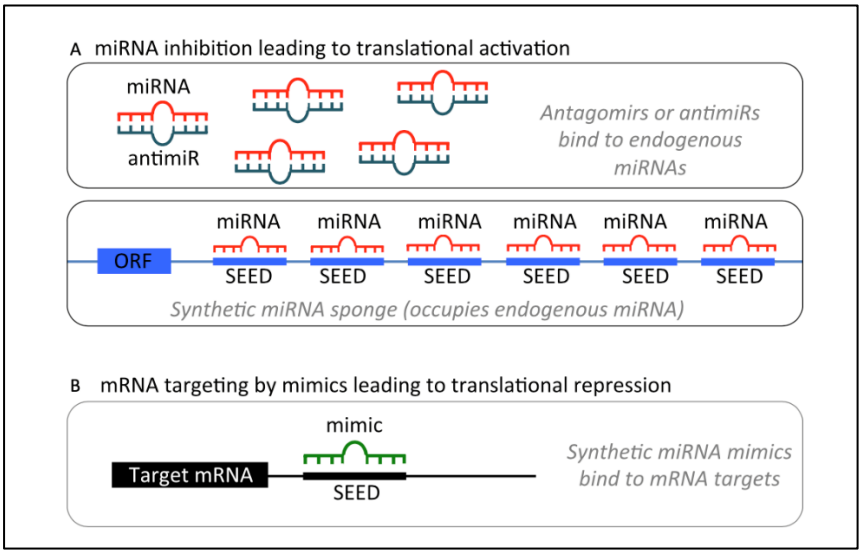

Figure 16. miRNA modulation strategies for therapeutic intervention (Shea et al., 2016)

These were followed by locked nucleic acid (LNA)-modified oligonucleotides, which have higher affinity to DNA and RNA nucleotides, higher stability, efficacy, and specificity as well as lower toxicity. LNA-linked oligonucleotides are currently the most widely used class of antagomirs and have shown promise for treating various conditions (Rupaimoole et al., 2016).

In general, beyond determining long-term effects, one of the greatest challenges with miRNA-based therapeutics is finding effective delivery systems, particularly

to the brain. There are various obstacles to efficient delivery including cellular resistance to the uptake of oligonucleotides, sequestration of treatments in the liver, and the blood–brain barrier, which prevents the delivery of most drugs to the brain. A recent study by Song et al. addressed the first issue, finding that R3V6 peptides were able to protect anti-miR-21 oligonucleotides from nucleases, while delivering the treatment into the cells more efficiently than other modifications, including polyethyleneimine. The peptide was also effective at reducing miR-21 levels and inducing apoptosis in GBM cells, suggesting that the R3V6 peptide may be a useful carrier for antisense oligonucleotides (Song et al., 2015). As mentioned above, miR-10b is involved in tumor invasion and is an optimal therapeutic target because of its high and generalized expression in all GB subtypes. A preclinical in vivo study focused on the inhibition of miR-10b in an orthotopic GB xenograft model compared the results of different delivery methods utilizing as endpoint the inhibition of the tumor growth. The antagonist of miR-10b administered by the three routes (brain injections, systemic injections, and intracranial osmotic pumps) resulted in the inhibition of miR-10b and in turn reactivated its target genes, attenuated tumor growth, and prolonged survival. Considering the possible translation from the bench to the bedside, the systemic injections of miR-10b inhibitor were less invasive compared to the other routes and had minimal or no side effects on extracranial tissues and with a good delivery through the BBB (Teplyuk et al., 2016). An alternative to antisense oligonucleotides is the miRNA sponge, which contains multiple binding sites for the miRNA of interest, competitively inhibiting it from binding to its target mRNA. Importantly, the sponge's binding sites are specific to the miRNA's seed region, allowing a single sponge to block all miRNA family members containing the same seed sequence (Figure 16) (Ebert et al., 2007). The utility of these "sponges" in GB was recently demonstrated for miR-23b both in glioma cell lines and orthotopic mouse model, using a miRNA sponge able to inhibit miR-23b. In vivo model showed the reduction of angiogenesis, migration and invasion, and in turn the malignancy of the tumor (Banelli et al., 2017).

The other side of therapies that can restore the functions of microRNAs are miRNA mimics, which are small synthetic double-stranded molecules that mimic endogenous miRNAs or their precursors (pre-miRNA); small molecules and DNA demethylating agents: all restore normal levels of tumor suppressor miRNAs

(Tutar et al., 2015). This can be achieved through administration of synthetic miRNA mimics, which have identical sequences to their naturally occurring equivalents. For example, Chen et al. found that miR-203 was significantly decreased in high WHO grade gliomas as compared to low WHO grade gliomas and normal brain tissue. Transfection of miR-203 mimics into U251 human GBM cells markedly downregulated expression of phospholipase D2, a target of miR-213 which is thought to be oncogenic in GBM. This suppressed the proliferation and invasion of U251 cells, demonstrating the utility of mimics for correcting miRNA depletion.

Table 6. miRNA-based therapeutics clinical trials

Product	Targeted miR	Disease type	Development phase
Miravirsen	miR-122	HCV	Phase 2
RG-012	miR-21	Alport Syndrome	Phase 2
Cobomarsen	miR-155	T-cell lymphoma	Phase 2
MRX34	miR-34	Liver cancer, Lymphoma, melanoma	Phase 1
MRG 110	miR-92	Wound healing, heart failure	Phase 1
MesomiR-1	miR-16	Mesothelioma,lung cancer	Phase 1

The lead candidate in the miRNA drug discovery process has most certainly been MRX34 from Mirna Therapeutics, which has represented a new class of anti-cancer agent. MRX34, a liposome-formulated mimic of miR-34 have been administered in a phase I clinical trial enrolling patients with unresectable primary liver cancer or advanced metastatic cancer with liver involvement (ClinicalTrials.gov Identifier: NCT01829971, A Multicenter Phase I Study of MRX34, MicroRNA miR-RX34 Liposomal Injection (Monroig-Bosque Pdel et al., 2015). In Table 6 is reported the list of miRNAs investigated as therapeutic agents. Nowadays not targeting GBM, but the expansion of miRNA use in treatment strategies represents promising advancement and possibilities also in this kind of tumors (Hanna et al., 2019; Bonneau et al., 2019).

2. Project Aim

The project focused on an innovative radiopharmaceutical, "Copper (64Cu) Chloride", that is under investigation as theranostic agent, in GBM patients. This Investigational Medicinal Product was developed by the company Acom Srl that is sponsor of the phase I clinical trial titled "Phase I study of $^{64}CuCl_2$ as theranostic agent in patients with relapse or progression of glioblastoma multiforme (GBM)".

This is a very preliminary phase in humans, and the therapeutic scheme is still under evaluation. The crucial points for the application of this theranostic agent are the identification of the proper dose that should reach the target in sufficient amounts, to carry out the therapeutic effect, but also the determination of the best dose scheme to avoid radioresistance uprising.

In fact, currently the lack of effective available treatments for GBM goes hand in hand with the development of resistance. GBM is a heterogenous tumor that often harbors genetic anomalies that affect different signaling pathways. Unfortunately, GBM are notoriously resistant to radiotherapy, and alterations in several molecular mechanism and signaling pathways, including miRNA deregulation, have been shown to be involved in inducing radioresistance in GBM.

On these grounds, the present research aimed to investigate on radioresistance associated to $^{64}CuCl_2$ treatment and in particular (I) the first aim of the project was to create two in vitro models of acquired radioresistant GBM lines to perform (Ia) from one point of view functional studies useful to implement the approach for dosimetric analysis and to identify the best dose scheme to avoid the establishment of radioresistance; (Ib) from the other point of view to analyze miRNA profiling in radiosensitive and radioresistant cell lines, in order to

- select miRNAs deregulated in sensitive cells (U87MG, U373MG) comparing to the resistant ones (U87MG-RR, U373MG-RR) to characterize the cell lines and selecting exosomal miRNAs differently expressed,
- identify miRNA aberrant expressions of specific miRNAs by comparing the expression profile of miRNAs obtained from cell pellets comparing to miRNAs obtained from exosomes of the cell culture medium.

Moreover, considering that copper chloride treatment is in phase I, a molecular biomarker for this therapy still lacks. Circulating miRNAs and exosomal miRNAs are showing their emerging role in oncology as optimal biomarkers of diagnosis, prognosis, or response to treatment due to their minimally invasive way to capture

tumour activities in real time. Therefore, introducing liquid biopsy for $^{64}CuCl_2$ treatment could help confirming the PET/CT findings and selecting the proper choice of a personalized treatment.

On the light of these premises (II) the second aim of the project focused on the detection of miRNA expression from plasma samples of the GBM patients enrolled in the phase I clinical trial (P. GBM.64Cu.2018) and their correlation with the different clinical responses to $^{64}CuCl_2$ treatment to (IIa) select, form one side, miRNAs as potential biomarkers of response to treatment and, from the other side, (IIb) to select predictive-biomarkers of response to $^{64}CuCl_2$ treatment.

In conclusion, miRNAs could bring to a better understanding of the $^{64}CuCl_2$ treatment, becoming useful tools both in detection of treatment response and as possible molecules that could restore treatment responsiveness.

3. Materials and Methods

3.1 Creation of GBM radioresistant cell lines

Glioblastoma Multiforme U87MG and U373MG are glioblastoma cell lines derived from primary tumor. The two GBM cell lines differ morphologically and genetically. Indeed, U87MG has an epithelial morphology whereas U373MG is pleomorphic/astrocytoid. With regard to the genetic profile, both lines are IDH1-Wildtype, while they differ in TP53, PTEN and NF1 status (Table 7)(Ghandi et al., 2019, Oh et al., 2017).

Table 7. Genetic profile cell lines U87MG, U373MG

	U87MG	U373MG
IDH1	wt	wt
P53	wt	Ho p.Arg273His
NF1	he p.Phe1247Ilefs*18	wt
PTEN	ho c.209+1G>T	p.Ile135_Ala137delinsThr

The cell lines were routinely grown in DMEM high glucose media supplemented with 10% FBS, 1% PS and cultured in at 37°C in a 5% CO2 humidified atmosphere.

Radioresistant cell lines U87MG-RR and U373MG-RR were generated by exposing the parental cell lines U87MG, U373MG to increasing doses of radiation for 32 weeks, starting with a dose of 0.0034 MBq and increasing gradually to 1 MBq. Fresh radionuclide was provided every 7 days. The development of radioresistance was evaluated though cell viability assays. The cells were considered resistant when they regained the ability to grow in the presence of a specific drug concentration and reached a viability of at least 90%.

3.2 Cell Survival Assays

MTT test

The cell viability of cell lines following radiation treatment was assessed by MTT test (Thiazolyl Blue Tetrazolium Bromide #M2128 Sigma). The cells were seeded in 96-wells black plates at a cell density of 10.000 cells/100ul x well and incubated at 37°C and 5% CO2 for 24 hours. After incubation, the medium was replaced with fresh medium containing increasing radioconcentrations of $^{64}CuCl_2$ [C1 = 0.0034, C2 =0.034, C3 = 0.34, C4 = 1.7, C5 = 3.4 MBq/well] and incubated for 24h. Cells treated with medium only served as a negative control. All tests were

performed in triplicate. Subsequently, after medium removal, cells were incubated with 50μl /well of MTT solution (0.5 mg/ml) for 2h at 37°C. Following MTT removal from each well and washing by DPBS, the resultant formazan crystals were dissolved in 50μl of isopropanol. The wells were left to stand for 15 minutes until complete crystals solubilization. The darker the solution (higher number of purple formazan crystals), the greater the number of viable, metabolically active cells. The optical density (OD) at a wavelength of 570nm was measured using a UV-Vis spectrophotometer. The degree of cell viability following treatment with the tested radiation dose was expressed as: % cell viability = [OD (570nm) tested dose] / [OD (570nm) negative control] x 100.

CellTiter-Glo® Luminescent Cell Viability Assay

The CellTiter-Glo® Luminescent Cell Viability Assay (Promega#G7570) is a method to determine the number of viable cells in culture based on quantitation of the ATP present, which signals the presence of metabolically active cells.

Cell were cultured in 96-wells black plates at a cell density of 10.000 cells/100μl /well) and incubated at 37°C and 5% CO2 for 24 hours. After incubation, cells were treated under the same conditions as the MTT test. After incubation, 100μl of fresh medium was replaced in each well and 100μl of CellTiter-Glo® Reagent were added directly to fresh medium. Addition of the reagent results in cell lysis and generation of a luminescent signal proportional to the amount of ATP present, which is directly proportional to the number of vital cells present in culture. In particular, the Assay generates a luminescent signal, produced by the luciferase reaction: the luciferase added to the cells is able to catalyze its substrate (luciferin) into oxyluciferin only in presence of ATP. The highest is the ATP content, the highest is the signal emitted by the oxyluciferin. The luminescent signal was measured by the EnSpire (Multimode Plate Reader – PerkinElmer).

3.3 Cell Uptake

^{64}Cu cell incorporation have been assessed measuring gamma-radiation emission through a gamma counter (Monogamma – l'acn, l'accessorio nucleare). ^{64}Cu cell incorporation was measured in all the cell lines at 24h, 48h, and 72h of treatment. Cells were grown on 100mm petri dish and seeded 24 hours before treatment at cell density of 2*106 cells/dish. At each timepoint two different concentrations

(C1= 6MBq, C2= 30MBq) were tested in duplicate. Cells treated with medium only served as a negative control. After incubation, surnatant was removed, then cells were washed with PBS , and a centrifugation at 1.400 rpm for 8 minutes let to separate pellet from surnatant. The activity was measured in the pellet and in all the surnatant fractions as counts per minutes. Cell pellets were stored at -80°C. The % of uptake was obtained as uptake in the pellet divided for the total activity measured. The uptake was normalized for the mg of total proteins contained in the cell pellet (see par.3.6 and par.3.7).

3.4 Subcellular ^{64}Cu Uptake

^{64}Cu uptake in the nucleus and in the cytoplasmatic fraction was also assessed. The detection of nuclear uptake was performed with the Nuclear Extraction Kit (abcam #ab113474) following the manufacturer's protocol. Cells were grown on 100mm petri dish, seeded and treated at the same conditions of par.3.3. Following treatments, cells were washed with PBS, scraped and centrifuged at 1150 rpm for 5 minutes. The cell pellet was resuspended in 400ul of 1XPre-Extraction Buffer and transferred to a microcentrifuge tube. Subsequently, the samples were incubated on ice for 10 minutes, then vortexed vigorously for 10 seconds and finally centrifuged for 1 minutes at 12.000 rpm. The surnatant, containing the cytoplasmatic fraction was removed and radioactivity was measured by a gamma counter. With regard to the nuclear pellet, it was added with 40μl of Extraction Buffer and incubated on ice for 15 minutes; during incubation the suspension was vortexed (5 seconds) every 3 minutes. After incubation the suspension was centrifuged 10 minutes at 14000rpm at 4°C and the supernatant was transferred to a new microcentrifuge tube. The radioactivity was measured also in the nuclear fraction.

3.5 Cytotoxicity and Genotoxity

To characterize radioresistant cell lines membrane permeability alterations (cytotoxicity) and DNA damage - induced γH2AX nuclear foci- (genotoxicity), as DNA double strand breaks (DSBs), were assessed with the HCS DNA Damage Kit (Invitrogen #H10292). Cells were seeded in 96-well black plates at a cell density of 10.000 cells/100ul x well and incubated at 37°C and 5% CO_2 for 24 hours.

Then, cells were incubated with treatment at different concentrations (C2= 0.034MBq, C3=0.34MBq, C4=1.7 MBq) tested in triplicate. After 24 hours of treatment the media was removed and replaced with 100μl/well of fresh FBS-depleted medium. Subsequently, 50μl/well of Image-IT DEAD green working solution was added and incubated 30 minutes at 37°C.

Image-iT® DEAD Green™ is a non-fluorescent and impermeant stain, but when the membrane permeability is compromised by $^{64}CuCl_2$ treatment, the stain is able to enter the cell forming highly fluorescent and stable complexes when bound to DNA. This property enables to make the discrimination between viable and dead cells. After incubation, the solution was removed, replaced with 100μl/well of Fixative solution and incubated for 15 minutes at room temperature. After washing with PBS 50μl/well of permeabilization solution was added, cells were incubated for 15 minutes at room temperature and after that, rinsed once with PBS. Afterwards, 100μl/well of blocking buffer were added and incubated for 1 hour. After blocking, primary antibody anti-pH2AX (50μl/well) was incubated for 60 minutes, wells were rinsed three times with PBS and secondary antibody solution containing Alexa Fluor 555 goat anti-mouse and Hoechst 33342 were added. The DSBs can be detected due to their capability to induce phosphorylation of the H2AX(Ser139) histones, forming DNA foci at the site of DNA DSBs. . After 60 minutes, wells were rinsed again three times with PBS. Finally,100μl of PBS was added to each well before proceeding to imaging. The plate was scanned in the EnSpire (Multimode Plate Reader – PerkinElmer) able to read the different fluorescent signals: the nuclear fluorescence intensity of Image-iT® DEAD GreenTM viability stain was assessed with FITC filter (Excitation=490 nm, Emission=525 nm); the fluorescence intensity of pH2AX signal was determined by using TRITC channel (Excitation=557 nm, Emission=576 nm) and to define the nucleus with Hoechst 33342 the DAPI filter was used (Excitation=358 nm, Emission=461 nm).

The same protocol was used for immunofluorescence microscope assay, to confirm quantitative data obtained by EnSpire by representative microscope images, with the only difference that cells were seeded in a chamber slide with a removable 3 well silicone chamber (Ibidi) at cell density of 105 cells/well/ml and tested in duplicate. Untreated cells (treated with medium only) were considered as negative control. Image analysis was performed using an Axio Imager M1 microscope (Carl

Zeiss, Oberkochen, Germany) and a computerized image analysis system (AxioCam MRc5) equipped with dedicated software (AxioVision Rel 4.8).

3.6 Protein extraction

Whole-cell protein extraction was performed from cell pellet obtained from the cell uptake assay (par. 3.3). The extraction was performed after 24h, 48h, and 72h of treatment. Pellets were lysed with a Lysis Buffer consisting of RIPA Buffer added with Phosphatase and Protease Inhibitors (1%) to prevent protein degradation or modification. In particular, 75μl of the Lysis Buffer was added to each sample, vortexed and maintained in agitation at 4°C for 2 hours. After that a centrifugation at maximum speed (14000 xg) for 15 minutes at 4°C was performed. The surnatant, containing the proteins, was collected and stored at -20°C until use.

3.7 Protein dosage

Protein dosage have been performed with the Bio-Rad Protein Assay, a simple, accurate colorimetric assay for total protein measurement (Bio-Rad Protein Assay Dye Reagent Concentrate, #5000006, BioRad), based on the Bradford method.
The method was used to dose protein obtained as described in par.3.6.
The Dye Reagent Concentrate was diluted 1:5 with distilled water. After that, using 2ml tubes, 999 μl of the Dye Reagent Diluted solution were added to 1μl of each sample. The Dye Reagent contains the Coomassie Blue dye that is able to bind to protein amino acid residues, and a differential color change of the dye occurs in response to various concentrations of protein: as the protein concentration increases, the color of the sample becomes darker.
The solution was then mixed and 200μl of each sample was added to a 96-wells plates. The plate was measured at 595 nm with a UV-Vis spectrophotometer considering that this value is the maximum absorbance of the dye.

3.8 miRNA analysis

3.8.1 RNA extraction

RNA extraction from cell pellet

In order to identify miRNAs deregulated in the cell lines, the mir*Vana*™ PARIS™ Kit was used to extract the RNA. The extraction was performed starting from cell pellets of 25 cm2 flasks at 80% confluence. The RNA extraction took place 48 hours post-seeding for the sensitive (U87MG and U373MG) and resistant cell lines (U87MG-RR and U373MG-RR). Resistant cell lines received a maintenance dose of $^{64}CuCl_2$ 24h before RNA extraction. The RNA extraction was performed following the supplier's protocol. Cells were pelleted and placed on ice and 300µl of ice-cold Cell Disruption Buffer was added, and the samples vortexed. For each sample the lysate was transferred to a new tube containing an equal amount of 2X Denaturing solution and incubated on ice for 5 min. After incubation, a volume of 600µl of the solution Acid-Phenol:Chloroform was added, the mix was vortexed for 60 seconds and a centrifugation was performed at maximum speed (10,000 x g) at room temperature for 5 min to separate the mixture into the aqueous and organic phases, respectively. The Acid-Phenol:Chloroform extraction provides a robust front-end purification that also removes most DNA. Centrifugation permits to separate the aqueous RNA-containing (upper) phase from the inter- and lower-phase and collect it to a new tube. Following the organic extraction, 1.25 volumes of 100% ethanol was added to the aqueous phase and mixed. 700µl of the lysate was added to the Filter cartridge (placed in the collection tube) and centrifuged at 10,000 xg for ~15 seconds. The Filter Cartridge contains a glass-fiber filter which immobilizes the RNA and allows washing. The following steps regards RNA washing: 700µl of miRNA Washing Solution 1 was added to the filter cartridge and centrifugation at 10,000 xg for ~15 seconds was repeated. 500µl of Wash Solution 2/3 was added to the filtered cartridge and centrifuged as in the previous step. This step was repeated twice, after discarding the flowthrough a centrifugation at 10,000 xg for 1 minute was performed to remove residual fluid from filter. Finally, the Filtered cartridge was transferred to a new collection tube, added of 100µl of preheated (95°C) Elution Solution and a final centrifugation of 30 seconds led to recover RNA.

RNA extraction from Medium Exosome

Identification of miRNA from exosome released in cell culture medium was performed using the Total Exome Isolation Reagent (Invitrogen #4478359) that permits to isolate exosomes. Exosomes were isolated from the cell medium (DMEM, 1% L-Glu, 1% PS) 48h post-seeding. To ensure that isolated exosome originate from the cell the medium have been depleted of FBS for 24 hours. 2ml of cell media was centrifuged at 2000 xg for 30 minutes to remove cells and debris; 1ml of the supernatant, containing the cell-free culture media was transferred to a new tube and 500μl of Total Exome Isolation Reagent was added. The solution was vortexed and incubated at 4°C overnight. After incubation, the samples were centrifuged at 10,000 xg for 1 hour at 4°C, the pellet containing the exosomes collected and resuspended in 100μl of 1XPBS.

Exosome RNA s was extracted using the Total Exome RNA and Protein Isolation Kit (Invitrogen #4478545), following producer protocol. In particular 100μl of 1X PBS (total volume 200μl) and then 200μl of 2X Denaturing Solution were added; after mixing the solution was incubated on ice for 5 minutes and then added of 400μl of Acid-Phenol:Chloroform and vortexed for 30-60 seconds. From the organic extraction to the washing steps the same procedure of the previous paragraph was followed (RNA extraction from cell pellet).

The filter cartridge was transferred into a fresh collection tube, applied 50μl of preheated (95°C) Elution Solution to the center of the filter and then centrifuged for 30 seconds. This step was repeated another time and the eluted RNA was collected.

RNA extraction from plasma exosome

Plasma samples

Plasma samples have been collected from patients enrolled in the phase I clinical trial titled "Phase I study of $^{64}CuCl_2$ as theranostic agent in patients with relapse or progression of glioblastoma multiforme (GBM)" (trial P.64Cu.GBM.2018). Before enrollment patients signed an Informed Consent for the inclusion in the clinical trial and the use of Banked biospecimens for research purposes (that is optional). The study was approved by the Ethics Committee of the University Clinical Center of the Republic of Srpska (Bosnia and Herzegovina), number of authorization 01-19-189.2/19.

The trial provides the enrollment of a total number of 16 patients; among those 10 patients will be analyzed for miRNA profiling, but at the moment, for this study 4 patients could be evaluated (G8: male, 34 years; G9: male, 43 years; G10: male, 62 years; G11: female, 55 years).

Patients were defined by nuclear medicine physicians as responder or non responder to treatment after comparing the PET/CT imaging obtained at day 0 with the Follow up imaging analysis. In particular, the response to $^{64}CuCl_2$, is expressed as objective responses defined as stable disease, reduction or disappearance of tumor mass as measured by imaging pre- and post-treatment and defined by RANO criteria.

For miRNA analysis was necessary to collect venous blood at two timepoints:

- blood samples collection at day 0, baseline - before first drug administration;
- blood samples collection at day 42, after 6 treatments of Copper chloride.

RNA extraction

15 ml of blood have been collected at two timepoint (pre-$^{64}CuCl_2$ treatment and at day 42) in commercially available anticoagulant-treated tubes (EDTA-treated Vacutainer). After collection, whole blood was immediately centrifuged at 1300 xg for 20 minutes at 4°C; the resulting plasma was transferred to a new tube and subjected to an additional centrifugation at 15000 xg for 10 minutes at 4°C. The resulting plasma was aliquoted and stored at -80°C until RNA extraction.

Exosomes RNA extraction was performed using the exoRNeasyMidi kit (Qiagen # 77144), following the manufacturer's protocol as schematized in Figure 17, 400μl of the filtered plasma sample were added to 400μl of XBP, mixed, loaded to the exoEasy spin column, and spun for 1 min at 500 x g. After that, exosomes bound to the spin column were washed with 3.5 ml of Buffer XWP, added to the exoEasy Midi spin column and removed by centrifugation. The spin column was transferred to a fresh collection tube, and 700μl of QIAzol were added to the column to lyse vesicles. After centrifugation, 90μl of chloroform were added to the collected eluate, the solution was incubated for 3 minutes. After incubation, a centrifugation at 12,000 x g for xx min at 4°C let to obtain 3 phases: 400 μl of the upper phase, containing the exosomal RNA, was transferred to a new collection tube with 800μl of 100% ethanol. The solution was added into the Rneasy MinElute spin column

and the column was then washed one time with Buffer RWT and twice with Buffer RPE. Finally, 14 µl of RNase free-water were added and the centrifugation in a new collection tubed, led to recover the exosomal RNA.

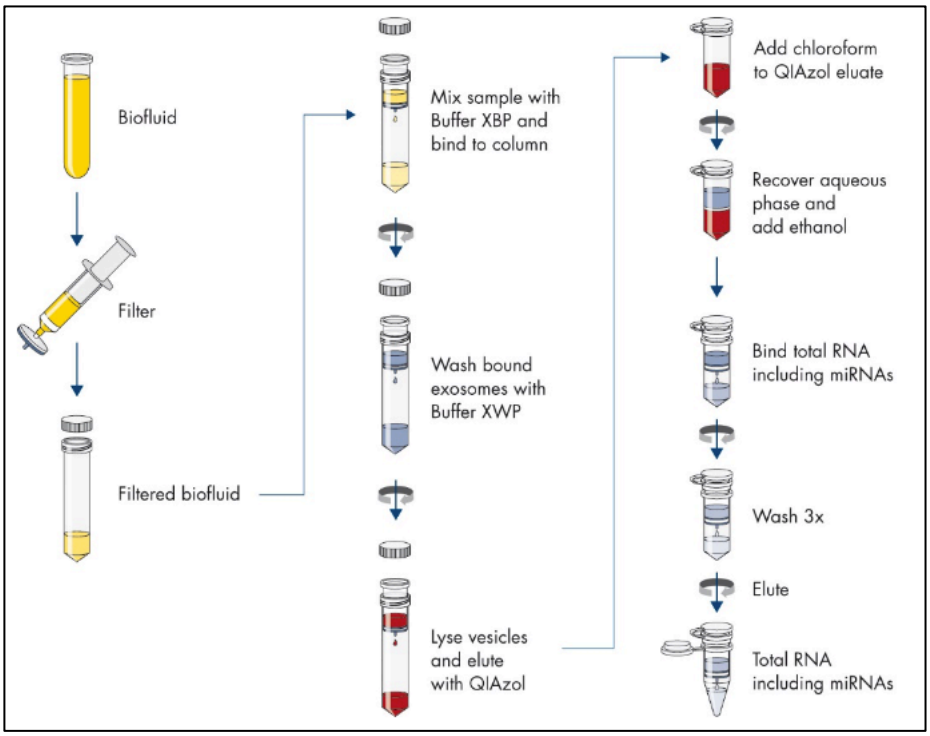

Figure 17. The exoRNeasy Midi kit procedure

3.8.2 RNA quantification

RNA quantification was necessary only for the RNA obtained from cell pellet. RNA has been determined using NanoDrop® 2000c, UV-visible spectrophotometer (220-750 nm) that allows to perform sample microvolume measurements (up to 1 µL) with high accuracy and reproducibility. Furthermore, the instrument allows to quantify even volumes of high concentrations samples, without having to make dilutions in order to obtain reliable measurements. Nanodrop technology exploits the surface tension exerted by small volumes placed between two neighboring surfaces. The voltage is developed by the reading plates of the instrument on which 1 µL of sample is placed. The reading plates are connected to two optical

Table 8. RNA samples concentration

N.	Sample	Conc. ng/µl	Abs 260/280 nm
1	U87MG (a)	328	2.10
2	U87MG-RR (a)	227.2	2.09
3	U373MG (a)	149.3	2.13
4	U373MG-RR (b)	313.0	2.13
5	U87MG (a)	728.2	2.12
6	U87MG-RR (a)	396.2	2.11
7	U373MG (a)	209.4	2.14
8	U373MG-RR (b)	255.6	2.12

fibers and the instrument source is a Xenon lamp. The instrument is connected to a software that directly processes the data, providing the absorption spectrum, concentration (ng/μL) and purity of the sample (Abs 260/280 nm).
The concentrations in Table 8 show the data obtained for the samples from cell pellet. Before proceeding with the following step RNA concentration has been diluted with water to a final concentration of 5ng/μl.

3.8.3 Reverse transcription reaction

To prepare cDNA templates from Retrotranscription reaction have been used TaqMan® Advanced miRNA cDNA Synthesis Kit (#A25576 Thermofisher Scientific) following producer protocol. The procedure to prepare the cDNA templates is composed by 4 steps:

1) poly(A) tailing reaction
2) adaptor ligation reaction
3) reverse transcription (RT) reaction
4) miR-Amp reaction

In the first stage of the workflow mature miRNAs from total RNA are modified by extending the 3' end of mature transcript through poly(A) addition (step 1) then, lengthening the 5' end by adaptor ligation. The modified miRNAs then undergo universal reverse transcription followed by amplification to increase uniformly the amount of cDNA for all miRNAs (miR-Amp reaction).

Step 1- poly(A)tailing reaction

In the first step 2μl of the sample has been added to 3μl of the Poly(A)Reaction Mix, prepared as shown in Table 9. The tubes were put in the thermal cycler using the following settings and standard cycling:

Table 9. Poly (A) Reaction Mix components

Poly(A) Reaction mix components	Volume for each sample (μL)
10X Poly(A)Buffer	0.5
ATP	0.5
Poly(A)Enzyme	0.3
RNase-free water	1.7
Total	3.0

Table 10. Poly(A) reaction PCR program

Step	Temperature	Time
Polyadenilation	37 °C	45 min
Stop reaction	65°C	10 min
Hold	4°C	∞

Step 2- adaptor ligation reaction

In the second step 10μl of Ligation Reaction Reaction Mix (Table 11) were transferred to each tube containing the poly(A) tailing reaction product. Before inserting the tubes in the thermal cycler (Table 12) they were shaked at 1,900 rpm for 1 min.

Table 11. Ligation Reaction Mix components

Ligation Reaction mix components	Volume for each sample (μL)
5X DNA Ligase Buffer	3
50% PEG 8000	4.5
25X Ligation Adaptor	0.6
RNA Ligase	1.5
RNase-free water	0.4
Total	3.0

Table 12. Ligation reaction PCR program

Step	Temperature	Time
Ligation	16 °C	45 min
Hold	4°C	∞

Step 3- reverse transcription (RT) reaction

In this step 15μl of the RT Reaction Mix (Table 13) were transferred to each tube containing the adaptor ligation reaction product.

Table 13. RT Reaction Mix components

Ligation Reaction mix components	Volume for each sample (μL)
5X RT Buffer	6
dNTP Mix	1.2
20X Universal RT Primer	1.5
10X RT Enzyme Mix	3
RNase-free water	3.3
Total	15

Table 14. RT PCR program

Step	Temperature	Time
Polyadenilation	42 °C	15 min
Stop reaction	85°C	5 min
Hold	4°C	∞

Step 4- adaptor ligation reaction

In this step 45μl of the miR-Amp Reaction Mix were transferred to a new tube and 5μl of the RT reaction product were added to have a final volume of 50μl per tube. Reaction in the thermal cycler followed the program in Table 16.

Table 15. miR-Amp Reaction Mix components

Ligation Reaction mix components	Volume for each sample (µL)
5X DNA Ligase Buffer	3
50% PEG 8000	4.5
25X Ligation Adaptor	0.6
RNA Ligase	1.5
RNase-free water	0.4
Total	3.0

Table 16. miR-Amp PCR program

Step	Temperature	Time	Cycles
Enzyme activation	95 °C	5 min	1
Denature	95°C	3 sec	14/16*
Anneal/extend	60°C	30 sec	
Stop reaction	99°C	10 min	1
Hold	4°C	∞	1

*for plasma samples 16 cycles

3.8.4 Endogenous Control RT-PCR

TaqMan® Advanced miRNA Assay miR-16-5p (A25576- Applied Biosystems) have been used for quantification of miRNA expression levels by qPCR analysis.

The cDNA template as miR-Amp reaction product have been diluted 1:10 with RNase free water (1µl of sample plus 9µl water). After transferring 7.5 µl of the PCR reaction Mix (Table 17) into PCR reaction plate (MicroAmp® Optical 96-well Reaction Plate-applied biosystems) 2.5 µl of the sample was added to each reaction well. The reaction plate has been loaded into 7900HT RT-PCR (Applied Biosystems) and the setting conditions have set up (Table 18).

Table 17. PCR Reaction Mix components

Component	Volume for each sample (µL)
TaqMan Fast Advanced Master Mix (2X)	5
TaqMan Advanced miRNA Assay (20X)	0.5
RNase-free water	2
Total	7.5

Table 18. Real-time PCR program

Step	Temperature	Time	Cycles
Enzyme activation	95 °C	20 sec	1
Denature	95°C	3 sec	40
Anneal/extend	60°C	30 sec	

3.8.5 miRNA profiling

In this step the DNA polymerase amplifies the preamplified cDNA using sequence specific primers and TaqMan of the MicroRNA Arrays probes. The TaqMan® MicroRNA Arrays are a set of two microfluidic cards with each 384 wells (Array A

and Array B) containing anhydrous TaqMan primers and probes. The assay allows for the quantification of gene expression levels of 384 miRNAs including their endogenous controls (Figure 19). This analysis takes place by loading the produced cDNA into the arrays and analyzing in Real-Time PCR. Each Card is composed by 8 port, in each port is charged 100µl of the sample (Figure 18).

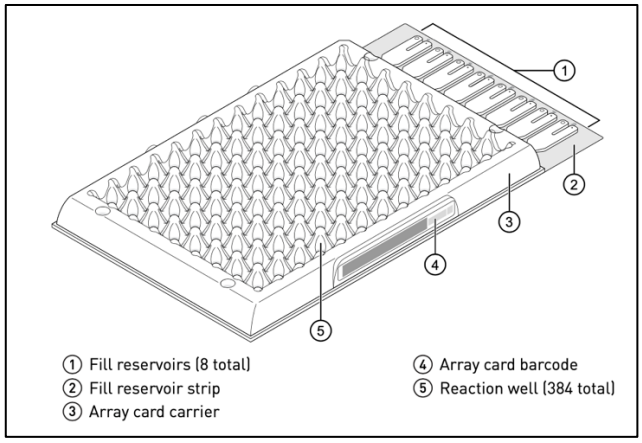

Figure 18. Card rapresentation

The cDNA template (miR-Amp reaction product) id diluted 1:10 with RNAase free water and for each card 212.5 µl of diluted cDNA template has added to TaqMan Fast Advance Master Mix as reported in Table 19.

Table 19. Reaction components for the Arrays

Component	Volume for each sample (µL)
Diluted cDNA template	220
TaqMan Fast Advanced Master Mix (2X)	440
RNase-free water	220
Total	880

Table 20. Real-time PCR program Array

Step	Temperature	Time	Cycles
Enzyme activation	95 °C	10 min	1
Denature	92°C	1 sec	40
Anneal/extend	60°C	20 sec	

The filled card is centrifuged and the thermal program for the 7900HT RT-PCR has set up as in Table 20.

For the correct use of the TaqMan™ MicroRNA Arrays the guidelines provided in the TaqMan Array User Guide protocol have been followed.

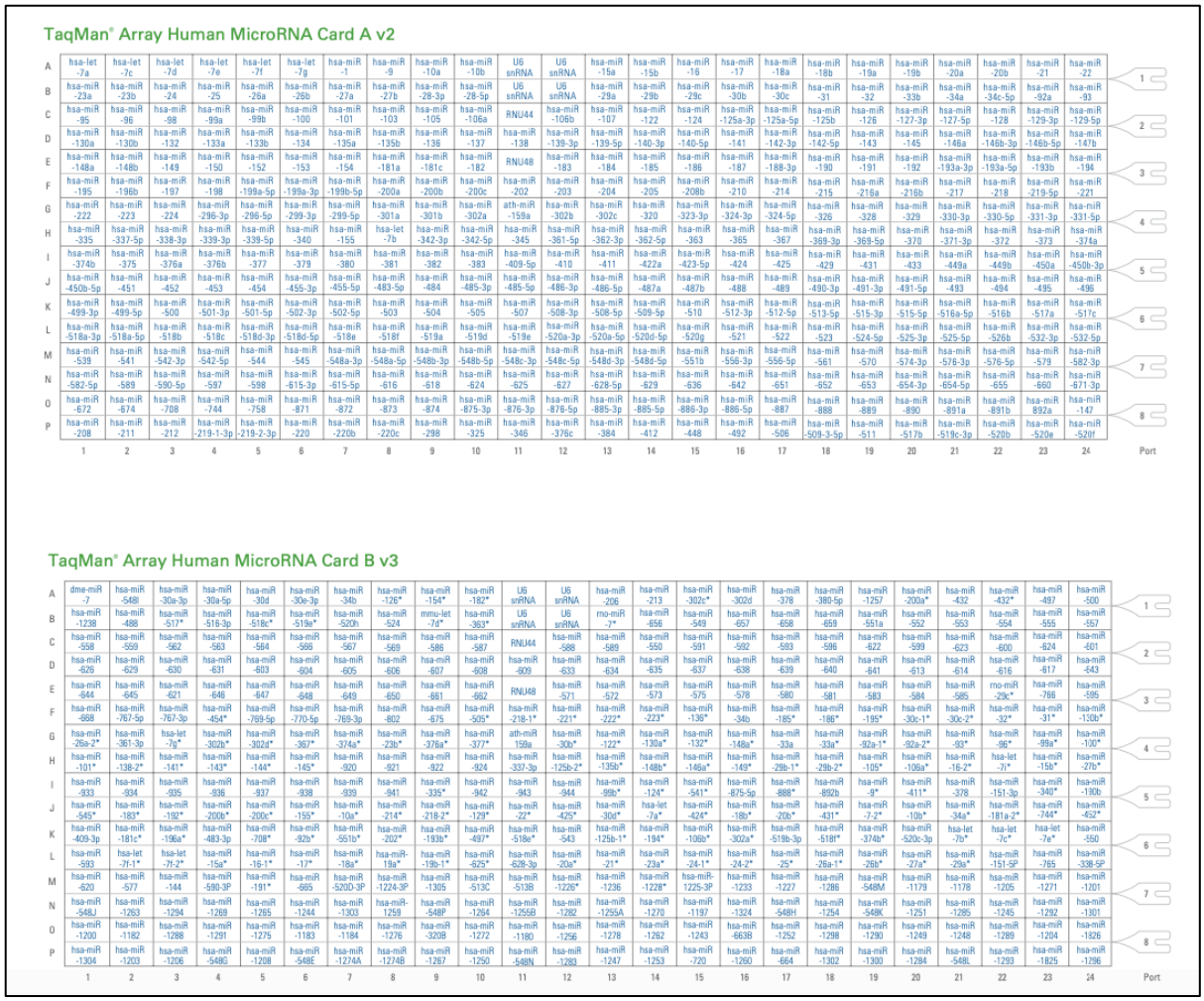

Figure 19. TaqManMicroRNA Arrays. Pool A Card and Pool B Card

miRNA expression levels normalization

I TaqMan® MicroRNA Arrays Ct data have been normalized on the basis on the endogenous miRNA has-miR-16-5p. Endogenous controls are reference genes that have an expression level that remain constant for all the samples independently of the experimental treatment. has-miR-16-5p was chosen as reference gene based on literature data (Lai et al., 2014; Yue et al., 2016; Zhang R et al., 2016; Lang et al., 2017).

Endogenous control was identified with a RT-PCR preliminary phase as explained in par.3.1.4. Pool A Cards contain 5 wells that amplify this control, whereas Pool B Cards contain 4 wells. Among the 768 Ct value analyzed for each Card, the samples with a Ct value ≥35 cycles were excluded considering the expression under the quantification limit. In fact, Ct value is inversely proportional to miRNA expression. Ct raw values have been used for the analysis and quantification of

genetic expression with the ΔΔCt method. The Ct average value of the control have been used for TaqMan Arrays miRNA normalization. For each single miRNA contained in the Card was calculated the ΔCt value as difference between the Ct value of each miRNA sample and miRNA endogenous control (*ΔCt = Ct (miRNA sample) – Ct (miR-16-5p)).*

3.8.6 *In silico* analysis

The target genes of the selected miRNAs were predicted by miRNET (https://www.mirnet.ca), a web-based platform designed to help elucidate microRNA (miRNA) functions by integrating users' data with existing knowledge via network-based visual analytics.

The platform has been used to perform Kyoto Encyclopedia of Genes and Genomes (KEGG) pathway analysis. The KEGG analysis was performed to also identify enrichment of deregulated miRNA target genes, which have been mapped to specific pathways. The p-values were calculated using hypergeometric tests and Benjamini–Hochberg FDR adjustment was used for multiple test correction. An FDR-adjusted p-value < 0.05 indicated the corresponding pathways are enriched in putative target genes.

3.9 Statistical analysis

After normalization of miRNA data of cell culture experiments, the analysis has been performed with the ΔΔCt method. To compare miRNA expression of the cell pellet and the miRNA released in the media the value of ΔΔCt was calculated as ΔΔCt = [ΔCt (Cell) - ΔCt (Exo)]. The ΔΔCt was calculated both for the Sensitive cell lines and for the Radioresistant ones. P-value calculation was performed with T-test. Only miRNA showing $-2 \geq \Delta\Delta Ct \geq +2$ and value <0.05 have been selected. Moreover, also in the miRNA expression comparison between sensitive and resistant cell lines the ΔΔCt have been used calculated as ΔΔCt= [ΔCt (Sensitive) - ΔCt (Resistant)], even in this case p-value calculation with t-test and selection of miRNA with $-2 \geq \Delta\Delta Ct \geq +2$ and pvalue <0.05.

The sample size of miRNA profiling from plasma sample is very small, and patient stratification have led to divide patients in only 1 non responder and 3 responders. Therefore, it was difficult to apply strong statistical analysis in this very small

samples. These are preliminary data that will need to be analyzed in a bigger cohort in which a statistical analysis can be applied. In this analysis the best tools to our knowledge have been used to render the data as much as possible realistic. miRNA levels contained in plasma exosomes of patients were calculated with the software miRNET. The Ct values of the timepoint (t0) were compared with the (t42) values (baseline Vs post-treatment) of the 3 patients Responder using Limma test. 9 miRNAs were identified with a p-value ≤ 0.05. Microsoft Excel was used as analytical tool to calculate the $\Delta\Delta$Ct values as $\Delta\Delta Ct = \Delta Ct\ (t0) - \Delta Ct\ (t42)$. The $\Delta\Delta$Ctvalues of the Responders were compared to the Non-responder patients, selecting the miRNAs with an opposite direction in all the 3 responder patients comparing to the Non-Responder patients.

The miRNA expression only at t(0) was performed with the $\Delta\Delta$Ct method. $\Delta\Delta$Ct of each responder patient was calculated subtracting the ΔCt of the Non responder patient ($\Delta\Delta Ct = \Delta Ct$ [Responder patient]-ΔCt [Non-Responder patient]) obtaining 3 $\Delta\Delta$Ct values. Among these the miRNAs showing a $\Delta\Delta$Ct value for each patient equal to $-2 \geq \Delta\Delta Ct \geq +2$ have been selected.

For miRNA analysis differences were considered to be statistically significant at $p \leq 0.05$ after false discovery rate [FDR] correction.

All experiments were performed ≥ 3 times and all the values are presented as mean ± SEM. Statistical evaluation for data analysis was performed using student's t-test. Differences were considered to be statistically significant at $p \leq 0.05$. Analyses were performed using PRISM software (GraphPad Software, USA).

4. Results

4.1 Establishment of GBM radioresistant lines

The research activity initially focused on the selection of the best dosage for the treatment of the GBM cell lines U87MG and U373MG with $^{64}CuCl_2$.

On the basis of preliminary tests 5 concentrations were selected as reported in Table 21.

Table 21. $^{64}CuCl_2$ radioactivity range	
C1	0.0034 MBq
C2	0.034 MBq
C3	0.34 MBq
C4	1.7 MBq
C5	3.4 MBq

These ranges have been selected on the basis of the dose reaching the brain lesion in the first three GBM patients enrolled in the phase I clinical trial (P.64Cu.GBM.2018). In particular, the volume of the brain lesion and the dose (in MBq) that reaches the lesion in comparison to the total activity administered was determined through PET/CT examination. The dose reaching the lesion (average of the three patients) and the volume of the lesion have been used to make a comparison with the cell density for in vitro tests.

Cell survival curve and corresponding IC50 were determined through Cell viability tests. The 5 concentrations have been tested with both MTT test and CellTiter-Glo® Luminescent Cell Viability Assay. Data are reported only for CellTiter-Glo (Figure 20) as at the high concentrations (C4 and C5) MTT assay showed false positive results.

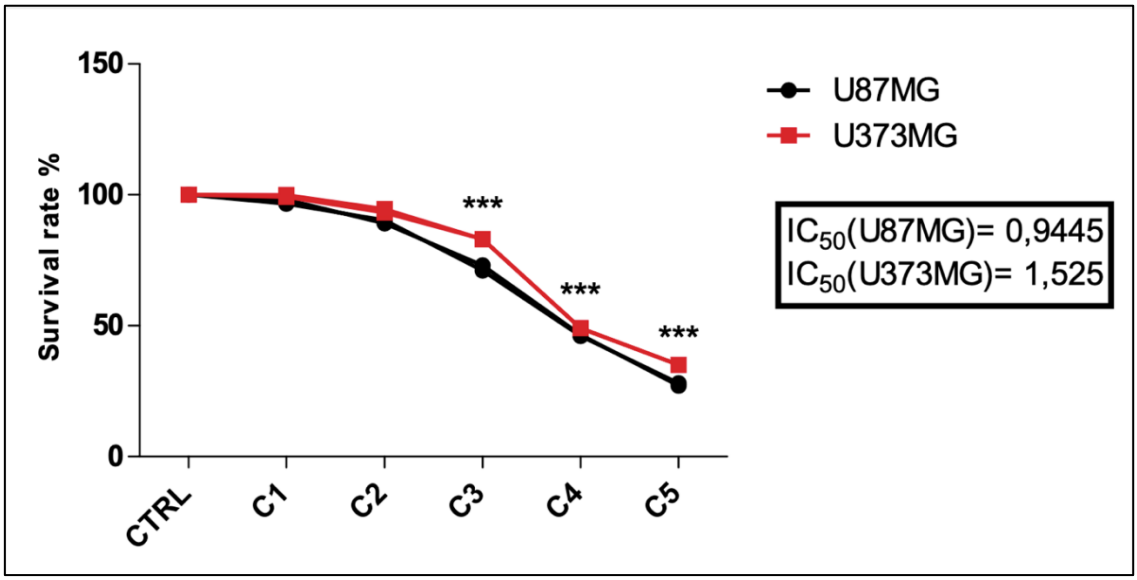

Figure 20. Cell survival curves for U87MG and U373MG (CellTiter-Glo® Luminescent Cell Viability Assay). Untreated cells were used as a control (* p ≤ 0.001).**

The viability of both cell lines was significantly affected from the concentration C3 equal to 0.34 MBq. The two cell lines showed a similar trend, even the U373MG line exhibited a higher IC50 value compared to the U87MG line (1.52 MBq vs 0.94 MBq) suggesting a more difficult capability of copper chloride to induce a cell-killing effect in this cell line.

These findings were crucial to establish the concentration to be used in the subsequent functional studies. In addition, the calculated IC50 was decisive for the generation of the in vitro radioresistant model. Radioresistant cell lines U87MG-RR and U373MG-RR were generated by exposing the two radiosensitive GBM lines (U87MG, U373MG) to increasing doses of radiation for 32 weeks. The starting dose used for the treatments was C1 (Table 21) and the cell lines were treated up to the corresponding IC50 and maintained at this concentration until viability was not significantly affected comparing to control. In the U87MG-RR line a viability above 100% was also observed, suggesting a mechanism of cell adaptation to the treatment (Figure 21a)

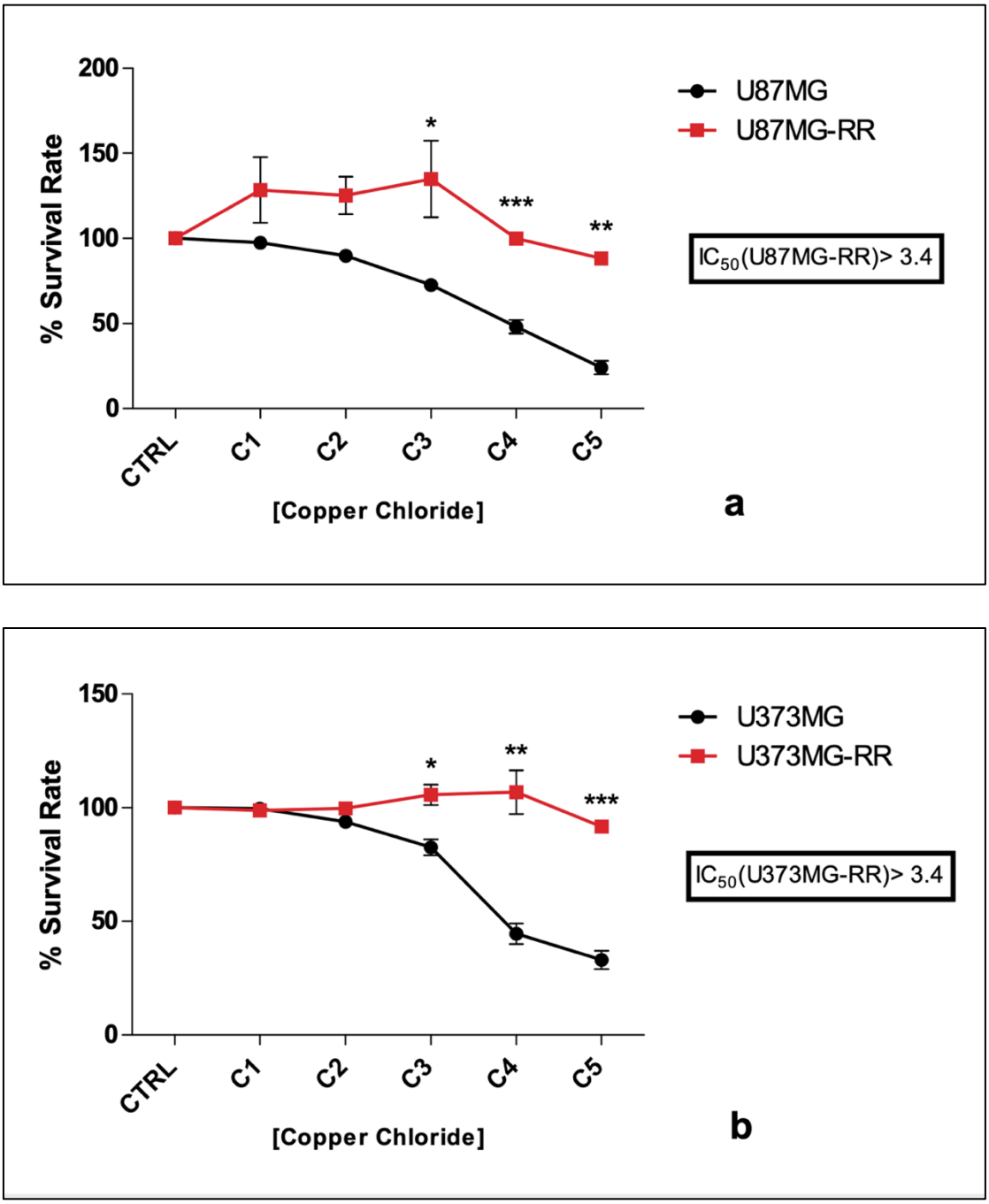

Figure 21. a) Survival curve of U87MG and U87MG-RR; b) Survival curve of U373MG and U373MG-RR. Value are expressed as mean ± SEM. (*p ≤ 0.05, **p ≤ 0.01 *** p ≤ 0.001 compared to sensitive lines).

4.2 Functional Studies

4.2.1 $^{64}CuCl_2$ cellular Uptake

Different studies were performed to characterize radioresistant lines and compare their behavior with the sensitive ones. In particular, $^{64}CuCl_2$ cellular internalization were tested at 24h, 48h, 72h after treatment with two different concentrations (C1= 6MBq, C2= 30MBq). Both the sensitive (U373MG and U87MG) and the radioresistant (U87MG-RR, U373MG-RR) lines were able to internalize $^{64}CuCl_2$; surprisingly at 24h the uptake was higher in the resistant cell lines than in the sensitive ones (Figures 22 and 23). The cell lines exhibited a different behavior as highlighted by comparing Figure 22 and 23. In particular, the uptake resulted higher in both U373MG and U373MG-RR compared to U87MG and U87MG-RR lines at 48h and 72h. Particularly, U87MG-RR showed a significantly higher uptake after 24h of treatment at both C1 and C2, compared to the sensitive line (Figure 22). On the contrary, U373MG-RR exhibited a lower uptake at C1, while is higher at C2, compared to U373MG, suggesting a dose-dependent grade of cell uptake.

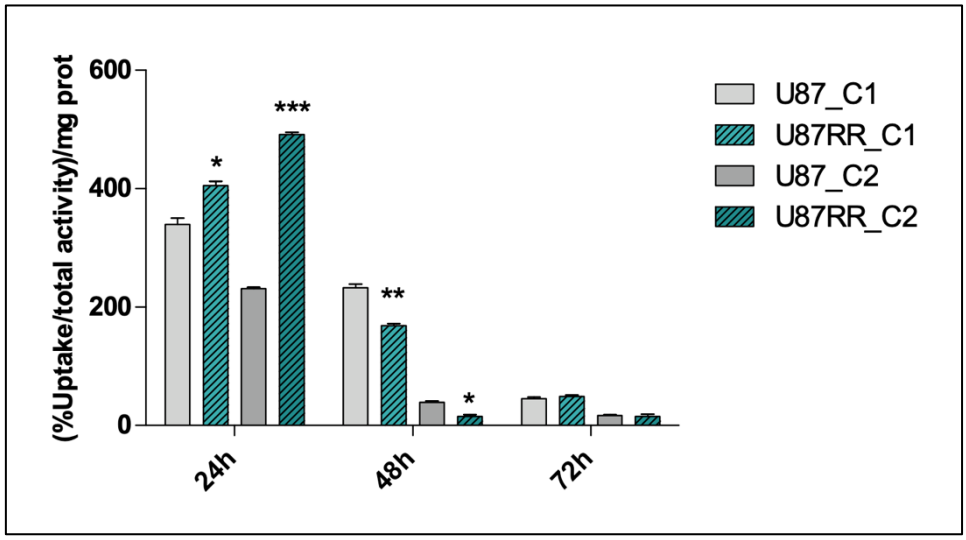

Figure 22. Copper-64 Cell Uptake in U87MG and U87MG-RR at two different concentrations C1=6MBq, C2=30MBq. Values are expressed as mean ± SEM. Statistical significance was calculated in comparison to the sensitive lines (*p ≤ 0.05, **p ≤ 0.01 *** p ≤ 0.001).

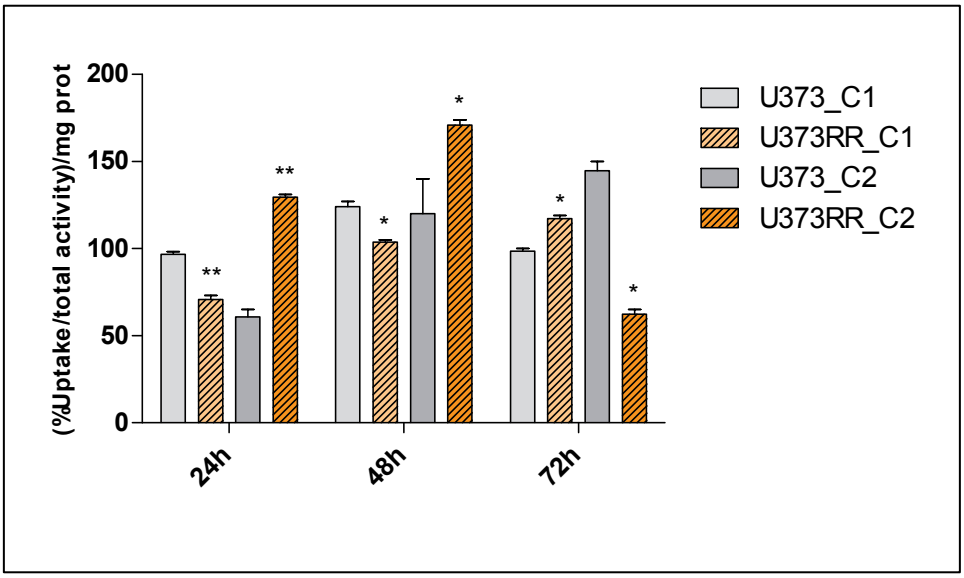

Figure 23. Copper-64 Cell Uptake in U373MG and U373MG-RR at two different concentrations C1=6MBq, C2=30MBq. Values are expressed as mean ± SEM Statistical significance was calculated in comparison to the sensitive lines (*p ≤ 0.05, **p ≤ 0.01 *** p ≤ 0.001).

The cell uptake in glioblastoma radioresistant cell lines was correlated to the Standardized Uptake Value (SUV_{max}) obtained from the PET/CT scans of the first 4 patients enrolled in the trial P.64Cu.GBM.2018. According to clinical data, 1 patient resulted non responder and the other 3 were classified as responder. Patients were classified in responder/non-responder on the basis of PET/CT examinations comparing the PET/CT imaging before and after treatment (follow up day 90). These preliminary results showed that the SUV_{max} of the non-responder patient was higher compared to the 3 responders (Table 22).

Table 22. SUV values of GBM patients		
Patient	**Day 90**	**Responder/**
	SUV_{max}	**Non resp.**
G8	1.5	Non Responder
G9	0.4	Responder
G10	0.6	Responder
G11	0.5	Responder

SUV, represent an index of tumor uptake in patients, therefore it can be correlated with the activity internalized by the cell lines. In particular, at high concentrations (C2), radioresistant cell lines showed an increased uptake in comparison to sensitive ones (Figures 22 and 23). These results are in analogy with what was observed in the 4 patients. In particular, the increased uptake in the radioresistant cells is in analogy with the high SUV observed in the non-responder patient (SUV=1.5), while the low uptake of $^{64}CuCl_2$ in sensitive cells is analogous to the low SUV observed in responder patients (SUV=0.5). Therefore, it would be interesting to confirm these results in a larger sample size in order to develop a method to evaluate sensitiveness to copper chloride: the signal intensity as capability to define cell uptake and treatment response.

4.2.2 $^{64}CuCl_2$ subcellular Uptake

In addition to cell internalization, the study focused on the distribution of $^{64}CuCl_2$ in the nuclear and cytoplasmatic fractions. Radioactivity was measured both in the sensitive and the radioresistant cell lines, at all the time points and for both the concentrations tested in the internalization test. The results showed a ^{64}Cu uptake from the nucleus in both sensitive and resistant cells of both the lines, however with different profiles (Figures 24 and 25). In general, U373MG and U373MG-RR showed a higher uptake at 24h compared to U87MG and U87MG-RR. With regard to the U87MG and U87MG-RR lines (Figure 24), radioactivity slowly migrate, in a similar way between the two lines and at both tested concentrations, into the nucleus, starting with a 5% of nuclear internalization at 24h up to 20% at 72h. In the U373MG and U373MG-RR cell lines (Figure 25) the nuclear uptake reached, at different times, different highest values according to the radiosensitivity status. In particular, differently from U87MG and U87MG-RR, nuclear uptake was not directly correlated to time and to concentrations. In fact, at 24h U373MG and U373MG-RR showed a similar uptake, differently from 48h and 72h results. After 48h of treatment a higher nuclear internalization was shown in U373MG-RR comparing to the sensitive one at both concentrations, reaching the 34% with 6 MBq for U373MG-RR (Figure 25-a). Indeed, at 72h the maximum nuclear uptake was with 30 MBq for the U373MG line (~40%;Figure 25-b).Overall, these results suggest that the U373MG and U373MG-RR lines have higher nuclear uptake comparing to U87MG and U87MG-RR.

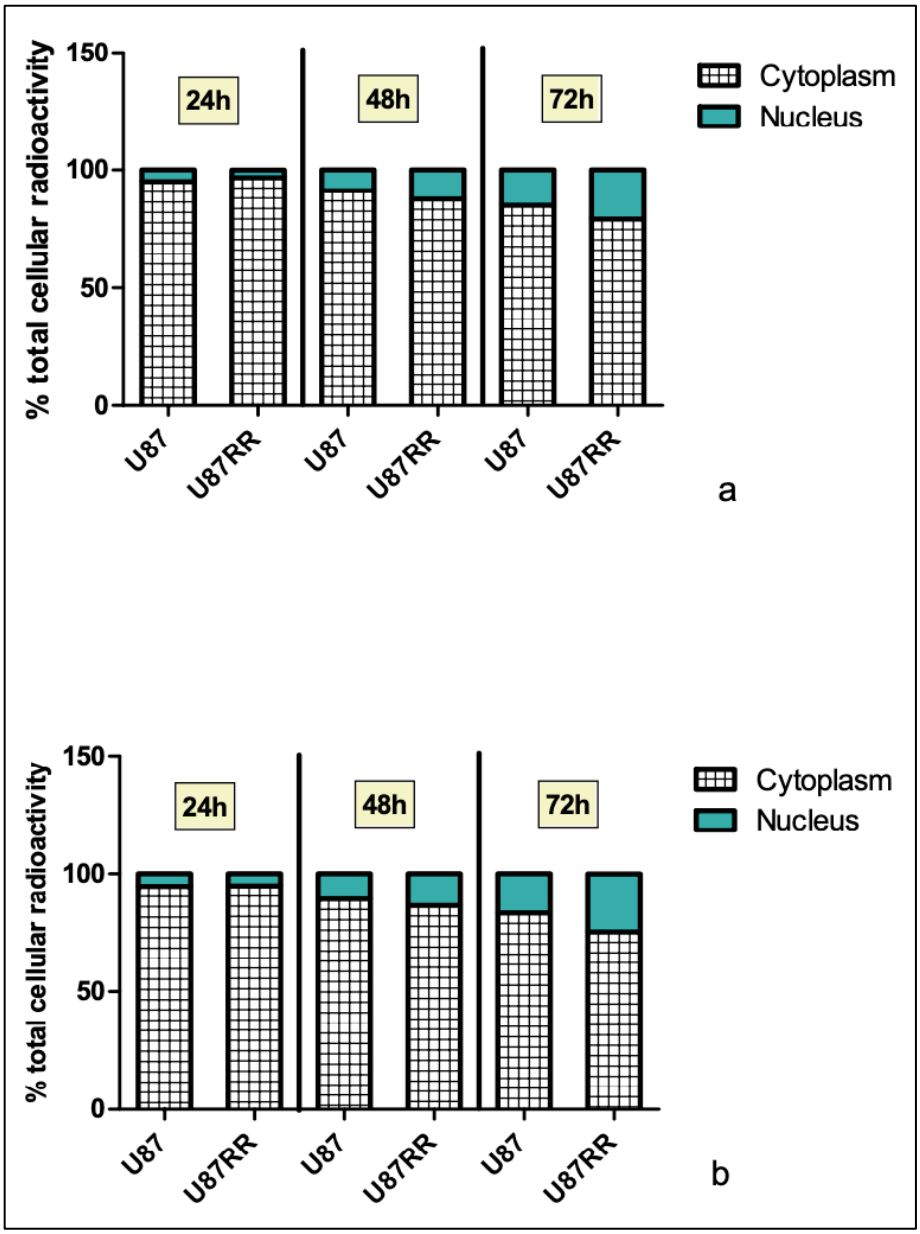

Figure 24. Subcellular distribution of $^{64}CuCl_2$ in U87MG and U87MG-RR at 6MBq (a) and 30MBq (b).

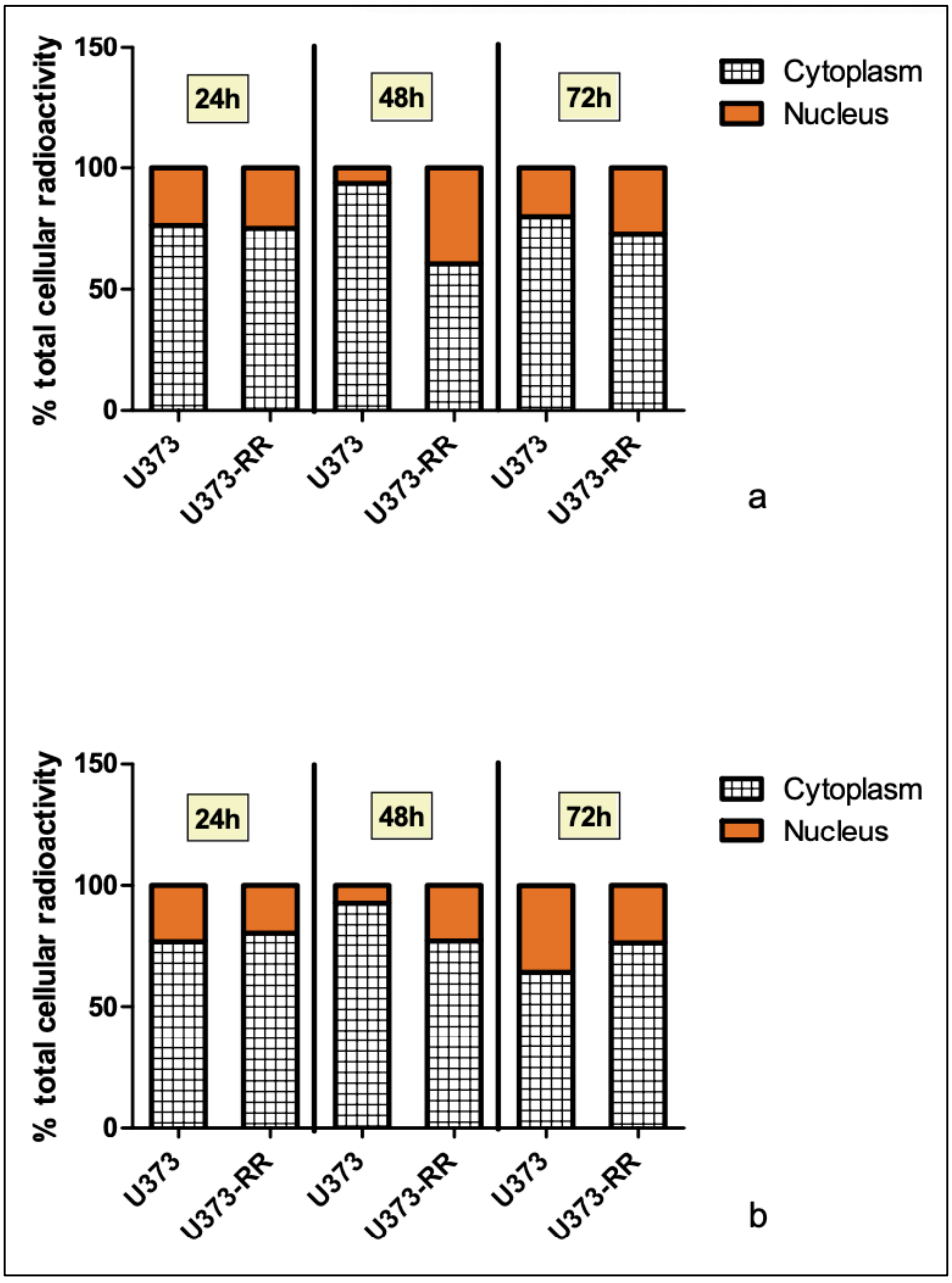

Figure 25. Subcellular distribution of $^{64}CuCl_2$ in U373MG and U373MG-RR at 6Mbq (a) and 30MBq (b).

4.2.3 Cytotoxicity and Genotoxicity

Afterwards, the study focused on cytotoxicity and genotoxicity, analyzing respectively membrane permeability alterations and DNA Double-Strand Breaks (DSBs), after copper chloride treatment of both sensitive and radioresistant cell lines. The data highlighted an increase in membrane permeability and DSBs with increasing dose, in both the radiosensitive lines U87MG and U373MG. In particular, regarding membrane permeability, U373MG exhibited significantly higher signal compared to control, whereas the U373MG-RR line showed a reduction in membrane permeability compared to control (Figure 26-a). Regarding the γH2AX DNA foci, also in this case the U373MG displayed a significantly increased value at all the concentrations compared to control; whereas the U373MG-RR was not affected by the treatment, at any tested concentrations, compared to control (Figure 26-b). The quantitative data were confirmed by the representative immunofluorescence microscope images, in which the membrane permeability is represented by the green signal while the γ-H2AX DNA foci are shown in very small red points (Figure 26-c). The images make the differences between the lines stand out, in particular resulted evident the red signal in the U373MG treated with C3, compared to the untreated (ctrl-U373MG), moreover this difference was not highlighted in the radioresistant line. Furthermore, the analysis showed alteration of membrane permeability, in particular the reduction of the green signal in U373MG-RR line compared to the control (ctrl U373MG-RR). Data obtained for U373MG and U373MG-RR were similar to the one obtained for U87MG and U87MG-RR both for membrane permeability and DNA DSBs. In fact, a significant value was obtained in membrane permeability for the treated U87MG lines compared to control for C3 and C4; on the contrary not significantly reduction in membrane permeability was observed for the U87MG-RR (Figure 27-a). Also, for γH2AX DNA foci U87MG line showed a higher signal compared to control, but this behavior is completely different from the U87MG-RR line in which there was no significant alteration by comparing treated cells to control.

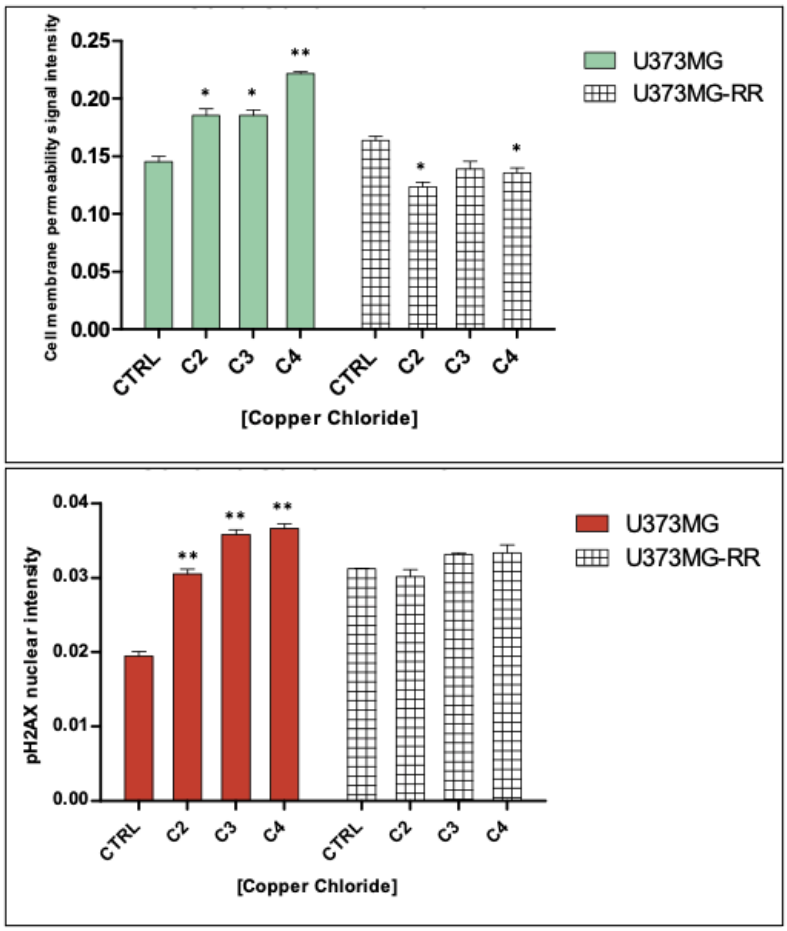

Figure 26. U373MG and U373MG-RR quantitative representation of (a) membrane permeability (b) DNA DSBs at incremental concentrations of $^{64}CuCl_2$. Values are expressed as mean ± SEM. Statistical significance was calculated in comparison to control (*p ≤ 0.05, **p ≤ 0.01). (c) immunofluorescence microscope images Magnitude 40X

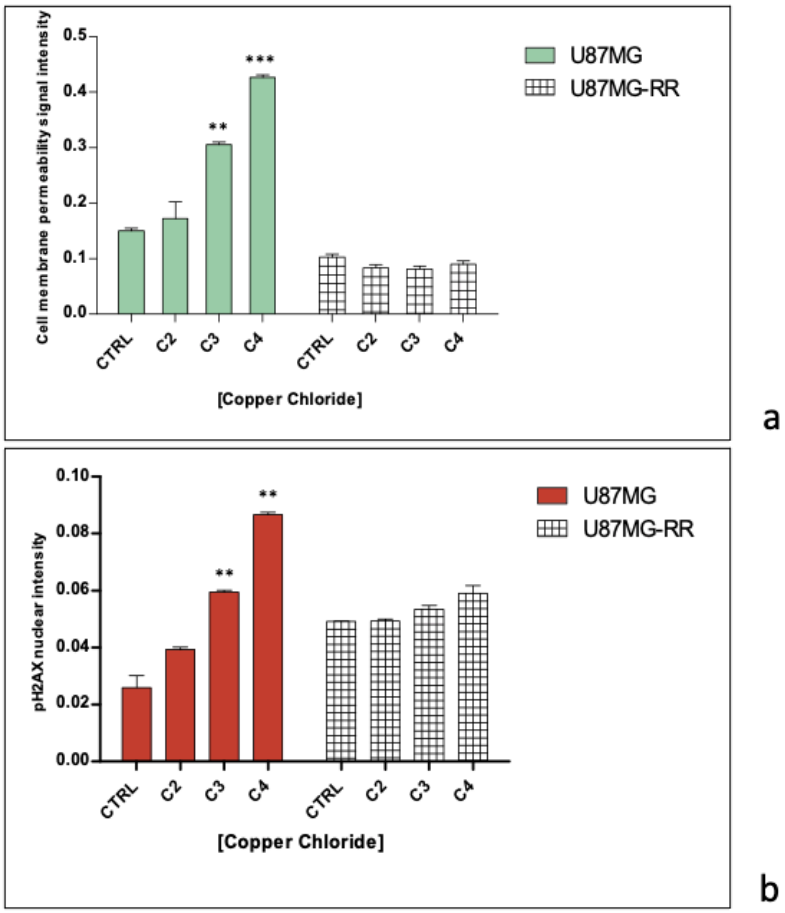

Figure 27. Quantitative representation of membrane permeability (a) and DNA DSBs (b) in U87MG and U87MG-RR at incremental concentrations of $^{64}CuCl_2$. Values are expressed as mean ± SEM. (*p ≤ 0.05, **p ≤ 0.01, ***p ≤ 0.001, compared to control).

4.3 miRNA analysis

4.3.1 GBM cell lines and exosomal miRNA profiling

In order to identify miRNAs differentially expressed under $^{64}CuCl_2$ treatment, miRNA expression was investigated in the sensitive and radioresistant lines. In addition, the profiling was conducted in exosomal miRNAs released in the culture medium of both cell lines.

Cellular and exosomal miRNAs analysis in radiosensitive and radioresistant cell lines.

The analysis focused on the identification of miRNAs expression deregulation comparing cellular and exosomal miRNAs in both radiosensitive (U87MG and U373MG) and radioresistant (U87MG-RR and U373MG-RR) cell lines. With regard to both the radiosensitive lines, 56 miRNAs showed deregulated expression in exosomes compared to cells (Figure 28–a). An in-silico search identified 272 validated target genes, that are involved in different signaling pathways among which are noteworthy the pathway of gene expression, intrinsic pathways of apoptosis, signaling by NGF, NGF signaling via TRKA from the plasma membrane. Nerve growth factor (NGF), and its signaling pathway, is known to promote survival and innervation of sympathetic and sensory neurons, indeed it is involved in cell death/survival processes. In GBM NGF resulted a significant promoter of pro-migratory and pro-proliferative activities of GBM cells (Brown et al., 2008).

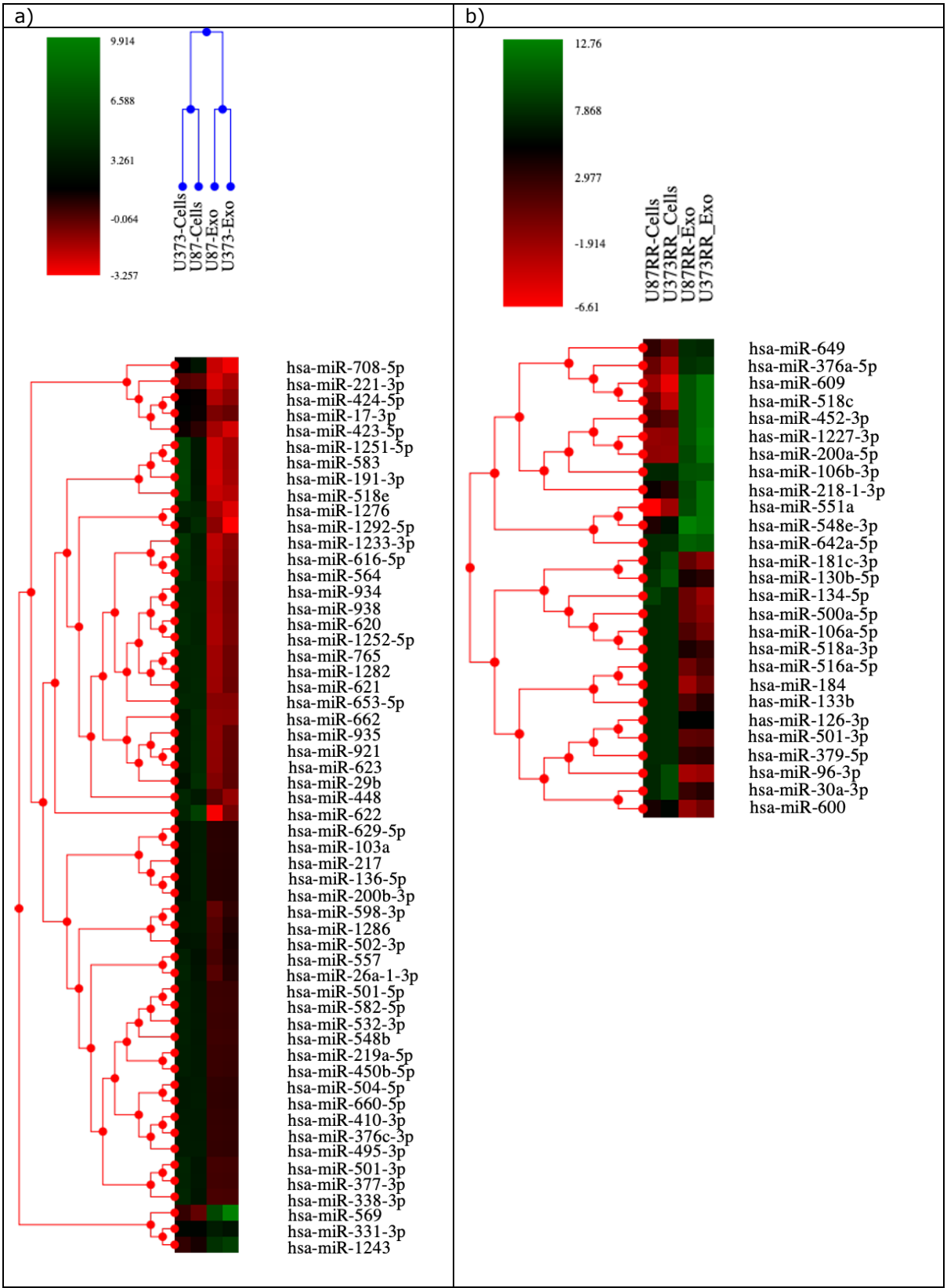

Figure 28. Heatmap of significantly deregulated miRNAs in (a) radiosensitive (U87MG, U373MG) cell lines compared to exosomes and (b) radioresistant (U87MG-RR, U373MG-RR) cell lines compared to exosomes

With regard to the radioresistant cell lines, (Figure 28-b), 27 exosomal miRNAs were significantly deregulated compared to the cells; an in-silico search showed 164 validated target genes, involved in different signaling pathways. Interestingly, results showed a different pattern of exosomal miRNAs expression in the radioresistant compared to the sensitive cells. In particular, the deregulated miRNAs in the radioresistant cell lines are involved in different signaling pathways among which are noteworthy Focal adhesion, signal and downstream signaling of activated FGFR1, FGFR2, FGFR3, FGFR4. All these FGFR pathways included the same target genes shown in Figure 29, and among these resulted of note fibroblast growth factor 2 (FGF2). Remarkably, a previous work showed the involvement of FGF1 and FGF2 in inducing radioresistance in GBM cell lines (Gouaze-Andersson et al., 2016).

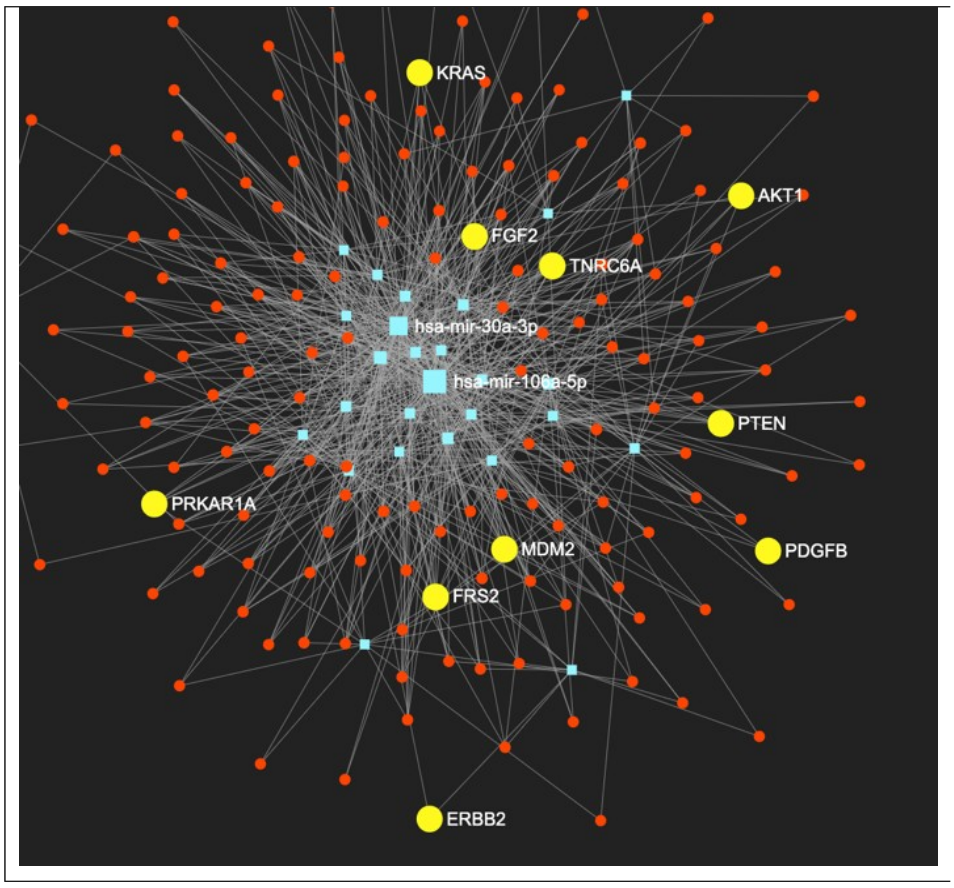

Figure 29. Downstream signaling of activated FGFR1, FGFR2, FGFR3, FGFR4. FGFR2 signaling pathways resulted involved in inducing radioresistance in GBM cell lines

miRNAs differentially expressed between radiosensitive and radioresistant glioblastoma cell lines.

miRNA analysis of the radiosensitive compared to the radioresistant cell lines identify 18 miRNAs significantly deregulated (Figure 30), targeting 101 genes. The most significant pathways in which these genes are involved resulted Apoptosis, Programmed Cell Death, Apoptotic execution phase, signaling by Rho GTPases, Rho GTPases effectors. The Rho family of small GTPases, which includes Rac1, Cdc42, and RhoA, is an important family whose members are key regulators of the invasion and migration of glioblastoma cells (Al-Koussa et al., 2020).

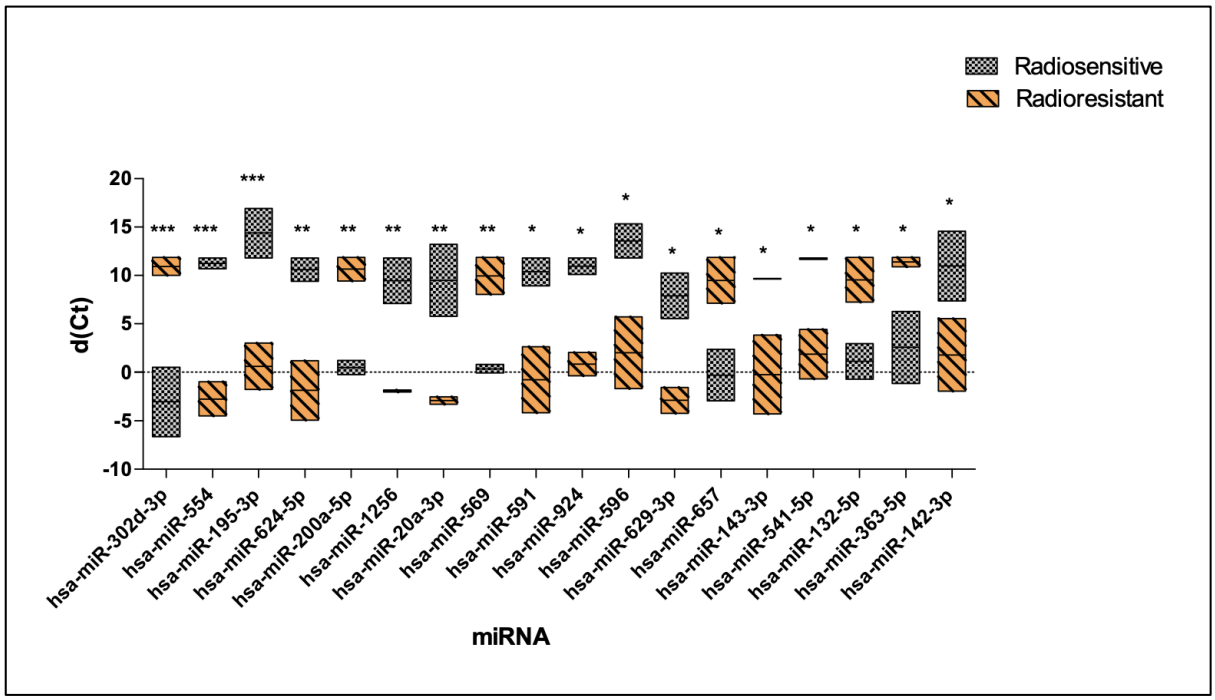

Figure 30. Significantly deregulated miRNAs in radiosensitive (U87MG, U373MG) compared to radioresistant cell lines (U87MG-RR, U373MG-RR). (*p ≤ 0.05, **p ≤ 0.01 *** p ≤ 0.001).

Subsequently, 20 miRNAs significantly deregulated (Figure 31) were identified comparing exosomal miRNAs expression in radiosensitive with radioresistant cell lines, suggesting a possible way of communication between cells promoting and sustaining the radioresistance process.

The in-silico search of validated target showed 107 target genes involved in different signaling pathways, including FGFR, PDGF, PI3K/AKT activation, pre-NOTCH expression and processing, pre-NOTCH transcription and translation.

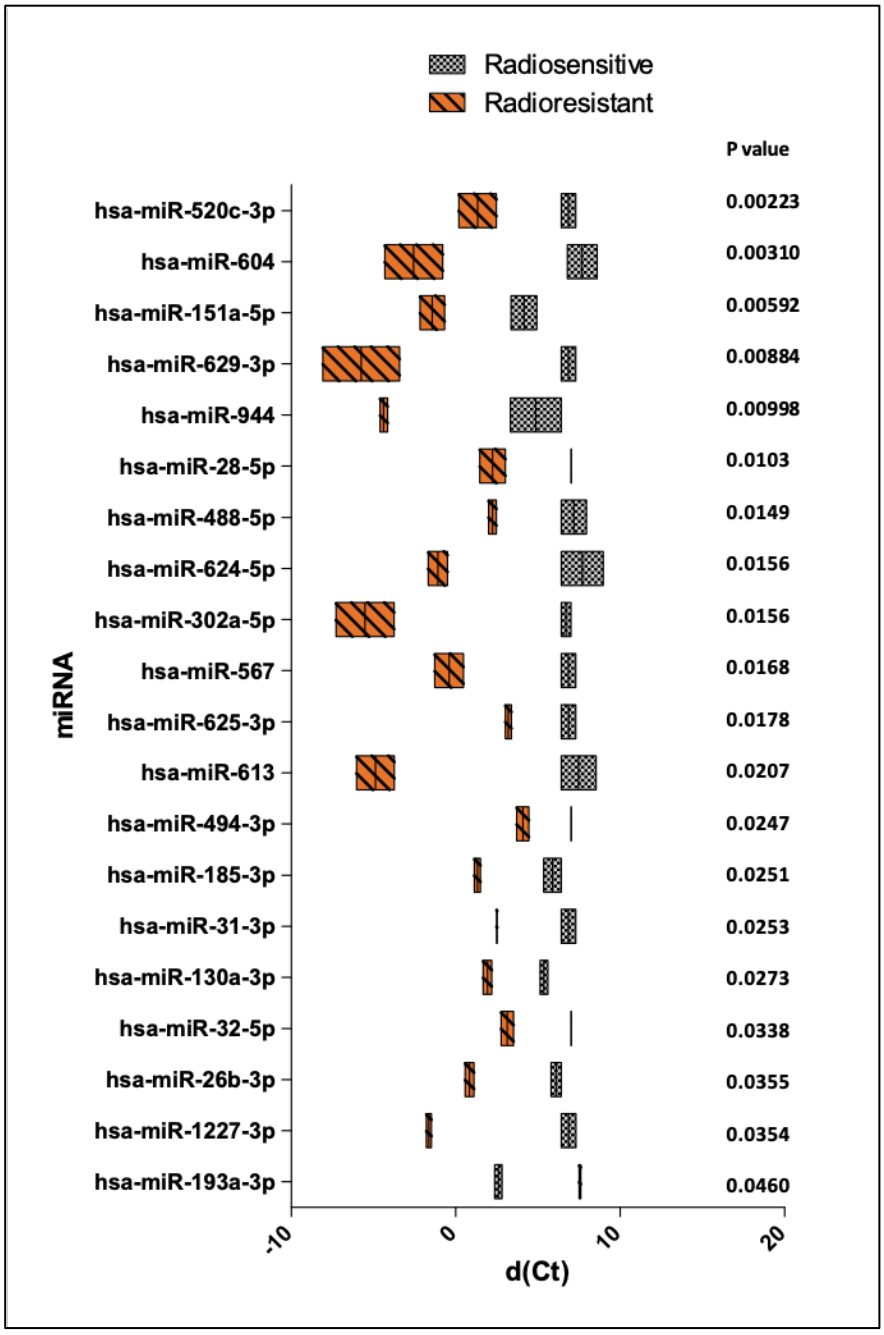

Figure 31. Significantly deregulated exosomal miRNAs in sensitive compared to radioresistant lines

4.3.2 miRNA analysis in glioblastoma patients

miRNA profiling was evaluated on plasma samples from patients enrolled in the trial P.64Cu.GBM.2018 in which the IMP administered is $^{64}CuCl_2$. The trial provides the enrollment of 16 patients, at the moment for this study 4 patients could be evaluated. Patients were defined by nuclear medicine physicians as responder or non responder after comparing the PET/CT imaging obtained at day 0 with the Follow up imaging analysis. In particular, the response to $^{64}CuCl_2$, is expressed as objective responses defined as stable disease, reduction or disappearance of tumor mass as measured by imaging pre- and post-treatment and defined by RANO criteria.

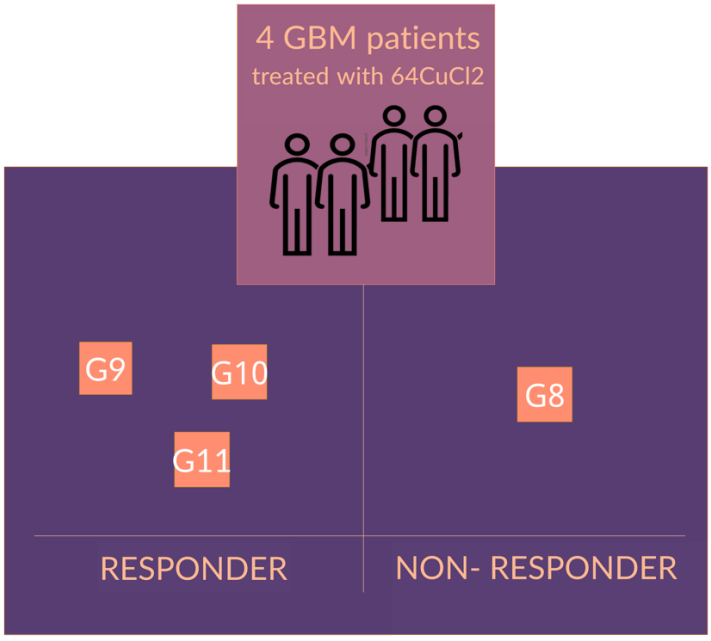

Figure 32. Stratification of GBM patients treated with $^{64}CuCl_2$ in responder (G9, G10, G11) and non responder (G8)

According to these criteria, among the 4 patients enrolled, and currently analyzed for miRNA profiling, one patient resulted non responder and 3 patients resulted responder (Figure 32). After stratification of the patients according to treatment response, the clinical outcome was correlated with miRNA profiling. In particular, miRNA analysis has been performed on plasma samples collected at day 0 (before IMP injections) and at day 42 (after 6 IMP injections).

In particular, considering that only one patient resulted non responder, to improve the analysis and not leave out data that could be significant, the analysis was performed into two different modalities.

The first analysis approach consisted in the identification of deregulated miRNAs among the three responder patients; subsequently, amongst these, miRNAs with opposite expression in responders compared to non responders and a DDDCt value of at least +/-2 were selected.

From the analyses 5 miRNA resulted with an opposite expression (Figure 33); in particular, 3 miRNAs - miR-339-3p, miR-133b and miR-103a-3p - resulted downregulated and 2 miRNAs- miR-32-5p and miR-335-5p - resulted upregulated in the non responder patient compared to the responder patients. These miRNAs, if validated in a larger sample size, could represent biomarkers of treatment response in GBM patients that undergo Copper chloride treatment.

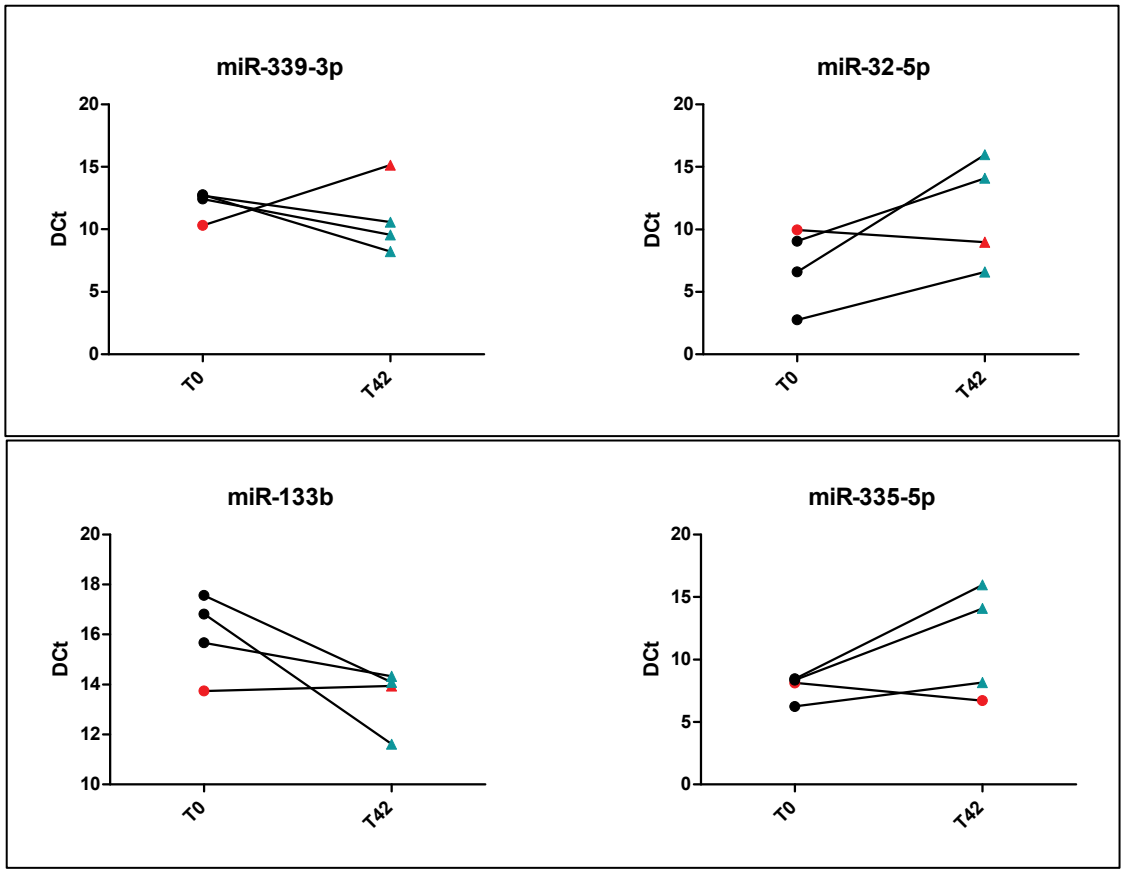

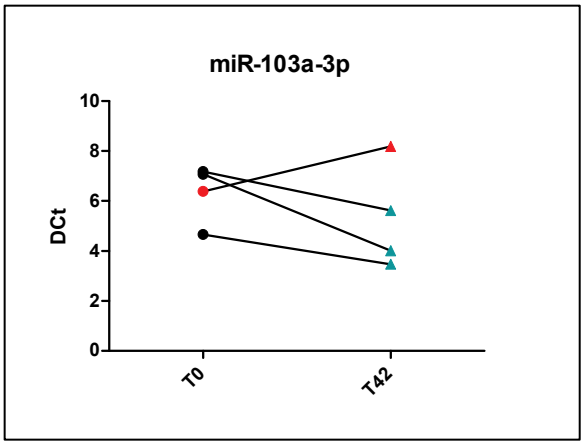

Figure 33. Representation of the selected miRNAs with their expression at t0 (baseline) and t42 (post-treatment) that showed a significant alteration between responder and non responder (red) patients

The analysis of the signaling pathways associated with the 5 miRNAs, performed using the miRNET software, highlighted 18 validated target genes. The most significant pathways included Post-transcriptional silencing by small RNAs, pre-NOTCH transcription and translation, pre-NOTCH expression and processing, signaling by NOTCH, FGFR (Table 23). All these pathways involve the same two genes the Trinucleotide Repeat Containing Adaptor 6A (TNRC6A) and 6B (TNRC6B) (Figure 34). They are two protein coding genes that encode for proteins also

known as GW182 family members that associate with Argonaute family members in the RISC to repress translation or promote mRNA degradation. In addition, knockdown of individual GW182 family members partially impaired miRNA-mediated gene silencing without affecting miRNA biogenesis or stability, indicating redundant roles of GW182 family members in controlling miRNA function (Jiang et al., 2011). Notably, genetic alterations at the TNRC6A loci have all been implicated in tumorigenesis in other tumor types as gastric and colorectal cancer, therefore could be interesting to investigate their role also in GBM (Sumazin et al., 2011).

Table 23. Signaling pathway for the selected 5 miRNAs

Pathway REACTOME	Pval		Pathway REACTOME	Pvalue
Post-transcriptional silencing by small RNAs	5.05E-05		Downstream signaling of activated FGFR4	0.0205
Pre-NOTCH Transcription and Translation	0.000407		alpha-linolenic (omega3) and linoleic (omega6) acid metabolism	0.021
Pre-NOTCH Expression and Processing	0.000654		alpha-linolenic acid (ALA) metabolism	0.021
Oncogene Induced Senescence	0.00102		Signaling by ERBB4	0.0216
Ca2+ pathway	0.00182		Cellular Senescence	0.0216
Signaling by NOTCH	0.00819		Downstream signal transduction	0.024
Oxidative Stress Induced Senescence	0.00856		Signaling by FGFR	0.024
PI3K events in ERBB4 signaling	0.00973		Signaling by FGFR1	0.024
PIP3 activates AKT signaling	0.00973		Signaling by FGFR2	0.024
PI3K events in ERBB2 signaling	0.00973		Signaling by FGFR3	0.024
PI-3K cascade:FGFR1	0.00973		Signaling by FGFR4	0.024
PI-3K cascade:FGFR2	0.00973		mRNA decay by 5' to 3' exoribonuclease	0.0242
PI-3K cascade:FGFR3	0.00973		Signaling by ERBB2	0.0243
PI-3K cascade:FGFR4	0.00973		DAP12 signaling	0.0249
Beta-oxidation of very long chain fatty acids	0.00974		Downstream signaling events of B Cell Receptor (BCR)	0.028
PI3K/AKT activation	0.0103		Signaling by EGFR	0.0292
GAB1 signalosome	0.0105		Fc epsilon receptor (FCERI) signaling	0.0296
Regulatory RNA pathways	0.011		DAP12 interactions	0.0302
Role of LAT2/NTAL/LAB on calcium mobilization	0.0116		Platelet calcium homeostasis	0.0306
beta-catenin independent WNT signaling	0.0138		Signaling by PDGF	0.0322
Folding of actin by CCT/TriC	0.0146		Formation of tubulin folding intermediates by CCT/TriC	0.0337
Association of TriC/CCT with target proteins during biosynthesis	0.0146		Peroxisomal lipid metabolism	0.0337
Reduction of cytosolic Ca++ levels	0.0162		NGF signaling via TRKA from the plasma membrane	0.0363

Early Phase of HIV Life Cycle	0.0178		Signaling by the B Cell Receptor (BCR)	0.0367
Signaling by SCF-KIT	0.0189		Signaling by BMP	0.0369
Downstream signaling of activated FGFR1	0.0205		Gene Expression	0.04
Downstream signaling of activated FGFR2	0.0205		Prefoldin mediated transfer of substrate to CCT/TriC	0.0432
Downstream signaling of activated FGFR3	0.0205		Cooperation of Prefoldin and TriC/CCT in actin and tubulin folding	0.0447
			Chaperonin-mediated protein folding	0.0463

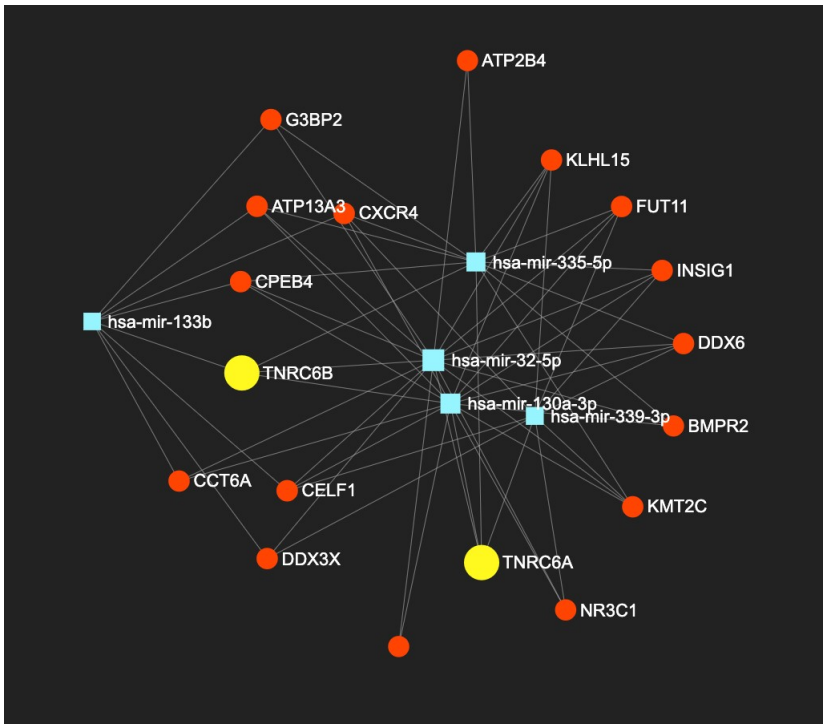

Figure 34. TNRC6B and TNRC6A targets of miR-133b, miR-335-5p, miR-32-5p, miR-339-3p, miR-130a-3p

The second analysis approach consisted in the correlation between miRNA levels at the baseline (t0) and the treatment response . From the analysis emerged that 6 miRNAs were deregulated between responder and non responder patients. In particular, 4 miRNAs resulted under-expressed (let- 7e-5p, miR-15a-5p, miR-29c-3p, miR-495) in non-responder patient, while 2 resulted over-expressed (miR-146b-5p, miR-199a-5p) (Figure 35). These miRNAs could represent predictive biomarker of treatment response . Indeed, if their predictive value would be confirmed in a large sample size, with a simple blood sample (liquid biopsy) and a miRNA analysis could be possible to identify before starting the treatment, patient responsiveness to the radiopharmaceutical.

The identified 6 miRNAs are involved in different signaling pathways (Table 24) typically deregulated in glioblastoma, including PI3K pathway, that is altered in

about 70% of GBM either by deletion of PTEN or amplification of EGFR and/or vascular endothelial growth factor receptor (VEGFR) and/or platelet-derived growth factor receptor (PDGFR) alpha. These genes are also involved in the PI3K/AKT activation, in fact PI3K generates phosphatidylinositol-3,4,5-triphosphate, which in turn activates Akt.

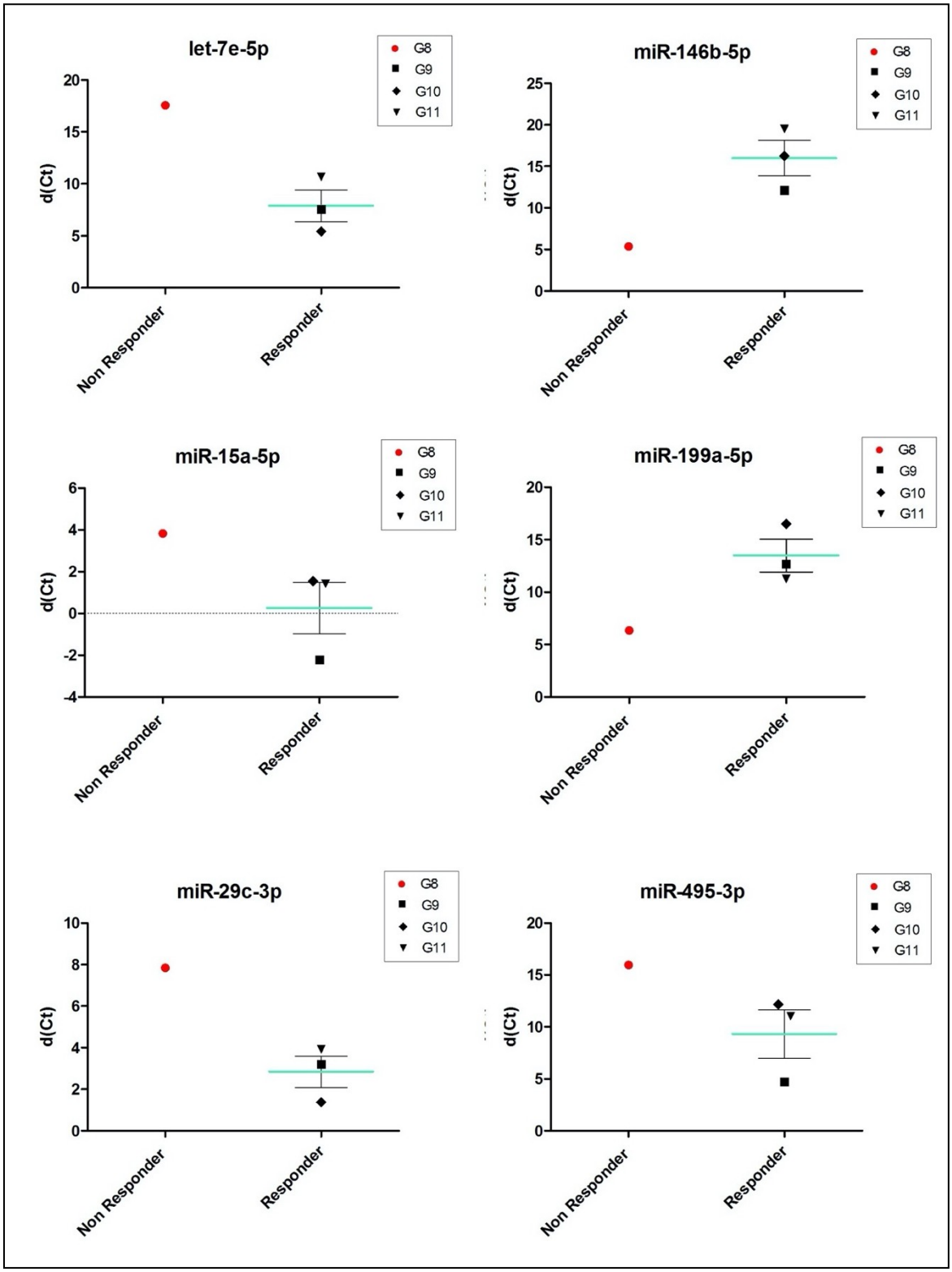

Figure 35. miRNAs deregulated at baseline in responder GMB patients compared to non responder

Table 24. Significant signaling pathway for the predictive miRNAs

Pathway	Pval	Pathway	Pval
Signaling by Wnt	0.01	AKT phosphorylates targets in the cytosol	0.0244
Fc epsilon receptor (FCERI) signaling	0.01	Signaling by NOTCH1 HD Domain Mutants in Cancer	0.0244
Signaling by PDGF	0.01	Constitutive Signaling by NOTCH1 HD Domain Mutants	0.0244
Beta-catenin phosphorylation cascade	0.01	beta-catenin independent WNT signaling	0.251
misplaced GSK3beta mutants stabilize beta-catenin	0.01	Synthesis of PE	0.0267
Platelet degranulation	0.01	Synthesis of Prostaglandins (PG) and Thromboxanes (TX)	0.0289
Signaling by NOTCH	0.02	Signaling by SCF-KIT	0.296
Response to elevated platelet cytosolic Ca2+	0.02	CRMPs in Sema3A signaling	0.0356
Apoptotic factor-mediated response	0.02	Downstream signaling of activated FGFR1	0.309
Post-transcriptional silencing by small RNAs	0.02	Downstream signaling of activated FGFR2	0.0309
Oxidative Stress Induced Senescence	0.02	Downstream signaling of activated FGFR3	0.0309
Cellular responses to stress	0.02	Downstream signaling of activated FGFR4	0.0309
PI3K events in ERBB4 signaling	0.02	Signaling by ERBB4	0.0318
PIP3 activates AKT signaling	0.02	Cellular Senescence	0.0318
PI3K events in ERBB2 signaling	0.02	Membrane Trafficking	0.0324
PI-3K cascade:FGFR1	0.02	Downstream signal transduction	0.0336
PI-3K cascade:FGFR2	0.02	Signaling by FGFR	0.0336
PI-3K cascade:FGFR3	0.02	Signaling by FGFR1	0.0336
PI-3K cascade:FGFR4	0.02	Signaling by FGFR2	0.0336
PI3K/AKT activation	0.02	Signaling by FGFR3	0.0336
GAB1 signalosome	0.02	Signaling by FGFR4	0.0336

Role of LAT2/NTAL/LAB on calcium mobilization	0.02		Signaling by ERBB2	0.0338
Nicotinate metabolism	0.02		DAP12 signaling	0.0342
Golgi to ER Retrograde Transport	0.02		NOTCH2 Activation and Transmission of Signal to the Nucleus	0.04
COPI Mediated Transport	0.02		Signaling by WNT in cancer	0.04
Activation of the AP-1 family of transcription factors	0.02		Pre-NOTCH Transcription and Translation	0.0422
WNT5A-dependent internalization of FZD4	0.02		Insulin processing	0.0489
O-glycosylation of TSR domain-containing proteins	0.02		disassembly of the destruction complex and recruitment of AXIN to the membrane	0.0489
			Constitutive Signaling by AKT1 E17K in Cancer	0.0489

5. Discussion

GBM is the most common adult primary malignant brain tumor and also the most lethal. Median progression-free and overall survival after initial diagnosis is 6.2–7.5 and 14.6–20.5 months, respectively, even with a highly aggressive standard-of-care treatment consisting of maximum safe surgical resection, radiation therapy, and chemotherapy. In light of this grim prognosis, substantial effort has been made to improve the overall survival of patients with GBM. However, over the last decade, all preclinical strategies that have shown promise failed to provide an overall survival benefit in large clinical trials. The main reason for these failures is attributable to the development of resistance to the standard therapeutic options for GBM, which include radiotherapy with concomitant chemotherapy. In particular, the development of adaptive radioresistance has been a major challenge. In this context, significant research has focused on defining the molecular mechanisms of adaptive radioresistance in GBM, with the aim of identifying a method to urgently overcome this clinical problem.

Copper Chloride is a new promising radiopharmaceutical that has recently shown in literature the capability to be a good candidate for prostate cancer diagnosis compared to standard tracers using PET/CT imaging (Piccardo et al., 2017). The radiopharmaceutical is also under investigation as a theranostic tracer, both as diagnostic and therapeutic tracer in GBM. $^{64}CuCl_2$ represents an ideal theranostic compound as, unlike from the tracers currently on the market, the chemically and biologically identical compound is administered for diagnosis and therapy. The crucial point for the application of a theranostic agent is the identification of the proper dose that should reach the target in sufficient amounts, in order to achieve an effective action. In the theranostic approach, the dose can be optimized on the basis of each patient and this is a considerable achievement for personalized medicine. Therefore, theranostic medicine could improve patient selection, reduce side effects, and enhance therapeutic efficacy. Moreover, theranostic approaches can be useful in estimating the safety and efficacy of a treatment, and, in particular, can be applied in monitoring the therapy course. With regard to $^{64}CuCl_2$, currently a phase I clinical trial (P.64Cu.GBM.2018) is evaluating the proper dose of the radiopharmaceutical, able to reach the therapeutic effect in GBM patients. Therefore, it is of crucial importance and timing to focus on the possible

development of radioresistance to this new radiopharmaceutical. In this context, is essential to define the appropriate therapeutic scheme that allow to avoid the establishment of radioresistance. Moreover, it is essential to identify a molecular biomarker of treatment response that could confirm, from a molecular point of view, the PET/CT data obtained after a diagnostic dose of copper chloride. For this reason, the company Acom Srl, sponsor of the phase I clinical trial on $^{64}CuCl_2$ as theranostic agent in GBM decided to focus on and improve the knowledge of the radioresistance associated with this new radiopharmaceutical. The idea behind this research is to improve the therapeutic scheme and identify, through liquid biopsy, biomarkers of treatment response. To reach the endpoints two GBM radioresistant cell lines have been generated (U87MG-RR and U373MG-RR) from the parental radiosensitive lines (U87MG and U373MG). The radioresistant cells showed the capability to skip the drug-killing effect in cell viability assays, therefore the established cell model was used to perform different functional studies, comparing the radiosensitive with the radioresistant cell lines. In particular, all the radiosensitive and the radioresistant cell lines were able to internalize $^{64}CuCl_2$, even with a different behavior. In particular, U373MG and U373MG-RR showed a constant rate of radioactivity internalization, which is still visible after 72h. On the other hand, U87MG and U87MG-RR showed a maximum rate of radioactivity internalization at 24h. The different behavior could point out the development of different mechanism of radioresistance due to the different characteristics of the cell lines, also reflecting patients' variability. A differential $^{64}CuCl_2$ uptake among various lines was also shown in other tumour types such as prostate cancer and melanoma. Guerreiro and coworkers analyzed $^{64}CuCl_2$ internalization on a panel of prostate cancer lines showing that all the tumoral lines exhibited a higher uptake comparing to a non-tumoral cell line, but with a differential uptake. The authors tried to correlate the differential uptake with the different expression of the copper transporter CTR1 characterizing the cell lines. In this regard, no significant result emerged, while different growth rates were observed according to chopper internalization. In particular, the PC3 cell line that had the fastest growth rate exhibited one of the lowest uptakes, whereas the LNCaP cell line, which grew more slowly, had a significantly higher uptake (Guerreiro et al., 2018). The influence of the tumor growth rate on cell uptake was also described for two different melanoma cell lines by Qin and coworkers (Qin et al., 2014). Similarly,

to the previous study, why different cell lines exhibited differential $^{64}CuCl_2$ uptake remained unclear. However, also these aspects could be connected to different mechanism of radioresistance and represent a starting point for further investigations on GBM lines.

The findings of cell uptake in radioresistant cell lines have a noteworthy value due to the possible correlation of the cell uptake with the SUV_{max} value obtained from the PET/CT scans of the 4 patients enrolled in the trial.

PET-based treatment response studies typically measure the change in the SUV to quantify response. The relative changes of different SUV measures can be used to classify patients into response categories, with quantitative thresholds separating the different categories (Vanderhoek et al., 2013).

Interestingly, in our study the SUVmax of the non-responder patient resulted higher comparing to the 3 responder patients. In the non-responder patient, in which PET/CT imaging examination shows $^{64}CuCl_2$ uptake, it is hypothesized that there is a higher uptake due to higher tumor replication but there is no response probably due to the fact that the dose necessary to reduce the tumour mass is under the efficacy dose threshold. This is important for the development of further dosimetric analysis focused on finding the best efficacy dose. This is a very preliminary and not statistically significant result however, the capability of the cell uptake to correlate with signal intensity and treatment response, if confirmed on a larger sample size makes cellular uptake an interesting biomarker of sensitiveness to copper chloride treatment.

After the cell internalization study, it was essential to understand how $^{64}CuCl_2$ is distributed within the cell between nucleus and cytoplasm. Indeed, nuclear uptake is crucial for the therapeutic action, as the radiopharmaceutical should reach the tumor DNA to show its therapeutic effect. Currently no data are available in literature regarding the exact radioactivity entering the nucleus in GBM lines, and this study highlights, for the first time, that ^{64}Cu is able to enter the nucleus not only of GBM radiosensitive lines but also of the radioresistant ones.

As observed before in the cell uptake study, the cell lines exhibited a different behavior. In particular, U87MG and U87MG-RR lines showed a linear uptake over time into the nucleus, which was not observed in the U373MG and U373MG-RR lines. From the data clearly emerged that ^{64}Cu uptake into the nucleus occurs in the radioresistant cell lines. Probably, despite the uptake inside the nucleus, in

the radioresistant lines the critical concentration of ^{64}Cu necessary for the cell-killing effect is not reached. Understanding the amount of radioactivity reaching the nucleus is essential to establish the therapeutic dose, and consequently it is the key requisite for dosimetric calculations. It has been already demonstrated that ^{64}Cu has a characteristic emission spectrum able to emit Auger electrons which allows its use as theranostic agent that is possible thanks to its capability to reach the nucleus and cause DNA damage of tumor cells (Cui et al., 2011; McMillan et al., 2015). In this context, the curative potential of the radiopharmaceutical depends on the scale and quality of DNA damage achieved in the tumor tissue. Indeed, the crucial point, on which the fate of a tumor cell following radiation exposure depends, is to reach a critical amount of DNA damage. The first of the "5R" of radiation biology is "Repair" and refers to DNA repair as one of the key determinants of tumor cell survival after radiation therapy (Schultz et al., 2019). Therefore, to avoid radioresistance, the balance between cell capability/incapability to repair the DNA damage should shift in favor of incapability. Certainly, if the levels of radiation-induced DSBs exceed the DNA repair capacity of tumor cells, this might result in cell cycle arrest, tumor cell senescence, and death. On the other hand, if the level of DNA lesions is low, DNA repair mechanisms and DNA damage checkpoints are activated, arresting cell cycle progression and allowing cells to repair the DNA. But, if the amount of DNA damage is unrepairable, the cells activate death programs. In confirmation of this, radioresistant cell lines showed a significant reduction of DNA DSB compared to the radiosensitive ones. This demonstrates the acquired capability of the radioresistant cells to overcome the copper chloride mechanism of action. A plausible explanation is the induction of adaptative and DNA repair mechanisms, that allow cells to survive.

Another aim of the project was related to identify resistance-associated epigenetic alteration, in particular focusing on miRNAs, that are considered to be master regulators of gene expression and critical in maintaining cellular homeostasis post-transcriptionally. Initially, the miRNA signature of both radiosensitive and radioresistant cell lines was characterized, and the different signaling pathways that resulted altered in radioresistant lines analyzed. Afterwards, the exosomal miRNAs, released in the culture medium, were also analyzed, showing a significantly different signature compared to cells. In addition, results showed that

the signature of miRNAs released by the cell via exosomes was different in the radioresistant compared to the sensitive cell lines. Exosomes are vesicles that play a crucial role in intercellular communication functioning as a bridge for information exchange between cells. In particular, there is mounting evidence that exosomal miRNAs can regulate tumorigenesis and cancer development by supplying the tumor niche with molecules favoring proliferation, invasion, and even drug resistance (He et al., 2018, Zhang et al., 2015, Jurj et al., 2020). In this context, a recent work by Lan and colleagues focused on the potential role of exosomal miRNAs, identifying miR-210 as a potential biomarker of diagnosis and prognosis of gliomas (Lan et al., 2020).

The generation of $^{64}CuCl_2$ radioresistant cells and the investigation of exosomal miRNAs released in the culture medium is important as it could represents a valid surrogate of patient plasma samples. Therefore, the model it might be useful for multiple purposes, including discovery of novel treatment strategy (out of the scope of the present work), biomarkers of resistance to copper chloride, and definition of strategies to overcome resistance to the radiopharmaceutical. In view of these considerations, is timing the choice to investigate exosomal miRNAs in GBM plasma samples, from the first 4 patients enrolled in the phase I clinical trial (P.64Cu.GBM.2018), before and after copper chloride treatment. Comparing the miRNA signature at the baseline (t0) with treatment response 6 miRNA (let-7e-5p, miR-15a-5p, miR-29c-3p, miR-495, miR-146b-5p, miR-199a-5p) were identified as significantly deregulated between Responder and Non responder patients. The finding is important, as these miRNAs could represent biomarkers of treatment response. In particular, with a simple blood sample (liquid biopsy) it could be possible to predict, even before starting the treatment, patient responsiveness; however, further confirmation in large sample size is mandatory. Noteworthy, among these miRNAs miR-29 was found deregulated in plasma samples of GBM patients compared to healthy subjects (Wu et al., 2014). The authors retained that miR-29 family could represent a biomarker for high-graded glioma screening, while the sensitivity and specificity for low-graded glioma detection might not be sufficient. Therefore, this miRNA family may play a role both in diagnosis and therapy. Another miRNA identified was miR-let-7e-5p, belonging to the let-7 miRNA family. It is interesting to note that miR-let-7 showed anti-tumorigenic effect on GBM cells (Lee ST et al., 2011) and low let-7 expression

was correlated with a poor prognosis of primary GBM patients (Wang XR et al., 2013). In addition, reduced expression of let-7 miRNA families is associated with low responsiveness to a number of chemotherapeutic agents including radiotherapy (Hummel et al., 2010). Accordingly, variation of let-7 expression associated with $^{64}CuCl_2$ therapeutic response of glioblastoma patients, is an interesting result which deserves further confirmatory studies.

To deepen the knowledge of the involvement of miRNAs in copper chloride response, pre- and post-treatment miRNA signature were analyzed in the 4 plasma samples from GBM patients enrolled in the phase I trial. 5 miRNAs resulted deregulated; in particular, miR-339-3p, miR-133b and miR-103a-3p were downregulated, and miR-32-5p and miR-335-5p were upregulated in the non-responder patient, compared to responders. Therefore, these miRNAs could also represent possible biomarkers of response to Copper chloride treatment in GBM patients. In addition, it could also be envisaged in future studies the possibility of having more samples for each patient at different timepoints. In particular, in the present project, the analysis, as stated above, was performed comparing the miRNAs signature before starting the treatment and only 42 days post-treatment, therefore, additional timepoints could be used during the follow-up to monitor the response over the time, promptly identifying non-responder patients. Among the miRNAs identified miR-339 significantly affected migration, invasion and apoptosis of GBM cells in vitro (Gulluoglu et al., 2018) whereas, Jiang et al. have suggested that miR-335 upregulation is associated with advanced tumor progression as well as a poorer survival time in patients with malignant glioma, indicating that miR-335 may become an independent prediction marker of clinical outcome in patients with gliomas (Jiang et al., 2012). Consistently with their findings, the study of Cheng and coworkers (Cheng et al., 2013) also revealed that a high miR-335 expression was significantly associated with a higher grade of glioma. In our study, the upregulation of miR-335-5p was observed in the non-responder patient, confirming it possible role as a marker of poor prognosis, as shown in literature, and $^{64}CuCl_2$ treatment response as well.

Interestingly, looking at the miRNAs identified as deregulated in the exosomes of the radioresistant lines with respect to miRNA deregulated in patients pre- and after- treatment, it is worth noting the presence of miR- 32-5p, that is upregulated in the exosomes of the radioresistant cells (considered as non-

responder cells), and it is also upregulated in the exosomes of the non-responder patient. Therefore, the lack of responsiveness to the treatment in the non-responder patient could be due to both insufficient radioactivity reaching the nucleus, and to an adaptive response mediated via exosomal miRNAs.

These findings are representative of the usefulness of generating an "in vitro liquid biopsy" model that could be of interest for further in vitro studies. Particularly, considering that miR-32-5p has already been involved in tumorigenesis of GBM, as regulator of p53 (Suh et al., 2012), it will be essential to plan in vitro tests evaluating the capacity of this miRNA to restore the radiopharmaceutical efficacy in radioresistant cells. p53 mutations play a significant role in the development of secondary GBMs and are often the earliest detectable genetic alteration in primary brain tumors p53 (Mao et al., 2012). The tumor suppressor protein p53 is a critical cellular mediator of the response to oxidative stress and genotoxic damage and is also implicated in the trafficking of Copper-64 to tumor cell nuclei. In particular, literature data demonstrated that ^{64}Cu is delivered to tumor cell nuclei with a direct dependence of p53 positive expression (Eiblmaier et al., 2008), moreover p53 may affect nuclear transport of copper by increasing the Atox1 expression level, the chaperon responsible for ^{64}Cu entrance into the nucleus (Beaino et al., 2014). Therefore, the involvement of p53 on copper trafficking encourage the use of miR-32-5p as possible miRNA to be used to restore the radiopharmaceutical efficacy in radioresistant cell lines.

Analysis of the signaling pathways of the deregulated miRNAs showed that they targeted genes, with post-transcriptional silencing by small RNAs, pre-NOTCH transcription and translation, pre-NOTCH expression and processing, signaling by NOTCH, FGFR as the most significant pathways involved. It is interesting to note that these pathways involve the same genes TNRC6B and TNRC6A. They are two protein coding genes that encode for GW182 family members that associate with Argonaute family members in the RISC complex to repress translation or promote mRNA degradation. Notably, genetic alterations at the TNRC6A loci have all been implicated in tumorigenesis in other tumor types as gastric and colorectal cancer, therefore it could be interesting to investigate their role in GBM (Sumazin et al., 2011).

Noteworthy, among these pathways the Notch signaling path is involved in radioresistance. Indeed, inhibition of Notch 1 and 2 restores radiosensitivity in

glioma stem cells, and Notch has been reported to induce radioresistance in GBM cells through regulation of the PI3-kinase/Akt pathway (Wang et al.,2009). In particular, authors identified the increase in AKT expression and activity as the main contributor to tumor progression, recurrence, and radioresistance (Li et al., 2009). In addition, Chautard and coworkers found that irradiation of GMB cells activates Akt and, enhancing DNA damage repair (DDR) by promoting γ-H2AX foci resolution, thereby contributing to the development of radioresistance (Chautard et al., 2010). On the other hand, downregulation of AKT facilitates the formation of unrepairable DNA DSB in irradiated U251 glioma cells (Chautard et al., 2010).

6. Conclusions

GBM is one of the most prevalent and aggressive malignant primary brain tumors in adult patients, usually with poor prognosis and low survival rates. Current treatment strategies have not significantly increased the overall survival and the vast majority of patients die within 2 years. Radiotherapy plays an important role in oncological treatment of GBM patients nevertheless, the brain tumors are well known for their frequent resistance to ionizing radiation and, thus, adjuvant therapy often fails, leading to early recurrences. This also applies to GBM, a heterogeneous tumor harboring anomalies in several molecular and signaling pathways, in which several alterations have been implicated in the observed radioresistance.

Lacking effective treatments raises the urgent need to seek and develop new effective molecules for this rare disease. $^{64}CuCl_2$ is an innovative radiopharmaceutical, showing its properties as a theranostic tracer in GBM patients. Currently the drug is an IMP in a phase I clinical trial, therefore the therapeutic dose, necessary to reach the best efficacy, is still under evaluation. Although it may seem premature, Acom Srl has already considered the possibility of radioresistance development and started to investigate this through an integrated cell/patient's approach.

In this context, this is the first study describing the establishment and miRNA characterization of two $^{64}CuCl_2$ radioresistant cell lines, contributing to understand the potential role of $^{64}CuCl_2$ as theranostic agent. In particular, this in-vitro evaluation allowed to investigate and highlight the critical point to avoid

radioresistance, including the proper dose reaching the nucleus, able to explicate the therapeutic effect. The results obtained will be useful to implement the approach for dosimetric analysis, with the aim to define the best dose scheme for each patient, trying to avoid radioresistance development. In this scenario, the key players responsible for modulating radioresistance could be miRNAs. Indeed, these regulators of gene-expression have been involved in the development of chemoresistance, therefore it is conceivable that they could be also implicated in the radioresistance process. Considering the crucial role of miRNA in cell-to-cell communication, circulating and exosomal miRNAs, , are widely investigated in GBM, as they could help monitoring therapeutic response or predict therapeutic effects. To the best of our knowledge, this is the first study bringing to an early identification of a miRNA signature associated with $^{64}CuCl_2$ treatment that could represent potential biomarkers of treatment response. In particular, this research led to the identification of different miRNA pattern both from plasma's samples and from cell lines, generating an "in vitro liquid biopsy" model for GBM, that could be of interest for further in vitro studies, including definition of strategies to overcome resistance to the radiopharmaceutical.

In the era of personalized medicine, the identification of these biomarkers is essential from one side to confirm, from a molecular point of view, the PET/CT imaging findings and, on the other side, to predict, even before starting the treatment, patient responsiveness, with a simple blood sample (liquid biopsy).

The study also opened the perspective towards the intriguing use of miR-32-5p as possible molecule able to restore $^{64}CuCl_2$ responsiveness in the radioresistant cell lines, representing a great challenge never faced in GBM studies. In particular, in the fight of $^{64}CuCl_2$ with DNA Repair system, miR-32-5p could represent a novel anti-tumorigenesis molecule to add to GBM therapy, enhancing its radio effect.

In conclusion, further studies, on large sample size are warranted to confirm the usefulness of the identified miRNAs signature in the generated radioresistant GBM models and plasma sample from GBM patients, as biomarker of treatment response. Nevertheless, the study added a better understanding of GBM radioresistance development, revealed some crucial points useful to clinical investigators to further improve the use of $^{64}CuCl_2$ as a theranostic agent in GBM, and highlighted a possible role of miRNAs in $^{64}CuCl_2$ treatment response.

7. List of References

Agnihotri S, Burrell KE, Wolf A, Jalali S, Hawkins C, Rutka JT, Zadeh G. Glioblastoma, a brief review of history, molecular genetics, animal models and novel therapeutic strategies. Arch Immunol Ther Exp (Warsz). 2013 Feb;61(1):25-41. doi: 10.1007/s00005-012-0203-0. Epub 2012 Dec 7. PMID: 23224339.

Al-Koussa H, Atat OE, Jaafar L, Tashjian H, El-Sibai M. The Role of Rho GTPases in Motility and Invasion of Glioblastoma Cells. Anal Cell Pathol (Amst). 2020 Jan 31;2020:9274016. doi: 10.1155/2020/9274016. PMID: 32089990; PMCID: PMC7013281.

Alexiou GA, Tsiouris S, Voulgaris S, Kyritsis AP, Fotopoulos AD. Glioblastoma multiforme imaging: the role of nuclear medicine. Curr Radiopharm. 2012 Oct;5(4):308-13. doi: 10.2174/1874471011205040308. PMID: 22642425.

Ali MY, Oliva CR, Noman ASM, Allen BG, Goswami PC, Zakharia Y, Monga V, Spitz DR, Buatti JM, Griguer CE. Radioresistance in Glioblastoma and the Development of Radiosensitizers. Cancers (Basel). 2020 Sep 3;12(9):2511. doi: 10.3390/cancers12092511. PMID: 32899427; PMCID: PMC7564557.

Ballinger JR. Theranostic radiopharmaceuticals: established agents in current use. Br J Radiol. 2018 Nov;91(1091):20170969. doi: 10.1259/bjr.20170969. Epub 2018 Mar 12. PMID: 29474096; PMCID: PMC6475961.

Banelli B, Forlani A, Allemanni G, Morabito A, Pistillo MP, Romani M. MicroRNA in Glioblastoma: An Overview. Int J Genomics. 2017;2017:7639084. doi: 10.1155/2017/7639084. Epub 2017 Nov 6. PMID: 29234674; PMCID: PMC5695025.

Barciszewska AM. MicroRNAs as efficient biomarkers in high-grade gliomas. Folia Neuropathol. 2016;54(4):369-374. doi: 10.5114/fn.2016.64812. PMID: 28139816.

Beaino W, Guo Y, Chang AJ, Anderson CJ. Roles of Atox1 and p53 in the trafficking of copper-64 to tumor cell nuclei: implications for cancer therapy. J Biol Inorg Chem. 2014 Mar;19(3):427-38. doi: 10.1007/s00775-013-1087-0. Epub 2014 Jan 21. PMID: 24445997; PMCID: PMC3951176.

Bonneau E, Neveu B, Kostantin E, Tsongalis GJ, De Guire V. How close are miRNAs from clinical practice? A perspective on the diagnostic and therapeutic market. EJIFCC. 2019 Jun 24;30(2):114-127. PMID: 31263388; PMCID: PMC6599191.

Müller Bark J, Kulasinghe A, Chua B, Day BW, Punyadeera C. Circulating biomarkers in patients with glioblastoma. Br J Cancer. 2020 Feb;122(3):295-305. doi: 10.1038/s41416-019-0603-6. Epub 2019 Oct 31. PMID: 31666668; PMCID: PMC7000822.

Bhaskaran M, Mohan M. MicroRNAs: history, biogenesis, and their evolving role in animal development and disease. Vet Pathol. 2014 Jul;51(4):759-74. doi: 10.1177/0300985813502820. Epub 2013 Sep 17. PMID: 24045890; PMCID: PMC4013251.

Boschi A, Martini P, Janevik-Ivanovska E, Duatti A. The emerging role of copper-64 radiopharmaceuticals as cancer theranostics. Drug Discov Today. 2018 Aug;23(8):1489-1501. doi: 10.1016/j.drudis.2018.04.002. Epub 2018 Apr 7. PMID: 29635027.

Broughton JP, Lovci MT, Huang JL, Yeo GW, Pasquinelli AE. Pairing beyond the Seed Supports MicroRNA Targeting Specificity. Mol Cell. 2016 Oct 20;64(2):320-333. doi: 10.1016/j.molcel.2016.09.004. Epub 2016 Oct 6. PMID: 27720646; PMCID: PMC5074850.

Brown MC, Staniszewska I, Lazarovici P, Tuszynski GP, Del Valle L, Marcinkiewicz C. Regulatory effect of nerve growth factor in alpha9beta1 integrin-dependent progression of glioblastoma. Neuro Oncol. 2008 Dec;10(6):968-80. doi: 10.1215/15228517-2008-047. PMID: 19074980; PMCID: PMC2719011.

Cai H, Wu JS, Muzik O, Hsieh JT, Lee RJ, Peng F. Reduced 64Cu uptake and tumor growth inhibition by knockdown of human copper transporter 1 in xenograft mouse model of prostate cancer. J Nucl Med. 2014;55: 622–8

Cai Q, Zhu A, Gong L. Exosomes of glioma cells deliver miR-148a to promote proliferation and metastasis of glioblastoma via targeting CADM1. Bull Cancer. 2018 Jul-Aug;105(7-8):643-651. doi: 10.1016/j.bulcan.2018.05.003. Epub 2018 Jun 18. PMID: 29921422.

Calin GA, Dumitru CD, Shimizu M, Bichi R, Zupo S, Noch E, Aldler H, Rattan S, Keating M, Rai K, Rassenti L, Kipps T, Negrini M, Bullrich F, Croce CM. Frequent deletions and down-regulation of micro-RNA genes miR15 and miR16 at 13q14 in chronic lymphocytic leukemia. Proc Natl Acad Sci U S A. 2002 Nov 26; 99(24):15524-9.

Capasso E., Durzu S., Piras S, et al. Role of 64CuCl2 PET/CT in staging of prostate cancer. Ann Nucl Med., 29:482–8, 2015;

Canelas HM, DeJorge FB, Pereira WC, Sallum J (1968) Biochemistry of cerebral tumours. Sodium, potassium, calcium, phosphatase, magnesium, copper and sulphur contents of astrocytoma, medulloblastoma and glioblastoma multiforme. J Neurochem 15:1455-1461

Carlson TA and White RM. Formation of Fragment Ions from CH3Te125 and C2H5Te125 Following the Nuclear Decays of CH3I125 and C2H5I125 The Journal of Chemical Physics 38, 2930 (1963);

Carmeliet, P., and Jain, R.K. (2000) Angiogenesis in cancer and other diseases. Nature 407, 249–257.

Chautard E, Loubeau G, Tchirkov A, Chassagne J, Vermot-Desroches C, Morel L, Verrelle P. Akt signaling pathway: a target for radiosensitizing human malignant glioma. Neuro Oncol. 2010 May;12(5):434-43. doi: 10.1093/neuonc/nop059. Epub 2010 Feb 4. PMID: 20406894; PMCID: PMC2940626.

Chakraborty C, Das S. Profiling cell-free and circulating miRNA: a clinical diagnostic tool for different cancers. Tumour Biol. 2016 May;37(5):5705-14. doi: 10.1007/s13277-016-4907-3. Epub 2016 Jan 29. PMID: 26831657.

Cheng CJ, Slack FJ. The duality of oncomiR addiction in the maintenance and treatment of cancer. Cancer J. 2012 May-Jun; 18(3):232-7.

Cheng Q, Cao H, Chen Z, Ma Z, Wan X, Peng R, Jiang B. PAX6, a novel target of miR-335, inhibits cell proliferation and invasion in glioma cells. Mol Med Rep. 2014 Jul;10(1):399-404. doi: 10.3892/mmr.2014.2150. Epub 2014 Apr 15. PMID: 24737483.

Chesler DA, Berger MS, Quinones-Hinojosa A. The potential origin of glioblastoma initiating cells. Front Biosci (Schol Ed). 2012 Jan 1;4:190-205. PMID: 22202053; PMCID: PMC3635065.

Cui X, Oonishi K, Tsujii H, Yasuda T, Matsumoto Y.Effects of Carbon Ion Beam on Putative Colon Cancer Stem Cells and Its Comparison with X-rays. Tumor and Stem Cell Biology 2011

Kudulaiti N, Zhang H, Qiu T, Lu J, Aibaidula A, Zhang Z, Guan Y, Zhuang D. The Relationship Between IDH1 Mutation Status and Metabolic Imaging in Nonenhancing Supratentorial Diffuse Gliomas: A 11C-MET PET Study. Mol Imaging. 2019 Jan-Dec;18:1536012119894087. doi: 10.1177/1536012119894087. PMID: 31889470; PMCID: PMC6997723.

D'Alessio A, Proietti G, Sica G, Scicchitano BM. Pathological and Molecular Features of Glioblastoma and Its Peritumoral Tissue. Cancers (Basel). 2019 Apr 3;11(4):469. doi: 10.3390/cancers11040469. PMID: 30987226; PMCID: PMC6521241.

D'Urso PI, D'Urso OF, Storelli C, Mallardo M, Gianfreda CD, Mon- tinaro A, Cimmino A, Pietro C, Marsigliante S. miR-155 is up-reg- ulated in primary and secondary glioblastoma and promotes tumour growth by inhibiting GABA receptors. Int J Oncol 2012; 41: 228-324.

Daniel KG, Harbach RH, Guida WC, Dou QP. Copper storage diseases: Menkes, Wilsons, and cancer. Front Biosci. 2004 Sep 1;9:2652-62. doi: 10.2741/1424. PMID: 15358588.

Delic S, Lottmann N, Stelzl A, Liesenberg F, Wolter M, Götze S, Zapatka M, Shiio Y, Sabel MC, Felsberg J, Reifenberger G, Rie- menschneider MJ. MiR-328 promotes glioma cell invasion via SFRP1-dependent Wnt-signaling activation. Neuro Oncol 2014; 16: 179-190.

Dissaux G, Basse V, Schick U, El Kabbaj O, Auberger B, Magro E, Kassoul A, Abgral R, Salaun PY, Bourhis D, Querellou S. Prognostic value of 18F-FET PET/CT in newly diagnosed WHO 2016 high-grade glioma. Medicine (Baltimore). 2020 Jan;99(5):e19017. doi: 10.1097/MD.0000000000019017. PMID: 32000446; PMCID: PMC7004648.

Drake LR, Hillmer AT, Cai Z. Approaches to PET Imaging of Glioblastoma. Molecules. 2020 Jan 28;25(3):568. doi: 10.3390/molecules25030568. PMID: 32012954; PMCID: PMC7037643

Ebert MS, Neilson JR, Sharp PA. MicroRNA sponges: competitive inhibitors of small RNAs in mammalian cells. Nat Methods. 2007 Sep;4(9):721-6. doi: 10.1038/nmeth1079. Epub 2007 Aug 12. PMID: 17694064; PMCID: PMC3857099.

Eiblmaier M, Meyer LA, Anderson CJ. The role of p53 in the trafficking of copper-64 to tumor cell nuclei. Cancer Biol Ther. 2008 Jan;7(1):63-9. doi: 10.4161/cbt.7.1.5130. Epub 2007 Oct 8. PMID: 17938576.

Eis PS, Tam W, Sun L, Chadburn A, Li Z, Gomez MF, Lund E, Dahlberg JE. Accumulation of miR-155 and BIC RNA in human B cell lymphomas Proc Natl Acad Sci U S A. 2005 Mar 8;102(10):3627-32.

Ebrahimkhani S, Vafaee F, Hallal S, Wei H, Lee MYT, Young PE, Satgunaseelan L, Beadnall H, Barnett MH, Shivalingam B, Suter CM, Buckland ME, Kaufman KL. Deep sequencing of circulating exosomal microRNA allows non-invasive glioblastoma diagnosis. NPJ Precis Oncol. 2018 Dec 12;2:28. doi: 10.1038/s41698-018-0071-0. PMID: 30564636; PMCID: PMC6290767.

Farazi TA, Spitzer JI, Morozov P, Tuschl T. miRNAs in human cancer. J Pathol. 2011 Jan;223(2):102-15. doi: 10.1002/path.2806.

Ferrari C., Asabella AN. And Villano C. Copper-64 dichloride as theranostic agent for glioblastoma multiforme: a preclinical study. BioMed Research International, 2015.

Fisher GL, Shifrine M (1978) Hypothesis for the mechanism of elevated serum copper in cancer patients. Oncology 35 : 22-25

Fuchs A, Lustig ED. Localization of tissue copper in mouse mammary tumors. Oncology 1989;46:183–7

Jie Gao and Liu The role of miR-26 in tumors and normal tissues (Review) Oncol Lett. 2011 Nov; 2(6): 1019–1023.

Gately L, McLachlan SA, Dowling A, Philip J. Life beyond a diagnosis of glioblastoma: a systematic review of the literature. J Cancer Surviv. 2017 Aug;11(4):447-452. doi: 10.1007/s11764-017-0602-7. Epub 2017 Feb 13. PMID: 28194640.

Ghandi M, Huang FW, Jané-Valbuena J, Kryukov GV, Lo CC, McDonald ER 3rd, Barretina J, Gelfand ET, Bielski CM, Li H, Hu K, Andreev-Drakhlin AY, Kim Next-generation characterization of the Cancer Cell Line Encyclopedia. Nature. 2019 May;569(7757):503-508. doi: 10.1038/s41586-019-1186-3. Epub 2019 May 8. PMID: 31068700; PMCID: PMC6697103

Ghaemmaghami AB et al. Role of exosomes in malignant glioma: microRNAs and proteins in pathogenesis and diagnosis. Cell Commun Signal. 2020;18(1):120. Published 2020 Aug 3. doi:10.1186/s12964-020-00623-9

Gabriely G1, Yi M, Narayan RS, Niers JM, Wurdinger T, Imitola J, Ligon KL, Kesari S, Esau C, Stephens RM, Tannous BA, Krichevsky AM. Human glioma growth is controlled by microRNA-10b.Cancer Res. 2011 May 15;71(10):3563-72. doi: 10.1158/0008-5472.CAN-10-3568. Epub 2011 Apr 6.

Gouazé-Andersson V, Delmas C, Taurand M, Martinez-Gala J, Evrard S, Mazoyer S, Toulas C, Cohen-Jonathan-Moyal E. FGFR1 Induces Glioblastoma Radioresistance through the PLCγ/Hif1α Pathway. Cancer Res. 2016 May 15;76(10):3036-44. doi: 10.1158/0008-5472.CAN-15-2058. Epub 2016 Feb 19. PMID: 26896280.

Gulluoglu S, Tuysuz EC, Sahin M, Kuskucu A, Kaan Yaltirik C, Ture U, Kucukkaraduman B, Akbar MW, Gure AO, Bayrak OF, Dalan AB. Simultaneous miRNA and mRNA transcriptome profiling of glioblastoma samples reveals a novel set of OncomiR candidates and their target genes. Brain Res. 2018 Dec 1;1700:199-210. doi: 10.1016/j.brainres.2018.08.035. Epub 2018 Aug 31. PMID: 30176243.

Guerreiro JF, Alves V, Abrunhosa AJ, Paulo A, Gil OM, Mendes F. Radiobiological Characterization of $64CuCl_2$ as a Simple Tool for Prostate Cancer Theranostics. Molecules. 2018 Nov 11;23(11):2944. doi: 10.3390/molecules23112944. PMID: 30423862; PMCID: PMC6278521.

Gutfilen B, Souza SA, Valentini G. Copper-64: a real theranostic agent. Drug Des Devel Ther. 2018 Oct 2;12:3235-3245. doi: 10.2147/DDDT.S170879. PMID: 30323557; PMCID: PMC6173185.

González-Gómez P, Sánchez P, Mira H. MicroRNAs as regulators of neural stem cell-related pathways in glioblastoma multi- forme. Mol Neurobiol 2011; 44: 235-249.

Han X, Xue X, Zhou H, Zhang G. A molecular view of the radioresistance of gliomas. Oncotarget. 2017 Oct 11;8(59):100931-100941. doi: 10.18632/oncotarget.21753. PMID: 29246031; PMCID: PMC5725073.

Hanahan D, Weinberg RA. The Hallmarks of cancer. Cell 2000;100:57–70.

Hanif F, Muzaffar K, Perveen K, Malhi SM, Simjee ShU. Glioblastoma Multiforme: A Review of its Epidemiology and Pathogenesis through Clinical Presentation and Treatment. Asian Pac J Cancer Prev. 2017 Jan 1;18(1):3-9. doi: 10.22034/APJCP.2017.18.1.3. PMID: 28239999; PMCID: PMC5563115.

Hanif F, Muzaffar K, Perveen K, Malhi SM, Simjee ShU. Glioblastoma Multiforme: A Review of its Epidemiology and Pathogenesis through Clinical Presentation and Treatment. Asian Pac J Cancer Prev. 2017 Jan 1;18(1):3-9. doi: 10.22034/APJCP.2017.18.1.3. PMID: 28239999; PMCID: PMC5563115.

Hanna J, Hossain GS, Kocerha J. The Potential for microRNA Therapeutics and Clinical Research. Front Genet. 2019 May 16;10:478. doi: 10.3389/fgene.2019.00478. PMID: 31156715; PMCID: PMC6532434.

He C, Zheng S, Luo Y, Wang B. Exosome Theranostics: Biology and Translational Medicine. Theranostics. 2018 Jan 1;8(1):237-255. doi: 10.7150/thno.21945. PMID: 29290805; PMCID: PMC5743472.

Howell R.W. Radiation spectra for Auger-electron emitting radionuclides: report No. 2 of AAPM NuclearMedicine Task Group No. 6. Med Phys. 1992 Nov-Dec;19(6):1371-83.

Hu G. Copper stimulates proliferation of human endothelial cells under culture; J. Cell. Biochem. 69:326-335, 1998.

Huang SW, Ali ND, Zhong L, Shi J. MicroRNAs as biomarkers for human glioblastoma: progress and potential. Acta Pharmacol Sin. 2018 Sep;39(9):1405-1413. doi: 10.1038/aps.2017.173. Epub 2018 Feb 8. PMID: 29417946; PMCID: PMC6289388.

Hummel R, Hussey DJ, Haier J. MicroRNAs: predictors and modifiers of chemo- and radiotherapy in different tumour types. Eur J Cancer. 2010 Jan;46(2):298-311. doi: 10.1016/j.ejca.2009.10.027. Epub 2009 Nov 28. PMID: 19948396.

Hung KF, Yang T, Kao SY. Cancer stem cell theory: Are we moving past the mist? J Chin Med Assoc. 2019 Nov;82(11):814-818. doi: 10.1097/JCMA.0000000000000186. PMID: 31469690.

Ishida S, Andreux P, Poitry-Yamate C, et al. Bioavailable copper modulates oxidative phosphorylation and growth of tumors. PNAS 2013;110:19507.

Jiang Z, Yu N, Kuang P, Chen M, Shao F, Martin G, Chui DH, Cardoso WV, Ai X, Lü J. Trinucleotide repeat containing 6a (Tnrc6a)-mediated microRNA function is required for development of yolk sac endoderm. J Biol Chem. 2012 Feb 17;287(8):5979-87. doi: 10.1074/jbc.M111.297937. Epub 2011 Dec 20. PMID: 22187428; PMCID: PMC3285365.

Jiang J, Sun X, Wang W, Jin X, Bo X, Li Z, Bian A, Jiu J, Wang X, Liu D, Hui X, Wang Y, Wang A, Ding L. Tumor microRNA-335 expression is associated with poor prognosis in human glioma. Med Oncol. 2012 Dec;29(5):3472-7. doi: 10.1007/s12032-012-0259-z. Epub 2012 May 27. PMID: 22644918.

John F, Robinette NL, Amit-Yousif AJ, Bosnyák E, Barger GR, Shah KD, Mittal S, Juhász C. Multimodal Imaging of Nonenhancing Glioblastoma Regions. Mol Imaging. 2019 Jan-Dec;18:1536012119885222. doi: 10.1177/1536012119885222. PMID: 31736437; PMCID: PMC6862774.

Jørgensen JT et al. "High tumor uptake of (64)Cu: implications for molecular imaging of tumor characteristics with copper-based PET tracers" Nucl Med Biol. 2013 Apr;40(3):345-50. doi: 10.1016/j.nucmedbio.2013.01.002.

Jurj A, Zanoaga O, Braicu C, Lazar V, Tomuleasa C, Irimie A, Berindan-Neagoe I. A Comprehensive Picture of Extracellular Vesicles and Their Contents. Molecular Transfer to Cancer Cells. Cancers (Basel). 2020 Jan 27;12(2):298. doi: 10.3390/cancers12020298. PMID: 32012717; PMCID: PMC7072213.

Kaiser J, Gullotta F (1980) Estimation of the copper content of astrocytomas, and glioblastomas by the cuproin method. Neurochirurgia 23: 20-23

Kassis A. The Amazing World of Auger Electrons INT. J. RADIAT. BIOL., NOVEMBER–DECEMBER, 2004, VOL. 80, NO. 11–12, 789–803

Kassis A. Strand Breaks in Plasmid DNA after Positional Changes of Auger Electron-Emitting lodine-125: Direct Compared to Indirect Effects RADIATION RESEARCH 152, 530-538 (1999)

Kassis A. Radiotoxicity of an 1251-LabeledD NA Intercalator in Mammalian Cells RADIATIORNE SEARC1H1 8, 283-294 (1989)

Kastan MB, Onyekwere O, Sidransky D, Vogelstein B, Craig RW. Participation of p53 protein in the cellular response to DNA damage. Cancer Res. 1991 Dec 1;51(23 Pt 1):6304-11. PMID: 1933891.

Kiess Ana P. Auger Radiopharmaceutical Therapy Targeting Prostate-Specific Membrane Antigen J Nucl Med. 2015 September ; 56(9): 1401–1407. doi:10.2967/jnumed.115.155929

Lah TT, Novak M, Breznik B. Brain malignancies: Glioblastoma and brain metastases. Semin Cancer Biol. 2020 Feb;60:262-273. doi: 10.1016/j.semcancer.2019.10.010. Epub 2019 Oct 22. PMID: 31654711.

Lan F, Yue X, Xia T. Exosomal microRNA-210 is a potentially non-invasive biomarker for the diagnosis and prognosis of glioma. Oncol Lett. 2020 Mar;19(3):1967-1974. doi: 10.3892/ol.2020.11249. Epub 2020 Jan 7. PMID: 32194691; PMCID: PMC7039075.

Lang FM, Hossain A, Gumin J, Momin EN, Shimizu Y, Ledbetter D, Shahar T, Yamashita S, Parker Kerrigan B, Fueyo J, Sawaya R, Lang FF. Mesenchymal stem cells as natural biofactories for exosomes carrying miR-124a in the treatment of gliomas. Neuro Oncol. 2018 Feb 19;20(3):380-390. doi: 10.1093/neuonc/nox152. PMID: 29016843; PMCID: PMC5817945.

Lapa C. Exciting Opportunities in Nuclear Medicine Imaging and Therapy. J Clin Med. 2019 Nov 12;8(11):1944. doi: 10.3390/jcm8111944. PMID: 31718092; PMCID: PMC6912644.

Lee RC, Feinbaum RL, Ambros V. The C. elegans heterochronic gene lin-4 encodes small RNAs with antisense complementarity to lin-14. Cell. 1993 Dec 3;75(5):843-54.

Lee ST, Chu K, Oh HJ, Im WS, Lim JY, Kim SK, Park CK, Jung KH, Lee SK, Kim M, Roh JK. Let-7 microRNA inhibits the proliferation of human glioblastoma cells. J Neurooncol. 2011 Mar;102(1):19-24. doi: 10.1007/s11060-010-0286-6. Epub 2010 Jul 7. PMID: 20607356.

Li,H.-F.;Kim,J.-S.;Waldman,T.Radiation induced Aktactivation modulates radioresistance in human glioblastoma cells. Radiat. Oncol. 2009, 4, 43.

Linder Maria C, Lisa Wooten, Philip Cerveza, Steven Cotton, Roman Shulze, and Norma Lomeli. Copper transport. Am J Clin Nutr 1998;67(suppl):965S–71S.

Linder MC. Biochemistry of copper. Plenum Press 1991

Linder MC; Hazegh-Azam M. Copper biochemistry and molecular biology. Am J Clin Nutr 1996, 63, 797S-811S.

Liu, C.-C.F. and D.M. Medeiros. 1986. Excess diet copper increases systolic blood pressure in rat. Biol. Trace Element Res. 9: 15-24.

Louis DN, Ohgaki H, Wiestler OD, et al: The 2007 WHO classification of tumours of the central nervous system. Acta Neuropathol 114: 97-109, 2007.

Lundy P, Domino J, Ryken T, Fouke S, McCracken DJ, Ormond DR, Olson JJ. The role of imaging for the management of newly diagnosed glioblastoma in adults: a systematic review and evidence-based clinical practice guideline update. J Neurooncol. 2020 Nov;150(2):95-120. doi: 10.1007/s11060-020-03597-3. Epub 2020 Nov 19. PMID: 33215340.

Lukas RV, Wainwright DA, Ladomersky E, Sachdev S, Sonabend AM, Stupp R. Newly Diagnosed Glioblastoma: A Review on Clinical Management. Oncology (Williston Park). 2019 Mar 13;33(3):91-100. PMID: 30866031; PMCID: PMC7278092.

Makarova JA, Shkurnikov MU, Turchinovich AA, Tonevitsky AG, Grigoriev AI. Circulating microRNAs. Biochemistry (Mosc). 2015 Sep;80(9):1117-26. doi: 10.1134/S0006297915090035. PMID: 26555465.

Malzkorn B, Wolter M, Liesenberg F, Grzendowski M, Stühler K, Meyer HE, Reifenberger G. Identification and functional characterization of microRNAs involved in the malignant progression of gliomas. Brain Pathol. 2010 May;20(3):539-50. doi: 10.1111/j.1750-3639.2009.00328.x. Epub 2009 Sep 19. PMID: 19775293.

Mao H, Lebrun DG, Yang J, Zhu VF, Li M. Deregulated signaling pathways in glioblastoma multiforme: molecular mechanisms and therapeutic targets. Cancer Invest. 2012 Jan;30(1):48-56. doi: 10.3109/07357907.2011.630050. PMID: 22236189; PMCID: PMC3799884.

Matsuyama H, Suzuki HI. Systems and Synthetic microRNA Biology: From Biogenesis to Disease Pathogenesis. Int J Mol Sci. 2019 Dec 24;21(1):132. doi: 10.3390/ijms21010132. PMID: 31878193; PMCID: PMC6981965.

McMillan DD, Maeda J, Bell JJ, Genet MD, Phoonswadi G, Mann KA et al Validation of 64Cu-ATSM damaging DNA via high-LET Auger electron emission. J Radiat Res.2015;56:784-91.

Metheetrairut C, Slack FJ. MicroRNAs in the ionizing radiation response and in radiotherapy. Curr Opin Genet Dev. 2013 Feb;23(1):12-9. doi: 10.1016/j.gde.2013.01.002. Epub 2013 Feb 28. PMID: 23453900; PMCID: PMC3617065.

Monroig-Bosque Pdel C, Rivera CA, Calin GA. MicroRNAs in cancer therapeutics: "from the bench to the bedside". Expert Opin Biol Ther. 2015;15(10):1381-5. doi: 10.1517/14712598.2015.1074999. PMID: 26372796; PMCID: PMC4890620.

Nasulewicza Anna, Andrzej Mazurb, Adam Opolskia et al. Role of copper in tumour angiogenesis—clinical implications. Journal of Trace Elements in Medicine and Biology 18 (2004): 1–8

O'Brien J, Hayder H, Zayed Y, Peng C. Overview of MicroRNA Biogenesis, Mechanisms of Actions, and Circulation. Front Endocrinol (Lausanne). 2018 Aug 3;9:402. doi: 10.3389/fendo.2018.00402. PMID: 30123182; PMCID: PMC6085463.

Oh SJ, Yang JI, Kim O, Ahn EJ, Kang WD, Lee JH, Moon KS, Lee KH, Cho D. Human U87 glioblastoma cells with stemness features display enhanced sensitivity to natural killer cell cytotoxicity through altered expression of NKG2D ligand. Cancer Cell Int. 2017 Feb 10;17:22. doi: 10.1186/s12935-017-0397-7. PMID: 28203118; PMCID: PMC5303255.

Ohgaki H, Kleihues P. The definition of primary and secondary glioblastoma. Clin Cancer Res. 2013 Feb 15;19(4):764-72. doi: 10.1158/1078-0432.CCR-12-3002. Epub 2012 Dec 3. PMID: 23209033.

Parmar A, Pascali G, Voli F, Lerra L, Yee E, Ahmed-Cox A, Kimpton K, Cirillo G, Arthur A, Zahra D, Rahardjo G, Liu GJ, Lengkeek N, Saletta F, Charil A, Kavallaris M, Vittorio O. In vivo [64Cu]CuCl2 PET imaging reveals activity of Dextran-Catechin on tumor copper homeostasis. Theranostics. 2018 Nov 9;8(20):5645-5659. doi: 10.7150/thno.29840. PMID: 30555570; PMCID: PMC6276294.

Peng F., Lu X. and Janisse J. PET of human prostate cancer xenografts mice with increased uptake of 64CuCl2. The jurnal of nuclear medicine, Vol 47 n° 10 pp 1649-1652, 2006.

Piccardo A, Paparo F, Puntoni M, et al. 64CuCl2 PET/CT in prostate cancer relapse. J Nucl Med. 8, 2017.

Pirtoli et al. Radiobiology of Glioblastoma- Recent Advances and Related Pathobiology-Current Clinical Pathology, Humana Press 2016

Pizzolo G, Savarin T, Molino AM, Ambosetti A, Todeschini G, Vettore L (1978) The diagnostic value of serum copper levels and other hematochemical parameters in malignancies. Tumori 64 : 55-61.

Qin C, Liu H, Chen K, Hu X, Ma X, Lan X, Zhang Y, Cheng Z. Theranostics of malignant melanoma with 64CuCl2. J Nucl Med. 2014 May;55(5):812-7. doi: 10.2967/jnumed.113.133850. Epub 2014 Mar 13. PMID: 24627435; PMCID: PMC4346241.

Qing Ji, Xinbao Hao, Min Zhang, Wenhua Tang, Meng Yang, Ling Li, Debing Xiang, Jeffrey T. DeSano, Guido T. Bommer, Daiming Fan, Eric R. Fearon, Theodore S. Lawrence, and Liang Xu MicroRNA miR-34 Inhibits Human Pancreatic Cancer Tumor-Initiating Cells PLoS One. 2009; 4(8): e6816.

Ross JS, Carlson JA, Brock G. miRNA: the new gene silencer. Am J Clin Pathol. 2007 Nov; 128(5):830-6.

Rupaimoole, R., Slack, F. MicroRNA therapeutics: towards a new era for the management of cancer and other diseases. Nat Rev Drug Discov 16, 203–222 (2017). https://doi.org/10.1038/nrd.2016.246

Scanni A, Tomirotti M, Licciardello L, Annibali E, Biraghi M, Trovato M, Fittipaldi M, Adamoli P, Curtarello G (1979) Variations in serum copper and ceruloplasmin levels in advanced gastrointestinal cancer treated with polychemotherapy. Tumori 65:331 338*

Saito Y, Liang G, Egger G, Friedman JM, Chuang JC, Coetzee GA, Jones PA.. Specific activation of microRNA-127 with downregulation of the proto-oncogene BCL6 by chromatin-modifying drugs in human cancer cells. Cancer Cell. 2006 Jun;9(6):435-43

Sasmita AO, Wong YP, Ling APK. Biomarkers and therapeutic advances in glioblastoma multiforme. Asia Pac J Clin Oncol. 2018 Feb;14(1):40-51. doi: 10.1111/ajco.12756. Epub 2017 Aug 25. PMID: 28840962.

Sayed D, Abdellatif M. MicroRNAs in development and disease. Physiol Rev. 2011 Jul;91(3):827-87.

Schulz A, Meyer F, Dubrovska A, Borgmann K. Cancer Stem Cells and Radioresistance: DNA Repair and Beyond. Cancers (Basel). 2019 Jun 21;11(6):862. doi: 10.3390/cancers11060862. PMID: 31234336; PMCID: PMC6627210.

Shea A, Harish V, Afzal Z, Chijioke J, Kedir H, Dusmatova S, Roy A, Ramalinga M, Harris B, Blancato J, Verma M, Kumar D. MicroRNAs in glioblastoma multiforme pathogenesis and therapeutics. Cancer Med. 2016 Aug;5(8):1917-46. doi: 10.1002/cam4.775. Epub 2016 Jun 10. PMID: 27282910; PMCID: PMC4971921.

Shankar GM, Balaj L, Stott SL, Nahed B, Carter BS. Liquid biopsy for brain tumors. Expert Rev Mol Diagn. 2017 Oct;17(10):943-947. doi: 10.1080/14737159.2017.1374854. Epub 2017 Sep 6. PMID: 28875730; PMCID: PMC5856481.

Shea A, Harish V, Afzal Z, Chijioke J, Kedir H, Dusmatova S, Roy A, Ramalinga M, Harris B, Blancato J, Verma M, Kumar D. MicroRNAs in glioblastoma multiforme pathogenesis and therapeutics. Cancer Med. 2016 Aug;5(8):1917-46. doi: 10.1002/cam4.775. Epub 2016 Jun 10. PMID: 27282910; PMCID: PMC4971921.

Shi R, Wang PY, Li XY, Chen JX, Li Y, Zhang XZ, Zhang CG, Jiang T, Li WB, Ding W, Cheng SJ. Exosomal levels of miRNA-21 from cerebrospinal fluids associated with poor prognosis and tumor recurrence of glioma patients. Oncotarget. 2015 Sep 29;6(29):26971-81. doi: 10.18632/oncotarget.4699. PMID: 26284486; PMCID: PMC4694967.

Silantyev AS, Falzone L, Libra M, Gurina OI, Kardashova KS, Nikolouzakis TK, Nosyrev AE, Sutton CW, Mitsias PD, Tsatsakis A. Current and Future Trends on Diagnosis and Prognosis of Glioblastoma: From Molecular Biology to Proteomics. Cells. 2019 Aug 9;8(8):863. doi: 10.3390/cells8080863. PMID: 31405017; PMCID: PMC6721640.

Soomro SH, Ting LR, Qing YY, Ren M. Molecular biology of glioblastoma: Classification and mutational locations. J Pak Med Assoc. 2017 Sep;67(9):1410-1414. PMID: 28924284.

Song et al., 2015Delivery of anti-microRNA-21 antisense-oligodeoxynucleotide using amphiphilic peptides for glioblastoma gene therapy

Steed TC, Treiber JM, Patel K, Ramakrishnan V, Merk A, Smith AR, Carter BS, Dale AM, Chow LM, Chen CC. Differential localization of glioblastoma subtype: implications on

glioblastoma pathogenesis. Oncotarget. 2016 May 3;7(18):24899-907. doi: 10.18632/oncotarget.8551. PMID: 27056901; PMCID: PMC5041878.

Stoyanov GS, Dzhenkov D, Ghenev P, Iliev B, Enchev Y, Tonchev AB. Cell biology of glioblastoma multiforme: from basic science to diagnosis and treatment. Med Oncol. 2018 Jan 31;35(3):27. doi: 10.1007/s12032-018-1083-x. PMID: 29387965.

Stupp R, Mason WP, van den Bent MJ, et al: Radiotherapy plus concomitant and adjuvant temozolomide for glioblastoma. N Engl J Med 352: 987-996, 2005

Suh S-S, Yoo JY, Nuovo GJ, Jeon Y-J, Kim S, Lee TJ, Kim T, Bakàcs A, Alder H, Kaur B, Aqeilan RI, Pichiorri F, Croce CM. MicroRNAs/TP53 feedback circuitry in glioblastoma multiforme. Proc Natl Acad Sci U S A. 2012; 109: 5316-5321.

Sumazin P, Yang X, Chiu HS, Chung WJ, Iyer A, Llobet-Navas D, Rajbhandari P, Bansal M, Guarnieri P, Silva J, Califano A. An extensive microRNA-mediated network of RNA-RNA interactions regulates established oncogenic pathways in glioblastoma. Cell. 2011 Oct 14;147(2):370-81. doi: 10.1016/j.cell.2011.09.041. PMID: 22000015; PMCID: PMC3214599.

Sun X and Anderson CJ. Production and Applications of Copper-64 Radiopharmaceuticals. Volume 386, 2004, 237-261.

Teplyuk NM, Uhlmann EJ, Gabriely G, Volfovsky N, Wang Y, Teng J, Karmali P, Marcusson E, Peter M, Mohan A, Kraytsberg Y, Cialic R, Chiocca EA, Godlewski J, Tannous B, Krichevsky AM. Therapeutic potential of targeting microRNA-10b in established intracranial glioblastoma: first steps toward the clinic. EMBO Mol Med. 2016 Mar 1;8(3):268-87. doi: 10.15252/emmm.201505495. PMID: 26881967; PMCID: PMC4772951.

Takahashi RU, Prieto-Vila M, Kohama I, Ochiya T. Development of miRNA-based therapeutic approaches for cancer patients. Cancer Sci. 2019 Apr;110(4):1140-1147. doi: 10.1111/cas.13965. Epub 2019 Feb 26. PMID: 30729639; PMCID: PMC6447849.

Taylor OG, Brzozowski JS, Skelding KA. Glioblastoma Multiforme: An Overview of Emerging Therapeutic Targets. Front Oncol. 2019 Sep 26;9:963. doi: 10.3389/fonc.2019.00963. PMID: 31616641; PMCID: PMC6775189.

Tutar L, Tutar E, Özgür A, Tutar Y. Therapeutic Targeting of microRNAs in Cancer: Future Perspectives. Drug Dev Res. 2015 Nov;76(7):382-8. doi: 10.1002/ddr.21273. Epub 2015 Aug 26. PMID: 26435382.

Vanderhoek M, Perlman SB, Jeraj R. Impact of different standardized uptake value measures on PET-based quantification of treatment response. J Nucl Med. 2013 Aug;54(8):1188-94. doi: 10.2967/jnumed.112.113332. Epub 2013 Jun 17. PMID: 23776199; PMCID: PMC6231399.

Verduin M, Compter I, Steijvers D, Postma AA, Eekers DBP, Anten MM, Ackermans L, Ter Laan M, Leijenaar RTH, van de Weijer T, Tjan-Heijnen VCG, Hoeben A, Vooijs M. Noninvasive Glioblastoma Testing: Multimodal Approach to Monitoring and Predicting Treatment Response. Dis Markers. 2018 Jan 17;2018:2908609. doi: 10.1155/2018/2908609. PMID: 29581794; PMCID: PMC5822799.

Wang,J.;Wakeman,T.P.;Latha,J.D.;Hjelmeland,A.B.;Wang,X.-F.;White,R.R.;Rich,J.N.;Sullenger,B.A. Notch Promotes Radioresistance of Glioma Stem Cells. Stem Cells 2009, 28, 17–28.

Wang XR, Luo H, Li HL, Cao L, Wang XF, Yan W, Wang YY, Zhang JX, Jiang T, Kang CS, Liu N, You YP; Chinese Glioma Cooperative Group (CGCG). Overexpressed let-7a inhibits glioma cell malignancy by directly targeting K-ras, independently of PTEN. Neuro Oncol. 2013 Nov;15(11):1491-501. doi: 10.1093/neuonc/not107. Epub 2013 Oct 3. PMID: 24092860; PMCID: PMC3813414.

Wen D, Danquah M, Chaudhary AK, Mahato RI. Small molecules targeting microRNA for cancer therapy: Promises and obstacles. J Control Release. 2015 Dec 10; 219:237-47.

Williams JR, Zhang Y, Russell J, Koch C, Little JB. Human tumor cells segregate into radiosensitivity groups that associate with ATM and TP53 status. Acta Oncol. 2007;46(5):628-38. doi: 10.1080/02841860601080407. PMID: 17562439.

Wollemann M (1974) Biochemistry of brain tumors. Mac- Millans Press Ltd, London

Wu J, Li L, Jiang C. Identification and Evaluation of Serum MicroRNA-29 Family for Glioma Screening. Mol Neurobiol. 2015 Dec;52(3):1540-1546. doi: 10.1007/s12035-014-8937-9. Epub 2014 Nov 4. PMID: 25367878.

Yao, M., Li, S., Wu, X. et al. Cellular origin of glioblastoma and its implication in precision therapy. Cell Mol Immunol 15, 737–739 (2018). https://doi.org/10.1038/cmi.2017.159

Yue X, Lan F, Hu M, Pan Q, Wang Q, Wang J. Downregulation of serum microRNA-205 as a potential diagnostic and prognostic biomarker for human glioma. J Neurosurg. 2016 Jan;124(1):122-8. doi: 10.3171/2015.1.JNS141577. Epub 2015 Jul 31. PMID: 26230475.

Zhang Q, Han Z, Zhu Y, Chen J and Li W: Role of hypoxia inducible factor-1 in cancer stem cells (Review). Mol Med Rep 23: 17, 2021

Zhang R, Pang B, Xin T, Guo H, Xing Y, Xu S, Feng B, Liu B, Pang Q. Plasma miR-221/222 Family as Novel Descriptive and Prognostic Biomarkers for Glioma. Mol Neurobiol. 2016 Apr;53(3):1452-1460. doi: 10.1007/s12035-014-9079-9. Epub 2015 Jan 31. PMID: 25636684.

Zhao Y, Song Y, Yao L, Song G, Teng C. Circulating microRNAs: Promising Biomarkers Involved in Several Cancers and Other Diseases. DNA Cell Biol. 2017 Feb;36(2):77-94. doi: 10.1089/dna.2016.3426. Epub 2017 Jan 6. PMID: 28060535. (a)

Yordanova A, Eppard E, Kürpig S, Bundschuh RA, Schönberger S, Gonzalez-Carmona M, Feldmann G, Ahmadzadehfar H, Essler M. Theranostics in nuclear medicine practice. Onco Targets Ther. 2017 Oct 3;10:4821-4828. doi: 10.2147/OTT.S140671. PMID: 29042793; PMCID: PMC5633297.

Zygogianni A, Protopapa M, Kougioumtzopoulou A, Simopoulou F, Nikoloudi S, Kouloulias V. From imaging to biology of glioblastoma: new clinical oncology perspectives to the problem of local recurrence. Clin Transl Oncol. 2018 Aug;20(8):989-1003. doi: 10.1007/s12094-018-1831-6. Epub 2018 Jan 15. PMID: 29335830.